THEORY AND DESIGN OF RELAXOMETRIC PROBES

Thesis by

Carlo Joseph Quiñónez

In Partial Fulfillment of the Requirements for the

degree of

Doctor of Philosophy

CALIFORNIA INSTITUTE OF TECHNOLOGY

Pasadena, California

2003

(Defended June 2, 2003)

ACKNOWLEDGEMENTS

First and foremost, I would like to express my deepest gratitude to my family and friends. Without them, I would not have been able to keep it together long enough to graduate. Of course I will never forget the support, advice and guidance of my mentor, Prof. Scott Fraser, and my lab mates.

ABSTRACT

In an effort to rationally design an apoptosis-sensitive MRI contrast agent, two novel gadolinium complexes were designed, synthesized and evaluated as components of a relaxometric probe. The first, AEDO3A will prove a useful building block for in the area of the relaxometric probe design. AEDO3A•Gd has a relaxivity of 2.2 mM-1s-1 and 3.4 mM-1s-1 at 60Mhz and 500MHz, respectively. If AEDO3A•Gd is the "on" state and assuming reasonable relaxivities for the "off" state, tissue contrast modeling of the smallest-detectable relaxivity change suggests AEDO3A is suitable for incorporation into relaxometric probes.

1-(2-Aspartryl-aminoethyl)-4,7,10-tri(carboxymethyl)-cyclen (Asp-AEDO3A) is evaluated as the second component of an apoptosis-sensitive relaxometric probe system. The synthesis and characterization of the ligand and its Gd and Tb complexes is described. Fluorescence lifetime data of the terbium complex indicate the presence of 0.6 water molecules in the inner coordination sphere. The gadolinium complex has a relaxivity of 1.4 $mM^{-1}s^{-1}$ and 1.7 $mM^{-1}s^{-1}$ at 60Mhz and 500MHz, respectively. Toxicity studies demonstrated *Xenopus* embryos tolerated Asp-AEDO3A•Gd at magnetically useful concentrations as predicted by tissue contrast modeling. X-ray crystallography data are presented for both the ligand and gadolinium complex.

Unfortunately, no enzymatic processing of Asp-AEDO3A•Gd was observed under any conditions. This phenomenon was attributed to heretofore-unknown coordination chemistry for gadolinium elucidated from the X-ray crystal structure. This novel N-carboxamido coordination, while problematic for the application of Asp-AEDO3A•Gd as a relaxometric probe, will be potentially useful in other areas of contrast agent design.

TABLE OF CONTENTS

LIST OF ILLUSTRATIONS AND/OR TABLES

Figures

Tables

Schemes

Equations

NOMENCLATURE

Apoptosis. An active and programmed process of cell elimination vital to homeostasis.

B_0. The constant (main) magnetic field of an MRI system. It is usually expressed in units of Telsa (10,000 Gauss or about 20,000 times the magnetic field of the Earth).

CA. See **Contrast Agent**.

Contrast Agent. A substance that enhances (shortens) the relaxation time of water molecules, making them appear 'brighter' in T_1 or T_2 weighted MR images. Abbreviated "**CA**".

Inner Coordination Sphere. Used to describe any water molecules that are directly coordinated to the metal ion inside a contrast agent.

Larmor Frequency. The Larmor frequency is the frequency of precession of the nuclear magnetic moment (spins) and is proportional to the magnetic field strength as shown in the Larmor equation, $\omega_I = \gamma_I B_0$, where ω_I is the Larmor frequency in Hertz, γ_I is the gyromagnetic ratio of the nucleus and B_0 is the magnetic field strength in Telsa.

MRI. Magnetic Resonance Imaging, a non-invasive technique using strong magnetic fields and radiofrequency pulse to create images of internal anatomy.

μMRI. Micro-MRI is a specialized form of MRI with better spatial resolution (< 500 μm). μMRI is typically performed in stronger field strengths than are typically employed in clinical settings.

NMR. Nuclear Magnetic Resonance, an analytical technique commonly employed in chemistry.

Outer Coordination Sphere. Used to describe any water molecules that are not in the inner- or second-coordination spheres.

P_m. The fraction of the solvent bound to the solvent. This is calculated by dividing the concentration of the contrast agent by the concentration of water (i.e., 55 M), $\frac{[M_{CA}]}{55\ M}$.

q**.** The symbol used to indicate the number of water molecules inside the inner-coordination sphere, i.e., directly coordinated to the metal ion in a CA.

Relaxation Time. The time it takes nuclear spins to return to their equilibrium state after excitation by an RF pulse. Intensity in MR image is proportional to relaxation time.

Relaxivity. The ability of a contrast agent to shorten the relaxation time of nearby water protons. The higher the relaxivity, the shorter the relaxation time.

Relaxometric Probe. A contrast agent that modulates, reversibly or irreversibly, its relaxivity in response to a physiological stimulus.

Second Coordination Sphere. Used to describe any water molecules that are coordinated to only the contrast agent ligand, not to the metal ion inside a contrast agent. For example, a water molecule that is hydrogen bound to a polar group on the ligand.

Smart Contrast Agent. A contrast agent that can serve as a reporter of a physiological or environmental stimulus. See Relaxometric Probe.

τ_m. The average length of time a water molecule spends in the inner coordination sphere.

τ_R. The rotational correlation time of a contrast agent. This is related to how fast the contrast is physically tumbling in solution.

T_1. The longitudinal or spin-lattice relaxation time. The longitudinal relaxation time is the time the longitudinal component of the net magnetization vector requires to return to the ground state after excitation by a radiofequency pulse. This is representative of the energy loss associated with high energy spins returning to their low energy state. The longitudinal axis is equivalent to the axis of the external magnetic field (B_0).

T_2. The transverse or spin-spin relaxation time. The transverse relaxation time is the time the magnitude of the transverse component of the net magnetization vector requires to return to zero after excitation by a radiofequency pulse. This is representative of the loss of proton spin phase coherence associated with the protons interacting with other protons. The transverse plane is perpendicular to the axis of the external magnetic field (B_0).

Voxel. A three-dimensional pixel in an MR image.

Chapter 1

INTRODUCTION

Magnetic Resonance Imaging (MRI) is a non-invasive technique using radio frequency (RF) pulses and strong magnetic fields to create images of internal organs and structures. Computer reconstruction of the data allows high-resolution arbitrary image planes to be generated from a single image imaging procedure. MRI has found applications in almost all areas of medicine, it is used to aid in the diagnosis of cancer, joint and musculoskeletal disorders, and neurodegenerative and cardiovascular diseases.

Apoptosis is an active and programmed process of cell elimination vital to homeostasis. It also has roles in development where the loss of cells serves many functions in deletion of cells and structures [1]. The abnormal activation or repression of apoptosis is also implicated in a wide variety of pathologies [2].

Magnetic Resonance Imaging

Magnetic resonance imaging is a valuable and versatile technique for visualizing internal structures technique first described in 1978 [3]. MRI is an extension of nuclear magnetic resonance spectroscopy used in chemistry. Certain atoms have an inherent magnetic dipole moment that results from their electrical charge and spin. When placed in a strong, steady magnetic field, these atoms begin to precess around the axis of the external magnetic field, B_0 (**Figure 1a**). The Larmor frequency, ω_L, is the frequency of precession of the atom. The orientation along the longitudinal axis, either with or against B_0, determines the energy level of the spin (**Figure 1b**). The difference in energy levels causes a net magnetization of the

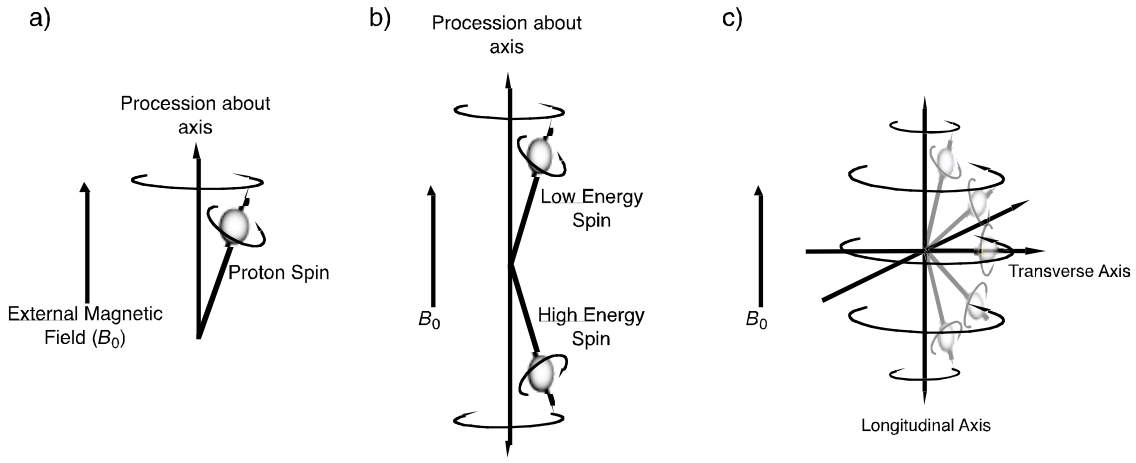

Figure 1. Panel A. Procession of protons in an external magnetic field. **Panel B.** Proton spin energy in a magnetic field. **Panel C.** Change in proton spin energy with increasing RF energy at the Larmor frequency.

sample along the longitudinal axis because of a small excess of spins in the low energy states vs. the high energy state, this net magnetization is best described as a vector. An RF pulse at the Larmor frequency may be used to add energy to the spins, moving spins from the low-energy state to a higher-energy state (**Figure 1c**). Consequently, the longitudinal component of the net magnetization vector diminishes and eventually becomes negative (against B_0) as more RF energy is added to the spins. The relaxation time is the time it takes nuclear spins to return to their equilibrium state. The relaxation time has two components, longitudinal and transverse relaxation times, known as T_1 and T_2 respectively.

The intensity of a magnetic resonance (MR) image depends primarily on three factors – the density of water protons, T_1 and T_2. The visual contrast is determined by the variation in these parameters among tissues. MR images are usually weighed to highlight differences in either T_1 or T_2, otherwise images would be fairly featureless because the density of water does not vary significantly. A small magnetic gradient is added to B_0, varying the strength of B_0

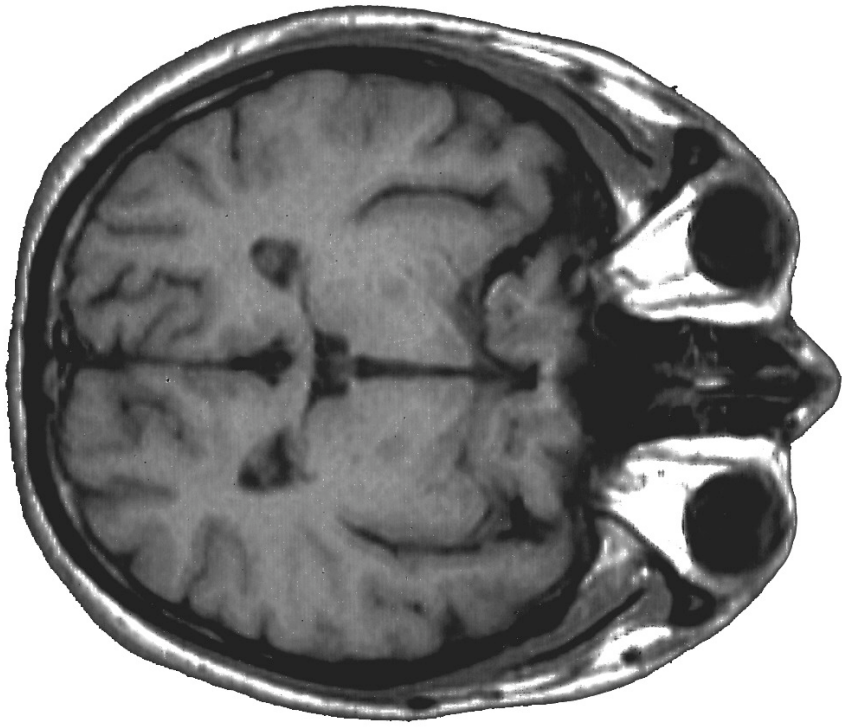

Figure 2. Example of an MR image depicting an axial section through a human subject's head. The eyes and nose are clearly visible on the right hand side of the image.

across sample. Protons within the stronger portion of the magnetic gradient will exhibit a higher Larmor frequency than protons located within the weaker segments. In this manner, spatial information is represented by the Larmor frequency of the protons. The signals from the water protons are detected by a sensitive receiver, and are analyzed by a computerized system to create a visual representation for display on a computer screen. An example of an MR image is presented (**Figure 2**).

Although satisfactory images are generated using T_1 or T_2 weighting, it is sometimes desirable to add additional contrast to an MR image in order to highlight regions of interest. This is accomplished by the use of small molecules called contrast agents (CA). CAs dramatically shorten the T_1 and T_2 of water and their presence is easily detected in MRI images

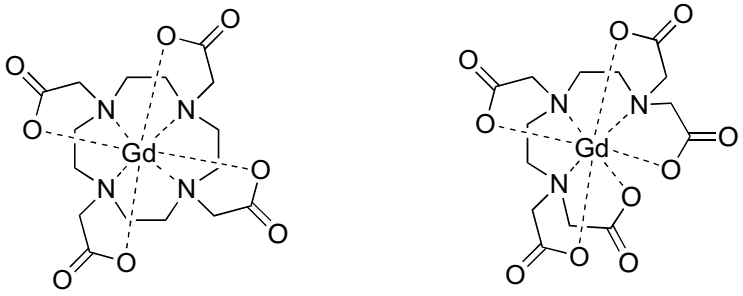

DOTA•Gd DTPA•Gd

Figure 3. Examples of two contrast agents. DOTA and DTPA are polyamino-carboxylate ligands capable of binding gadolinium ions.

at levels as low as 0.1 mM. At the core of all CAs is a metal ion such as gadolinium, manganese or iron. Among the ions, gadolinium has the greatest effect on T_1 and hence is more commonly used than the other ions. The unpaired electrons of gadolinium shorten the relaxation time of nearby water protons, making voxels appear 'brighter' in T_1-weighted images. Through-space dipole-dipole interactions between nearby water protons and the unpaired electrons cause this enhancement. Unfortunately, gadolinium ions also interfere with calcium-dependant processes and are toxic. Consequently gadolinium is used in the form of a chelate such as DOTA•Gd or DTPA•Gd (**Figure 3**). Both DOTA and DTPA make gadolinium complexes that are exceedingly stable, ameliorating the toxicity while still allowing the gadolinium ion to affect the T_1 of water protons.

Apoptosis: Programmed Cell Death

It is well known cells in the body are constantly being replaced and replenished. In fact, every year a mass of cells equal to the body weight is eliminated in order to make room for these new cells [4]. The cells that are eliminated undergo a process of programmed cell death called apoptosis. This process was first identified and coined in 1972 [5]. Apoptosis

literally means "falling leaves" in Greek, relating apoptosis in an organism to the annual shedding of leaves by deciduous tree in the autumn.

Apoptosis is different from necrotic cell death [6]. Although the difference between the two may not always be clear, apoptosis is generally characterized by distinct morphological characteristic such as cytoplasmic shrinkage, chromatin condensation, membrane blebbing and fragmentation into vesicles. There are also extensive biochemical changes that accompany the visible indicators of apoptosis. The composition of the cell membrane changes so that cells undergoing apoptosis are recognized by macrophages that will eventually consume the apoptotic cell. Chromosomal DNA is fragmented and a specific family of intracellular proteases becomes activate. These proteases are collectively known as caspases and disable cellular repair enzymes while activating other downstream proteases to quickly dissemble and package the apoptotic cell for efficient recycling.

Apoptosis can be triggered by many stimuli such as lack of growth factors, hormonal influences or mild toxic insults; active T-cells can also induce apoptosis in other cells. Apoptosis is important to homeostasis and its inappropriate activation or suppression can lead to many different pathologies. Abnormal apoptosis activity has been implicated in immune system disorders [7, 8], carcinogenesis and treatment [9-11], viral infections [12], diabetes [13], stroke [14-16], traumatic brain injury [17, 18], aging [19, 20] and even neurodegenerative diseases [21].

Common assays for apoptosis detection typically rely on one of three phenomenon, (1) activation of proteases, (2) DNA fragmentation or (3) changes in the plasma membrane. The protease whose presence is typically detected in the first type of assay is caspase. Caspase

are a family of proteases which were first identified in *C. elegans* as necessary for programmed cell [22] and their activation is considered the defining biochemical event of apoptosis [23]. In the second type of assay, DNA fragmentation is detected using a variety of enzymatic or chromatographic methods. The pattern of DNA fragmentation that occurs during apoptosis is distinctive, fragments are multiples of 180 base pairs – the distance between the histone nucleosome cores on DNA. In the final type of assay, changes in the asymmetry or permeability of the plasma membrane are used as markers for apoptosis. For instance, during apoptosis phosphatidylserine translocates from the cytoplasmic side of the plasma membrane to the extracellular side. This translocatation is detected using Annexin V, which binds extracellular phosphatidylserine. All of these techniques rely on colormetric, fluorogenic or chromatographic detection and hence are limited in their application *in vivo*. This project seeks to develop a novel MRI-based assay for apoptosis as the first step in an *in vivo* diagnostic.

Chapter 2

RELAXOMETRIC PROBES

Relaxometric probes serve as reporters of physiological function by altering their relaxivity in response to a variety of stimuli, such as pH [24, 25], O_2 saturation [26, 27], presence of specific proteins [28, 29], temperature [30, 31], metal ion concentration [32, 33] or enzyme activity [34-37]. These relaxometric probes modulate their relaxivity through a myriad of mechanisms. In order to best appreciate the different mechanisms involved in relaxometric probes, the theoretical basis of relaxivity will need to be explored in some detail.

Relaxivity

In a T_1-weighted image, the signal intensity of the voxel will be inversely proportional to the T_1 of the water protons contained within that voxel. The observed relaxation time is the sum of the intrinsic relaxation time of the solvent and the contribution from the CA (**Equation 1**). The superscripts "OBS," "SOL," and "CA" are used to respectively indicate the observed, solvent and contrast agent terms.

$$\frac{1}{T_1^{OBS}} = \frac{1}{T_1^{SOL}} + \frac{1}{T_1^{CA}} \qquad \textbf{[1]}$$

T_1^{CA} is modeled as the sum of three independent components (**Equation 2**). The superscripts "IS", "SS" and "OS" are used to respectively indicate the inner-, second- and outer-sphere contributions to T_1^{CA}. The relaxation time of water molecules in the inner-coordination sphere (i.e., directly coordinated to the paramagnetic metal ion) is expressed as

T_1^{IS}. The relaxation time of nearby water molecules is also affected and their contribution to T_1^{CA} is expressed in two separate terms, T_1^{SS} and T_1^{OS}.

$$\frac{1}{T_1^{CA}} = \frac{1}{T_1^{IS}} + \frac{1}{T_1^{SS}} + \frac{1}{T_1^{OS}} \quad \textbf{[2]}$$

Inner-Sphere Relaxivity

The inner-sphere contribution to T_1^{CA} is given in **Equation 3**, where q is the number of water molecules in the inner-coordination sphere, P_m is the fraction of water molecules inside the inner-coordination sphere, τ_m is the average length of time a single water molecule resides within the inner-sphere coordination sphere and T_{1m} is the relaxation enhancement experienced by the inner-sphere water molecules.

$$\frac{1}{T_1^{IS}} = \frac{qP_m}{T_{1m} + \tau_m} \quad \textbf{[3]}$$

Solomon-Bloembergen-Morgan theory [38, 39] provides a foundation to understand the basis of T_{1m} (**Equations 4-8**). The two components of T_{1m} term (**Equation 4**) are dipole-dipole and scalar interactions, noted by the "DD" and "SC" superscripts respectively.

$$\frac{1}{T_{1m}} = \frac{1}{T_1^{DD}} + \frac{1}{T_1^{SC}} \quad \textbf{[4]}$$

$$\frac{1}{T_1^{SC}} = \frac{2}{3} S(S+1)\left(\frac{A}{\hbar}\right)^2 \left[\frac{\tau_{e2}}{\left(1+\omega_s^2\tau_{e2}^2\right)}\right] \quad \textbf{[5]}$$

$$\frac{1}{T_1^{DD}} = \frac{2}{15}\frac{\gamma_H^2 g^2 \mu_B^2 S(S+1)}{r^6}\left[\frac{3\tau_{c1}}{\left(1+\omega_H^2\tau_{c1}^2\right)} + \frac{7\tau_{c2}}{\left(1+\omega_s^2\tau_{c2}^2\right)}\right] \quad \textbf{[6]}$$

$$\frac{1}{\tau_{ci}} = \frac{1}{T_{ie}} + \frac{1}{\tau_m} + \frac{1}{\tau_R} \qquad i = 1,2 \quad \textbf{[7]}$$

$$\frac{1}{\tau_{ei}} = \frac{1}{T_{ie}} + \frac{1}{\tau_m} \qquad i = 1,2 \quad \textbf{[8]}$$

The scalar interaction is given in **Equation 5**. The hyperfine coupling constant $\left(\frac{A}{\hbar}\right)$ is quite small in most CAs, consequently the contribution of T_1^{SC} to T_{1m} may be safely ignored and will not be considered further.

Thus T_{1m} is largely determined by the magnitude of the dipole-dipole interactions given in **Equation 6**. γ_H is the proton gyromagnetic ratio, g is the electronic g factor, μ_B is the Bohr magneton, S is the number of unpaired electron in the paramagnetic metal ion, r is the distance between the water protons and the unpaired electrons of paramagnetic metal ion, ω_H/ω_s are the Larmor frequencies of protons and electrons respectively, and τ_{1c}, is the local correlation time of the contrast agent. The electronic contributions (the "7" term inside the square brackets) may be conveniently ignored because at field strengths used in MRI, $\omega_s^2\tau_{c2}^2 >> 1$, reducing the electronic contributions to an insignificant amount. The nuclear contribution (the "3" term inside the square brackets) is determined by ω_H^2, the proton Larmor frequency, and τ_{1c}, the local correlation time. The relaxation enhancement efficiency of the CA depends on how closely matched the proton frequency (i.e., the Larmor frequency, ω_H) is to the correlation

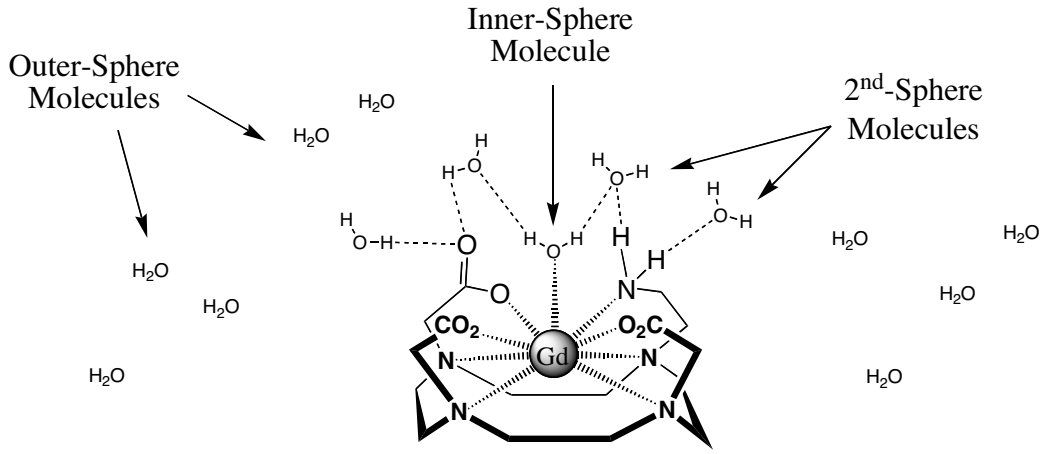

Figure 4. Three coordination spheres, the inner-sphere molecules are directly bound to the metal, the second sphere consists of water molecules coordinated to other parts of the CA while the remaining water molecules comprise in the outer sphere.

frequency of the contrast agent ($1/\tau_{c1}$). The nuclear contributions to relaxation are maximized when $1/\tau_{1e}$ approaches the Larmor frequency of the protons.

The local correlation time (τ_{1e}) has three components, T_{1e} – the electronic relaxation time of the unpaired electrons, τ_m – the water residency lifetime, and τ_R – the rotational correlation lifetime (**Equation 7**). The high-field strengths used in MRI again simplify matters, T_{1e} is long enough to reasonably ignore the contributions from the $1/T_{c1}$ term. τ_m is the same term from **Equation 3**. τ_R is rotational correlation time and is related to physical tumbling time of the CA in solution.

Second- and Outer-sphere Relaxivity

Water molecules not directly coordinated to the metal ion also experience relaxation enhancement in the presence of the CA. These water molecules may be organized into a second- and outer-coordination sphere (**Figure 4)**. Solomon-Bloembergen-Morgan theory may also be applied second-sphere water molecules, thus T_1^{SS} may be modeled from

Equations 3 and **6**. The deviating terms are noted with a prime, e.g., q', r' and $\boldsymbol{\tau}_m'$, to differentiate them from the unvarying terms, w_H and S. Outer-sphere relaxation enhancement may be modeled using theories developed by Hwang and Freeman [40, 41]. T_1^{OS} is estimated using **Equations 9-12**. Essentially T_1^{OS} is determined by T_{1e} (*vide supra*), a – the minimum distance of approach between the metal complex and the outer-sphere water molecules, and D – the sum of the diffusion constants of outer-sphere water molecules and the CA. The remaining terms are N_A - Avogadro's Number and M – concentration of CA.

$$\frac{1}{T_1^{OS}} = C\left[3j(\omega_H) + 7j(\omega_s)\right] \qquad \textbf{[9]}$$

$$C = \left(\frac{32\pi}{405}\right)\gamma_H^2 g^2 \mu_B^2 (S+1)\frac{N_a M}{1000aD} \qquad \textbf{[10]}$$

$$j(\omega_i) = \mathrm{Re}\left[\frac{1+\frac{1}{4}z_i}{1+z_i+\frac{4}{9}z_i^2+\frac{1}{9}z_i^3}\right] \qquad i = H,s \qquad \textbf{[11]}$$

$$z_j = \sqrt{i\omega_j \frac{a^2}{D} + \frac{a^2}{DT_{1e}}} \qquad i \equiv \sqrt{-1},\ j = H,s \qquad \textbf{[12]}$$

Separating the inner-, second- and outer-sphere components of T_1^{CA} is problematic. An approach often used to approximate T_1^{IS} of a CA is to simply deduct the T_1^{CA} of a second, related CA that has $q = 0$. In the case of the second CA, T_1^{IS} is zero (because q = 0) and the observed relaxation enhancement is attributed solely to T_1^{SS} and T_1^{OS}. This provides a reasonable estimate of T_1^{SS} and T_1^{OS} for the first CA because these parameters are not

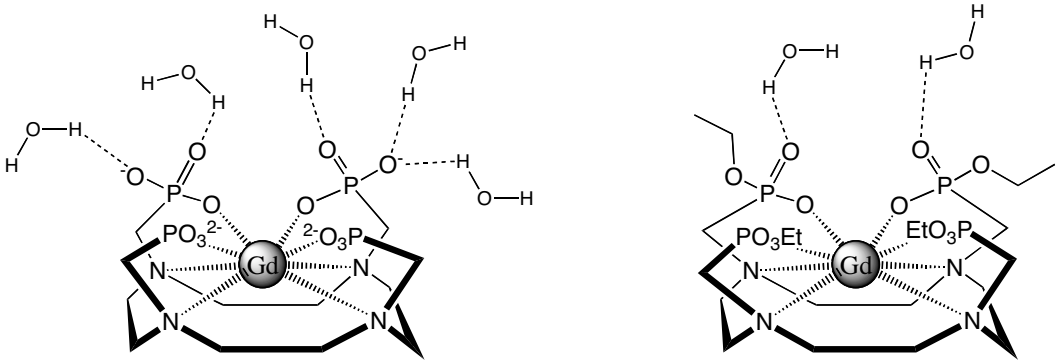

DOTP•Gd DOTPME•Gd

Figure 5. Neither DOTP•Gd nor DOTPME•Gd have any water molecules in the inner-coordination sphere, yet their respective relaxivities are 5.0 $mM^{-1}s^{-1}$ and 2.0 $mM^{-1}s^{-1}$. This disparity is presumably caused by the phosphonate arms of DOTP•Gd that are capable of forming a more extensive second-coordination sphere.

expected differ significantly among structurally related CAs. However there are notable exceptions to this assumption and this approach must be carefully applied (**Figure 5**). Presently, there is no satisfactory experimental method to partition the second- and outer-sphere components of T_1^{CA}

Relaxometric Probes

Relaxometric probes serve as reporters of specific environmental events or conditions by modulating their degree of the relaxation enhancement. This modulation occurs because the environmental event or condition alters one or more of the parameters in **Equations 2-12**. In order to better understand the potential of the different parameters to affect T_1^{CA}, **Equations 2-12** are condensed and presented into **Equation 13**. Two reasonable assumptions

are made in simplifying the equations, [1] $\frac{1}{T_1^{SC}}$ is omitted because $\left(\frac{A}{\hbar}\right)^2 \approx 0$ for water proton-metal interactions in CA's and [2] $\frac{7\tau_{c2}}{\left(1+\omega_s^w \tau_{c2}^2\right)} \approx 0$ because B_0 is sufficiently strong.

$$\frac{1}{T_1^{CA}} = \overbrace{k_{IS}\frac{qM}{\frac{1}{S(S+1)\left(\frac{\tau_{c1}}{1+\omega_H^2\tau_{c1}^2}\right)}+\tau_m}}^{Inner\ Sphere\ Contribution} + \overbrace{k_{SS}\frac{q'M}{\frac{1}{r'^6 S(S+1)\left(\frac{\tau'_{c1}}{1+\omega_H^2\tau'^2_{c1}}\right)}+\tau'_m}}^{Second-Sphere\ Contribution} + \overbrace{k_{OS}\frac{1}{S(S+1)M\left[3j(\omega_H)+7j(\omega_s)\right]}}^{Outer-Sphere\ Contribution} \quad \textbf{[13]}$$

The overriding criterion for the utility of a relaxometric probe is the change in T_1^{CA}, therefore parameters that are unfixed are the most relevant. These parameters are q, q', r, r', τ_{c1}, τ_{c1}', τ_m, τ_m', S and M. The remaining parameters are either physical constants or determined by B_0.

M-based Relaxometric Probes

Recalling that contrast is proportional to $\frac{1}{T_1}$, it is desirable to increase M in response to an environmental trigger because $\frac{1}{T_1^{CA}} \propto M$. Modulation of M is accomplished *in vivo* by designing a CA with a specific affinity for the tissue of interest. In this way, the CA may be administered systemically but accumulates in specific tissues, increasing the local concentration and hence the contrast. Many CAs have utilized antibodies [42-44] and receptor ligands [45-49]

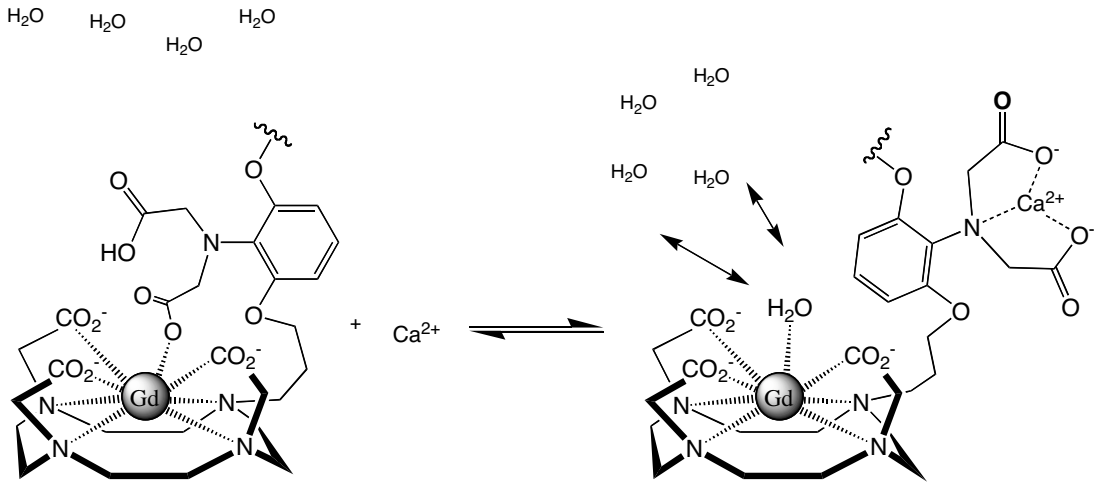

Figure 6. The mechanism for relaxation enhancement in a Ca^{2+} sensitive contrast agent [32]. In the absence of calcium ions, a loosely coordinated carboxylate fills the coordination sphere of the gadolinium ion, preventing water molecules from approaching. The addition of calcium ion removes this blockade.

for this purpose. This method is perhaps the most straightforward, both conceptually and practically, although there some difficulties involved with overcoming the low concentration of antigens and receptors.

q-based Relaxometric Probes

It is desirable to increase q in response to an environmental trigger because $\frac{1}{T_1^{CA}} \propto q$.

Modulating q in a relaxometric probe requires altering the coordination environment of the complex. This has been accomplished via two methods. The first method uses coordinating groups that bind the paramagnetic metal ion in the CA, serving to displace water molecules from the inner coordination sphere. These coordinating groups are only loosely bound and will preferentially bind other metal ions (**Figure 6**). This mechanism has been used in Ca^{2+} and Zn^{2+} sensitive relaxometric probes [32, 33]. The second method for increasing q is the use of a group that is not coordinated to the paramagnetic metal ion, but still serves to exclude water

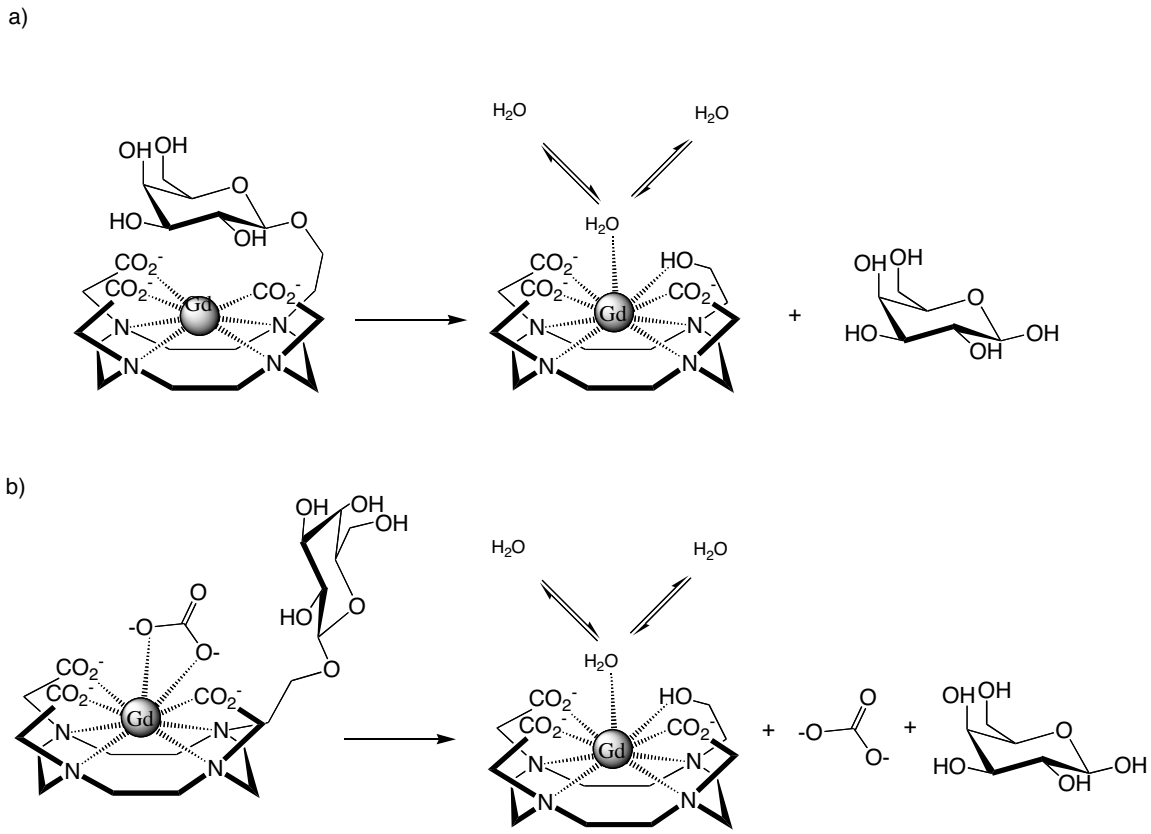

Figure 7. Panel A. The action of β-galactosidase removes the galactosyl residue from the contrast agent, thus allowing water molecules to enter the inner coordination sphere. **Panel B.** Bidentate ligands, such as CO_3^{2-} or PO_4^{3-} present in the solvent may displace the galactosyl moiety and coordinate to the gadolinium. This fills the inner-coordination sphere and prevents water molecules from entering. Enzymatic processing reveals a hydroxyl group, an efficient ligand, which in turn displaces the bidentate ligand, removing the blockade.

molecules by virtue of steric bulk. Two β-galactosidase-sensitive CAs function through this mechanism [35, 36] (**Figure 7A**), although data cannot exclude an alternate mechanism (**Figure 7b**).

τ_{c1}-based Relaxometric Probes (or τ_R-based Relaxometric Probes)

It is desirable to maximize the nuclear dipole-dipole interations, $\left[\frac{3\tau_{c1}}{\left(1+\omega_H^w\tau_{c2}^2\right)}\right]$,

because $\frac{1}{T_1^{CA}} \propto \left[\frac{3\tau_{c1}}{\left(1+\omega_H^w \tau_{c2}^2\right)}\right]^{-1}$ if $T_{1m} >> \tau_m$. The nuclear dipole-dipole interactions are maximized when $\tau_{c1} = \frac{1}{\omega_H}$. τ_{c1} has three components, T_{1e}, τ_m, and τ_R (**Equation 7**), but as previously pointed out, T_{1e} may be sensibly ignored in most μMRI regimes. Accordingly τ_{c1} is approximately equal to the smallest of τ_R and τ_m.

It is generally true in CAs that $\tau_R << \tau_m$ and $\tau_R < \frac{1}{\omega_H}$, consequently the short τ_R is a limiting factor in $\frac{1}{T_1^{CA}}$ and lengthening τ_R is desirable. This has been accomplished dynamically in relaxometric probes through a myriad of methods (**Figure 8**). In one example, an enzyme catalyzed the oligomerization of a relaxometric probe, lengthening τ_R wherever the enzyme was active [37]. In another, the relaxometric probe is processed enzymatically into an effective ligand for a ubiquitous protein, human serum albumin [34]. Different specific receptor-ligand interactions with DNA-transcription factors [29], carbonic anhydrase [28] or oxyhemoglobin [27] are utilized in other relaxometric probes. In the final example, the relaxometric probe undergoes pH-dependant changes to its secondary-structure, altering its τ_R [24].

Although τ_m –based relaxometric probes do exist, the fundamental explanation for their responsiveness in $\frac{1}{T_1^{CA}}$ is not through modulation of τ_{c1} (*vide infra*). They will be described in a separate section below.

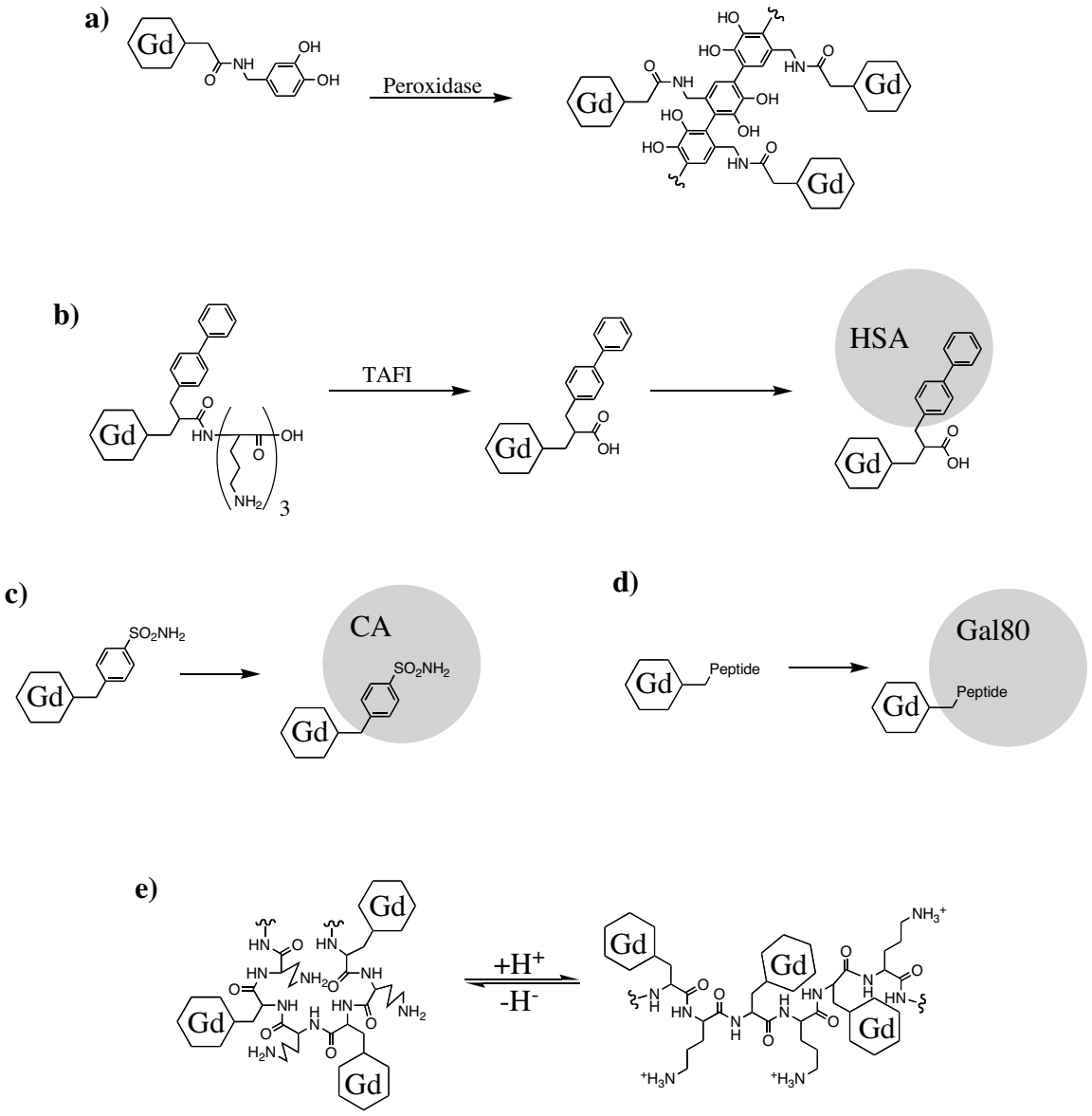

Figure 8. Several representations of τ_R-based relaxometric probes. **Panel A.** Enzyme-catalyzed oligomerization increases molecular weight [37]. **Panel B.** Thrombin-activatable fibrinolysis inhibitor (TAFI) removes polar amino acids, increasing the probe's affinity for human serum albumin [34]. **Panel C.** A pseudo-inhibitor (a sulfonamide-derivatized probe) of carbonic anhydrase (CA) forms a non-covalent adduct with the enzyme [28]. **Panel D.** A peptide-conjugated probe is recognized and bound by Gal80, a yeast DNA transcription factor [29]. **Panel E.** A pH-sensitive relaxometric probes undergoes extensive remodeling of the secondary structure in response to protonation and deprotonation of the lysine side chains. For example, acidifying the pH would increase the rigidity of the structure as the protonated amines began repelling one another [24].

Note: The "Gd"/hexagon symbol represents a gadolinium chelate and the gray circles represent proteins.

τ_m-based Relaxometric Probes

In macromolecular CAs, τ_R is sufficiently long so as not to be a limiting factor in $\frac{1}{T_1^{CA}}$. In this case $\frac{1}{T_1^{CA}}$ is instead limited by τ_m. This limitation is not a function of the local correlation time of the complex, τ_{c1}, rather it is purely a function of the number of water molecules cycling through the inner-coordination sphere. The magnitude of $\frac{1}{T_1^{CA}}$ is limited by the longest term between T_{1m} and τ_m in **Equation 3**. While it is desirable to have $\tau_m << T_{1m}$ so water exchange rates are never a limiting factor, in practice τ_m is extremely difficult control. In any case, the limiting effects of slow water exchange in complexes with very long rotational correlation times has been utilized to make a temperature-sensitive relaxometric probe [31].

S-based Relaxometric Probes

It is desirable to increase *S* in response to an environmental trigger because $\frac{1}{T_1^{CA}} \propto S$ if $T_{1m} >> \tau_m$. A relaxometric probe which incorporates this mechanisn is a pO_2-sensitive relaxometric probe incorporating a redox-sensitive $Mn^{2+/3+}$ ion [26]. It should be noted that in this specific case, the change in *S* is not the primary mechanism for the relaxation enhancement, however this serves to illustrate the potential applications of an S-based relaxometric probe in a redox sensitive contrast agent.

Other mechanisms

A relaxometric probe that functions by modulating *r* has not reported. It is theoretically possible to modulate *r*, the design of such a ligand would be difficult. However even a small change in r, for example 0.2 Å, results in a 30% change in relaxivity because of the r^6-dependence of T_{1m}.

Deliberate modulation of the second- or outer-sphere contributions in a relaxometric probe have only been reported in T_2-contrast agents [50, 51]. There are no reports of a T_1-contrast agent purposely designed to modulate the second and outer spheres.

Finally, there is also an emerging class of CAs have nothing to do with relaxation time. These CAs utilize chemical-exchange saturation transfer (CEST) pulses to reduce the contrast wherever they are present. Instead of enhancing relaxation rates, these contrast agents serve as 'antennas' for saturating RF pulses that 'erase' nearby water protons for a short time from subsequent MR images, resulting in areas that appear darker than the surrounding tissue in MR images. For a detailed description of the mechanism, the reader is referred to the published literature on this subject [52, 53]. Smart CEST agents have been designed that report on temperature and lactate concentration [54, 55].

Practical Aspects

It would be useful to apply real numbers to these equations to obtain an understanding of the contributions of τ_m and τ_R in a typical CA. For this purpose we'll work at a typical magnetic field employed μMRI (B_0 = 11.7 Tesla), at this field ω_H is 500 Mhz. Starting with some prototypical values, τ_R = 50 ps, τ_m = 250 ns, $q = 1$ and $r = 3.1\,\text{Å}$, we have a CA with a

relaxivity of 4.0 $mM^{-1}s^{-1}$. This CA has τ_{c1}= 50 ps, far shorter than the optimal value of 2 ns (ω_H^{-1}, 500 MHz^{-1}).

It is valuable to consider how changes in τ_m and τ_R affect the relaxivity. Since $\tau_R << \omega_H^{-1}$, the relaxivity is not limited by slow water exchange. Consequently, shortening τ_m to 125 ns only increases the relaxivity to 4.1 $mM^{-1}s^{-1}$, a minimal improvement of .1 $mM^{-1}s^{-1}$. Lengthening τ_R to 100 ps has a more pronounced effect; the relaxivity increases to 7.6 $mM^{-1}s^{-1}$. In general for small molecule contrast agents, τ_R is the primary determinate of relaxivity and τ_m has very little effect. Only a relatively small number of polyamide derivatives of DOTA and DTPA have τ_m's long enough to adversely affect the relaxivity of small molecule contrast agents with short τ_R's.

Linking this CA to a large protein such as albumin will typically lengthen τ_R to ~2000. Under these conditions, τ_{c1} is 1.9 ns – very close to being optimal – and the "theoretical" relaxivity, T_{1m}, is 84 $mM^{-1}s^{-1}$. Unfortunately if τ_m remains unchanged at 250 ns, the actual relaxivity is only 40 $mM^{-1}s^{-1}$ because it is now limited by the long water exchange time. Shortening τ_m to 50 ns ameliorates this limitation and increases the relaxivity to 68 $mM^{-1}s^{-1}$.

Designing an apoptosis-sensitive relaxometric probe

A relaxometric probe will be synthesized and evaluated in an effort to detect apoptosis *in vivo*. A *q*-based relaxometric probe was chosen because of extensive experience with the design and synthesis of such molecules [32, 35, 36]. In a scheme analogous to prior relaxometric probes synthesized in this lab, a suitable effector moiety will be attached to DO3A. The effector moiety would serve to exclude water molecules from inner-coordination sphere and lower the relaxivity. Theoretically, the removal of the effector moiety is

accomplished by the specific action of an enzyme, restoring the relaxivity of the contrast agent and producing a detectable signal in the MR image.

The first step was choosing the enzymatic target. The criteria for the enzyme are straightforward, (1) the enzyme must be capable of hydrolyzing a bond and (2) it should specific to apoptosis. Caspases were immediately identified as the preferred enzymatic target because their activation is the defining biochemical event associated with apoptosis. Furthermore, caspases have many aspects that make them an ideal enzyme to target. They are activated fairly early in the apoptotic cell [56], allowing a longer period for the enzymatic processing to occur which can be quite prolonged in relaxometric probes. Caspases also have a relatively short 4 amino-acid consensus sequence and are exo-peptidases rather than endo-peptidases [57] facilitating the design of the linker between the CA and effector moiety. Finally, caspases are rather promiscuous enzymes, they can efficiently process a diversity of single amino-acid substrates including L-Asp, L-Arg, L-Glu and even D-Asp [58]. This also served as a preliminary indication the enzyme would recognize and process the relaxometric probe being designed.

Initially the entire consensus sequence for caspase-3 was considered for incorporation into the relaxometric probe, however when it was discovered that a single aspartate is also an efficient substrate, the tetra-peptide was dropped in favor of the single amino acid as the effector moiety. The single aspartate is sufficient bulky to block water molecules from entering the inner-coordination sphere. Furthermore, the carboxylate side chain and N-terminal amine might coordinate to the metal ion, saturating the inner coordination sphere instead just

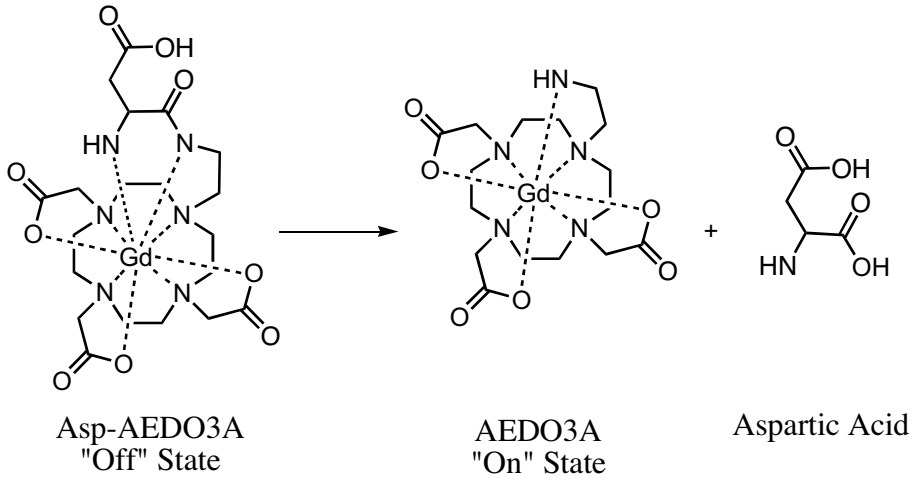

Figure 9. Proposal for an apoptosis-sensitive relaxometric probe. The Asp-AEDO3A, the "Off" state, would be processed by caspase to liberate AEDO3A, the "On" state.

blocking water molecules. When the bond between the amino acid and the CA is cleaved, these inhibitory effects will be removed, restoring the relaxivity.

After the molecular target was chosen, a survey of known CAs was conducted in order to find one that would serve as suitable building block. Although there are many examples of CAs linked to peptides or amino acids, this linkage is usually either (1) accomplished by recruiting a carboxyl group on the ligand to couple to an amine on the peptide [59] or (2) through a amine group on the ligand located distal to the apical coordination site [60, 61]. A promising candidate was the ligand 1-(2-aminoethyl)-4,7,10-tri(carboxymethyl)-cyclen (AEDO3A). **Figure 9** illustrates how AEDO3A would be incorporated into a relaxometric probe.

AEDO3A was chosen because it contains a pendant amine, allowing the attachment of the effector moiety – the single aspartate – through an amide bond. This amide bond could be cleaved by a caspase to liberate AEDO3A [62]. Secondly, the length and geometry of the

pendant amine are likely to place it adjacent to the apical coordination site, maximizing the likelihood that the effector moiety will be able to efficiently displace water molecules from the inner-coordination sphere. However, the application of AEDO3A as a CA ligand has not been reported, therefore the synthesis of the gadolinium and terbium chelates had to be undertaken to before AEDO3A could confidently be included as a component of the apoptosis-sensitive relaxometric probe.

Chapter 3

ESTIMATION AND REDUCTION OF ERRORS IN RELAXIVITY

The ordinary linear fit of $1/T_1$ vs. concentration has traditionally been used to estimate the relaxivity of CAs. However, the ordinary linear fit is not well suited to handling $1/T_i$ data, errors are neither weighed nor propagated properly. Consequently, errors in the T_1 data do not 'average' out and its use should be avoided. Two novel methods of estimating relaxivity are evaluated as alternatives. The first method is a weighted least-squares fit directly to the T_1 data. The second method is a distribution-free (or non-parametric) method. A Monte Carlo simulation used to evaluate the accuracy and precision of each method. Both the direct fit and distribution-free methods proved more precise than the ordinary linear fit. These novel methods will prove in reducing uncertainty in relaxivity estimate.

Introduction

The relaxivity change that occurs during the relevant physiological event is a major criterion for the utility of any relaxometric probe. Tissue contrast modeling suggests that changes as small as 0.9 $mM^{-1}s^{-1}$ in the relaxivity of CAs may reasonably be detectable in T_1-weighted images [63]. Thus, the precision of the estimates is an important concern when evaluating the utility of relaxometric probes. Unfortunately relaxivity estimates can be elusive; for example the relaxivity of a well-known CA, DOTA, has been independently reported to be anywhere between 3.5 $mM^{-1}s^{-1}$ [64] and 4.8 $mM^{-1}s^{-1}$ [65] – a range of 1.3 $mM^{-1}s^{-1}$ which is larger than the smallest-detectable relaxivity change in a relaxometric probe system. On the surface, this uncertainty in the estimation of relaxivity appears to make *in vitro* evaluation of relaxometric probes untenable. Fortunately a substantial portion of this variability is accounted

for by differences in experimental conditions such as temperature, buffer or field strength. When measuring relaxivity changes in relaxometric probes, these factors are kept constant and a comparison between the different relaxivities may more confidently be made.

In order to estimate relaxivity, relaxation times of solutions with differing concentrations of CA are measured. Relaxivity is defined as the concentration dependence of $1/T_1$. The simple linear relationship between $1/T_1$ and concentration appears to make the estimation of r_1 a trivial calculation of the least-squares 'best' fit line. This is not the case. The ordinary linear least-squares fit does not properly propagate nor weigh the errors in the data. A simple non-technical explanation of these points follows. For a more thorough discussion of these points, the reader is directed to the published literature on these topics [66].

Formal error propagation is necessary when taking the reciprocal distorts errors in T_1 data (i.e., it is a nonlinear transformation). Taking the reciprocal of T_1 increases errors in one direction and decreases them in the other. This becomes readily apparent in an extreme example such as 1 s ± 0.5 s, the range of possible values is 0.5 s - 1.5 s. Taking the reciprocal results in $1 s^{-1}$ with a possible range of 2 s^{-1} - 0.66 s^{-1}. The error after the reciprocal transformation is clearly no longer Gaussian, this violates a basic assumption of the linear least-squares fit. Proper weighing of errors is also important. Most experimental techniques to estimate T_1 give constant relative errors (i.e., ± 3%) rather than constant absolute error (i.e., ± 5 ms). After the reciprocal transformation, this inadvertently results in points with lower T_1 values (e.g., higher concentrations) being weighed more heavily when estimating the r_1.

This mishandling of errors is a minor, but significant, violation of the assumptions made in a simple linear fit. Consequently, the simple linear least-squares fit only provides a

reasonable estimate of r_1 not the *best* estimate. Although it is certainly possible to derive the appropriate corrections to enable the use of a linear fit, it is more expeditious to use a simplex algorithm to find an r_1 that most closely matches the observed T_1 data. Furthermore, a non-parametric method to estimate r_1 is proposed and evaluated.

Methods

Linear fit

The linear fit is the traditional method of calculating relaxivities. It is simply the slope of the best-fit line of $1/T_{1,i}$ versus $[M_i]$. This is calculated using the Linest() function in Microsoft Excel (Redmond, WA). The *Y*-intercept was not fixed and calculated by the algorithm.

Direct fit

The direct fit uses a simplex algorithm that iteratively calculates an r_1 that minimizes the weighted sum-of-squared deviations in T_1 (**Equation 14**).

$$\sum_{i=1}^{N}\left(T_{1,i}-\hat{T}_{1,i}\right)^2\omega \qquad \textbf{[14]}$$

The weight (ω) is $1/\hat{T}_{1,i}^{\,2}$ and corrects for the difference in the magnitude of the variation at different T_1's. The value $\hat{T}_{1,i}$ is calculated (**Equation 15**) using the empirically determined T_1 of the buffer system as T'_{01}.

$$\hat{T}_{1,i}=\left(\frac{1}{T'_{01}}-r_{1,i}[M_i]\right)^{-1} \qquad \textbf{[15]}$$

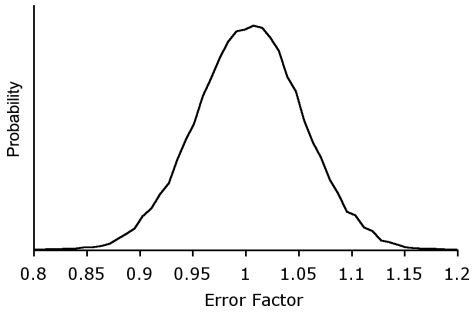

Figure 10. Distribution of the errors factors used in the Monte Carlo simulations. N=25,000

This model was constructed using Excel and solved using a simplex algorithm accessed via the Solver plug-in. A sample spreadsheet of this model is included in the Appendix.

Distribution-free method

The distribution-free method calculates $r_{1,ij}$ (**Equation 16**) for all possible pairs of T_1's in the data set and returns the median (*not* the average) value. There are (N)*(N-1)/2 unique pairs in a data set consisting of N samples. For example, in a data set consisting of three CA concentrations $\{(T_{1,a},[M_a]), (T_{1,b},[M_b]), (T_{1,c},[M_c])\}$ and one blank measurement $\{(T_{01,d},[0.0])\}$, there are six unique pairs of data. (i.e., A-B, A-C, A-D, B-C, B-D, C-D). The relaxivity for each unique pair is calculated and median value is considered the relaxivity of the CA. A sample spreadsheet of this model is included in the Appendix.

$$r_{1,ij} = \frac{\frac{1}{T_{1,i}} - \frac{1}{T_{1,j}}}{[M_i] - [M_j]} \qquad \textbf{[16]}$$

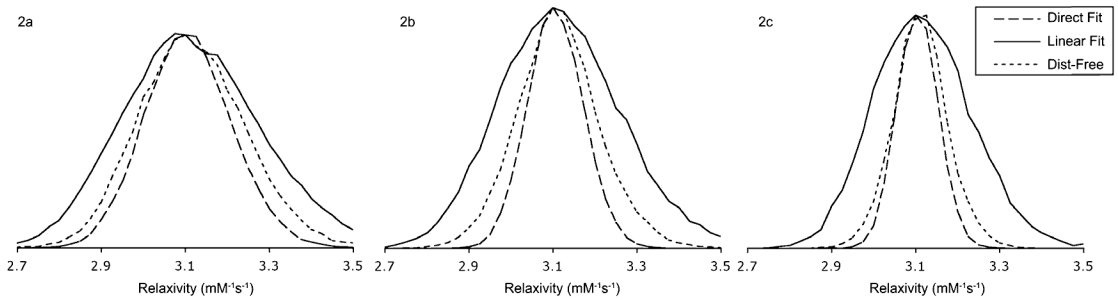

Figure 11. Distribution of relaxivity estimates produced by the direct fit (solid line), distribution-free method (short dashes) and the ordinary linear fit (long dashes) for data sets consisting of 3, 6 or 12 concentrations (**Panels A**, **B** and **C**, respectively). These curves assume 5% error in the underlying T_1 data.

Monte Carlo Simulations

The Monte Carlo simulation was performed using Excel. Theoretical T_1 values were calculated from Equation 3 (r_1 = 3.1 $mM^{-1}s^{-1}$, T_{01} = 2.0 s) at several concentrations of CA. An 'observed' T_1 was calculated by introducing stochastic error into the theoretical T_1. The error was randomly generated for each individual data point and was normally distributed (**Figure 10**) with a fixed mean and standard deviation. The relaxivities were then estimated using the linear fit, direct fit and the distribution-free methods.

The simulations were performed under a variety of error conditions (SD= 2.5%, 5%, 10%) and data set sizes (N=2-7).

Results

The results of simulated relaxivity estimates were analyzed to ascertain their accuracy and precision (**Figure 11**). For example, if one uses 6 data points and assumes 5% error in the underlying T_1 data, then the error in the relaxivity estimate will be approximately ± 4.6% using the direct fit or ± 9.5% using the linear fit. Although the difference in accuracies (data not

shown) between the methods is statistically significant because of the large sample sizes used in the simulations, the magnitude of the differences, less than 0.5%, is not relevant to most discussions of CA relaxivity. Hence when judged solely on the basis of accuracy, all methods performed equally well.

However, the precision of relaxivity estimates differed by a noteworthy amount. As expected, the direct fit returned the most precise estimates while the linear fit performed the worst. Indeed, using linear fit is not much better than simply estimating relaxivity solely from most concentrated sample – regardless of the actual number of concentrations used in the fit. This is expected from the incorrect weighing of the individual data points and is borne out in the Monte Carlo simulations.

The direct fit estimates were the most precise of the three methods evaluated. Directly comparing T_1 and $\hat{T}_1$, as opposed to $1/T_1$ and $1/\hat{T}_1$ in the linear fit, avoids the confounding reciprocal transformation required in the linear least-squares estimation. Furthermore, the variation at each $[M_i]$ is weighed for more accurate treatment of error. Consequently, the precision of the direct fit method increases with increasing number of data points used. As one would expect, this decrease in variation is roughly proportional to the square root of the number of data points used.

In contrast to the direct fit method that assumes a normal distribution of error and a constant proportional variance, the distribution free method uses a much simpler assumption – positive errors are as likely as negative errors. The detriment to this method is that it produces a weaker conclusion (more uncertainty) because it relies upon weaker assumptions. In the event that the classical assumptions are true, a parametric method such as the direct fit

will always produce results that are more precise. However, a non-parametric analysis such as the distribution free method will provide better estimates, in general, than a poorly chosen parametric analysis, as is the case with estimating relaxivity with the linear fit.

Goodness of fit is best assessed visually (**Figure 12**). The reciprocal plot of T_1 can be misleading because it visually distorts the magnitude of the error in all the data points and gives misleading information to the viewer about the goodness of fit. Neither is the direct plot ideal either for the visual inspection of the goodness of fit. A plot of the weighted residuals $[1-(\hat{T}_{1,i}/T_{1,i})]$ is the most useful visual indicator of goodness of fit. It is vital to consider that the data in Fig. (2) contains a reasonable amount of error (5%) and the Linear Fit *appears* optimal, yet the error in the resulting relaxivity estimate is 8.4%. This

N	*Direct Fit*	*Linear Fit*	*Distribution Free*
	2.5% Error		
2	1.71%	2.55%	2.55%
3	1.64%	2.61%	1.94%
4	1.42%	2.68%	1.84%
5	1.32%	2.48%	1.84%
6	1.10%	2.32%	1.68%
8	3.77%	8.36%	6.04%
10	0.77%	1.91%	1.33%
12	0.72%	1.75%	1.19%
	5% Error		
2	3.65%	4.94%	4.94%
3	3.42%	5.45%	4.06%
4	2.87%	5.10%	3.52%
5	2.52%	4.90%	3.58%
6	2.29%	4.77%	3.29%
8	1.89%	4.25%	2.98%
10	1.62%	3.92%	2.73%
12	1.40%	3.46%	2.29%
	10% Error		
2	7.39%	10.45%	10.45%
3	6.52%	10.65%	7.84%
4	5.87%	11.06%	7.58%
5	4.90%	10.35%	7.23%
6	4.39%	9.26%	6.39%
8	3.77%	8.36%	6.04%
10	3.25%	8.22%	5.57%
12	2.72%	7.30%	4.75%

Table 1. The standard deviations of the various simulated relaxivity estimates are presented. Each line in the table presents standard deviations (expressed as a percentage) of relaxivity estimates generated by the three methods using 2000 sets of T_1 data with the stated error and number of data points (not including the blank). These values are useful for approximating the error in individual relaxivity estimates because 95% of the time the 'true' relaxivity will be ± 2 standard deviations away.

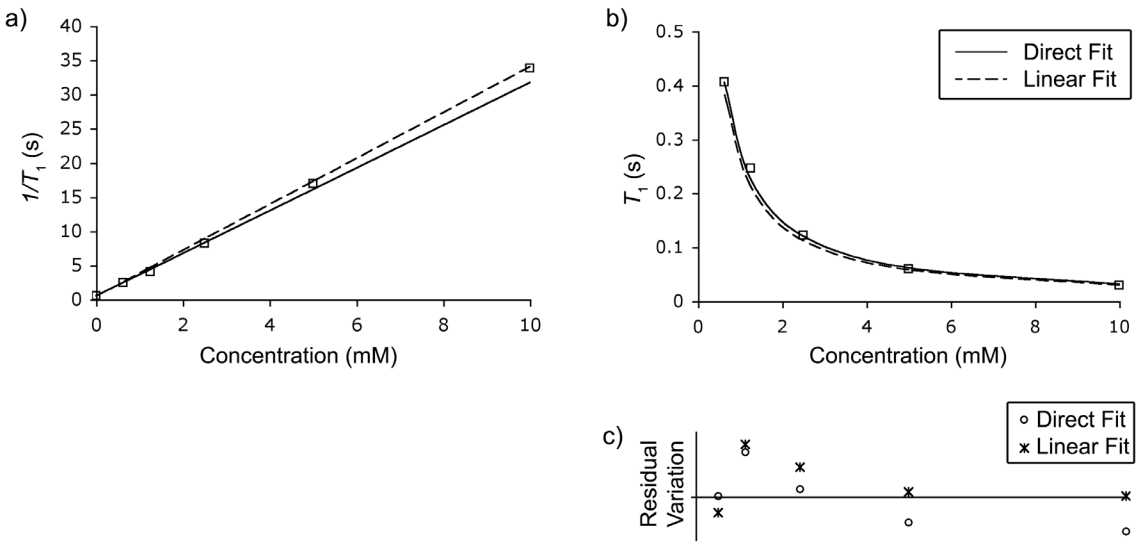

Figure 12. Panels 2a and 2b present reciprocal and direct plots of the following T_1 data ($[M_i]$, $T_{1,i}$) = [(0 mM, 1.93 s), (0.63 mM. 405 ms), (1.25 mM, 246 ms), (2.5 mM, 122 ms), (5 mM, 59.1 ms), (10 mM, 29.6 ms)] with superimposed Direct and Linear Fits using T_{01} of 1.93 s. This T_1 data was generated from a 'true' r_1 of 3.1 $mM^{-1}s^{-1}$ with a random error (ε_i) = (0.932, 0.946, 1.000, 1.078, 0.988, 0.969). **Panel a**. The Linear Fit (dashed line) appears to fit the data quite well, while the Direct Fit (solid line) seems to miss the 5mM and 10mM points. **Panel b**. The direct plot is not better for judging the goodness-of-fit. The difference between the two fits appears minor. **Panel c**. The plot of the weighted residuals is the most useful visual indicator of goodness of fit. The residuals from the direct fit appear centered on the X-axis while residuals from the linear fit lie mostly above the X-axis. Although visually the differences appear minor, the calculated relaxivities from the Linear and Direct Fits are 3.36 $mM^{-1}s^{-1}$ and 3.12 $mM^{-1}s^{-1}$ respectively. For comparisons sake, the Distribution Free method estimated a relaxivity of 3.31 $mM^{-1}s^{-1}$.

highlights the uncertainty present in relaxivity estimates regardless of the visual appearance of the plotted data.

Discussion

The errors associated with estimating relaxivities are numerous and the statistical model used should reduce these errors. The ubiquity of Excel and other spreadsheets make the calculation of the direct fit and distribution free methods only slightly more laborious than the

linear fit. The use of the linear fit should be avoided and either the direct fit or distribution free method substituted in its place. The direct method provides the most precise estimates of relaxivity, however like all parametric methods it is sensitive to outliers. Because visually detecting outliers or assessing the goodness of fit is difficult, unless residuals plots are inspected the distribution free method should be employed. This method handles errors, including outliers, in a robust manner yet still produces more precise estimates than the linear fit. The uncertainty reported in relaxivity should reflect the number of concentrations used in the determination and allow statistically significant conclusions to be made.

Chapter 4

AEDO3A – A USEFUL BUILDING BLOCK FOR A RELAXOMETRIC PROBE

1-(2-Aminoethyl)-4,7,10-tri(carboxymethyl)-cyclen (AEDO3A) is evaluated as a component of a relaxometric probe system. The synthesis and characterization of the ligand and its Gd and Tb complexes is described. The gadolinium complex has relaxivities of 2.2 $mM^{-1}s^{-1}$ and 2.4 $mM^{-1}s^{-1}$ at 60Mhz and 500MHz respectively. Fluorescence lifetime data of the terbium complex indicate the presence of 0.9 water molecules in the inner coordination sphere. X-ray crystallography data are presented for both the ligand and gadolinium complex. Assuming reasonable relaxivities for the "off" state, tissue contrast modeling of the smallest-detectable relaxivity change suggests AEDO3A is suitable for incorporation into relaxometric probe the desired relaxometric probe.

Synthesis

Attempts to synthesize this agent using the literature procedure produced unsatisfactory yields in this laboratory. Consequently, a new synthetic route (**Scheme 1**) was developed that required neither silica-gel chromatography nor HPLC to purify intermediates.

AEDO3A was synthesized in four steps starting from 2-bromoethylamine. The 2-bromoethylamine was acylated with BOC-anhydride to yield the BOC-protected derivative (1) that was then reacted with a 5-fold excess of cyclen to promote monoalkyation. Compound **2** was exhaustively alkylated with t-butyl bromoacetate to yield the fully protected ligand **3**. Deprotection using TFA yielded the final ligand **4**. The final complexes, **5a** and **5b**, were formed from the correct lanthanide chlorides under slightly acidic conditions, pH 6-7. The

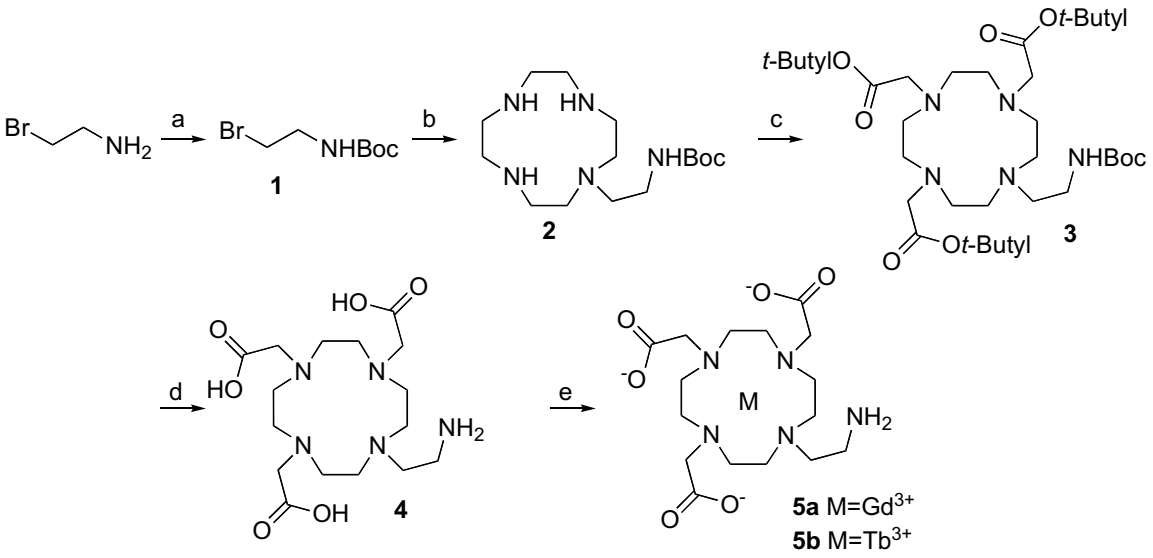

Scheme 1: Synthetic Scheme for AEDO3A. a) BOC-anhydride, NaOH, DCM/H_2O, yield 70%; b) cyclen, MePh, yield 56%; c) t-Butyl bromoacetate, Na_2CO_3, yield 85%; d) TFA, Triisopropylsilane, yield 45%; e) MCl_3, LiOH, pH 6-7, H_2O, yield 50%

final complexes were purified by precipitation followed by column chromatography (Biorad Chelex) and dialysis to remove any trace heavy metals.

All reagents and solvents were purchased from Aldrich, Fluka, or Strem (cyclen) and were used without further purification. Ion exchange resins purchased from Bio-Rad.

N-Boc-2-aminoethyl bromide (1). A 1N solution of sodium hydroxide (160 ml) was added dropwise over 15 minutes to a vigorously stirring biphasic system of bromoethylamine hydrobromide (17.85 g, 87.1 mmol) in water (100 ml) and di-t-butyl pyrocarbonate (9.5 g, 43.5 mmol) in dichloromethane (100 ml). After 2 hours, the layers were separated and the organic layer was washed with 1H HCl (25 ml) twice and a saturated sodium chloride (25 ml) once. The organic layer was then dried over sodium sulfate and concentrated *in vacuo* to a colorless oil. The oil was dissolved in hexanes (10ml) and placed at –80° C overnight. 1.9 grams of a

white solid that crystallized was filtered and washed with cold hexanes. The combined filtrates were again placed at –80°C for 1 hour to precipitate a second batch of crystals weighing 4.9 grams. Total yield, 6.8 grams (30.3 mmol or 70% yield). ^{13}C NMR ($CDCl_3$, 300 MHz) δ 155.6, 79.8, 42.3, 32.8, 28.3. ^{1}H NMR ($CDCl_3$, 300 MHz) 5.03 (s, 1H), 3.53 (t, 2H), 3.46 (t, 2H), 1.46 (s, 9H). HR-CI+GC, m/z 224.0286 (M+H) theoretical 224.0286.

(N-Boc-2-aminoethyl)-cyclen (2). A solution of **1** (10.3 g, 45 mmol) and cyclen (30.96 g, 180 mmol) in toluene (400 ml) was stirred at 70°C overnight. The following day, the product was extracted from the reaction mixture using water (100 ml, 4x). The combined aqueous layers were washed with toluene (50 ml) followed by dichloromethane (100 ml, 4x). The dichloromethane layers were combined, dried over sodium sulfate and then concentrated *in vacuo* to a colorless oil. The oil was dissolved in dichloromethane (15 ml), diethyl ether was added until the solution was cloudy and placed at -80°C overnight. The white solid that precipitated was filtered and washed with cold ether. Total yield, 7.5 grams (24 mmol, 56% yield). ^{13}C NMR ($CDCl_3$, 300 MHz) δ 155.99, 81.73, 80.43, 50.66, 41.17, 37.17, 31.67, 28.32, 28.04. ^{1}H NMR ($CDCl_3$, 300 MHz) 5.65 (s, 1H), 3.21 (q, 2H), 2.72-2.48 (m, 21H), 1.44 (s, 9H). HR-FAB, m/z 316.2728 (M+H) theoretical 316.2712.

(N-Boc-2-aminoethyl)-4,7,10-tri(t-butoxycarbonylmethyl)-cyclen (3). A solution of **2** (950 mg, 3 mmol), sodium carbonate (3.3 g, 31 mmol) and t–butyl bromoacetate (2.4 ml, 15 mmol) in acetonitrile (100 ml) was stirred at 70°C overnight. The following day, the reaction was filtered and washed with heptane (250 ml, 3x). The acetonitrile layer was then concentrated in vacuo to a pale yellow oil. The oil was dissolved in dichloromethane (15 ml), heptane was added until the solution was cloudy and placed at –80°C overnight. The white

solid that precipitated was filtered and washed with heptane. Total yield, 1.68 grams (2.5 mmol, 85% yield). ^{13}C NMR ($CDCl_3$, 300 MHz) δ 173.36, 172.84, 172.58, 156.42, 82.80, 81.42, 81.94, 79.20, 56.51, 55.69, 53.95, 50.34 (m), 37.84, 28.41, 28.01, 27.82. ^{1}H NMR ($CDCl_3$, 300 MHz) 5.43 (s, 1H), 3.4 - 2.2 (m, 26H), 1.6-1.4 (m, 36H). HR-FAB, m/z 658.4750 (M+H) theoretical 658.4754.

1-Aminoethyl-4,7,10-tri(carboxymethyl)-cyclen (4). A solution of **3** (1.6 grams, 2.5 mmol) in triisopropyl silane (500 μl) and trifluoroacetic acid (50 ml) was stirred overnight at room temperature. The following day the solution had turned orange and the solvent was removed in vacuo until less than 1 ml remained. The remained solution was added dropwise to cold diethyl ether. The pale orange solid that formed immediately was filtered, and then resuspended in a minimal amount of water (~3 ml). The final product was titurated and filtered off by the addition of a large excess of acetone (~100 ml). Total yield, 420 mg (1.1 mmol, 45% yield). ^{13}C NMR (D_2O, 500 MHz) δ 175.70, 170.50, 57.31, 52.69, 52.27, 50.60, 50.30, 48.39, 48.17, 36.29. ^{1}H NMR (D_2O, 500 MHz) 3.8-2.6 (m). HR-FAB, m/z 390.2355 (M+H) theoretical 390.2352.

1-(Aminoethyl)-4,7,10-tri(carboxymethyl)-cyclen, gadolinium salt (5a). A solution of **4** (289 mg, 743 μmols) and gadolium chloride (235 mg, 891 μmols) was stirred at 80° C overnight. The pH was periodically checked and adjusted to 6.0~7.0 using a solution of lithium hydroxide (1M) as needed. After 12 hours, lithium hydroxide was added to bring the pH to ~12 and reaction was syringed through a nylon .2 μm filter. The filtrate was then lypohilized to a white powder that was resuspended in a minimal amount of methanol (~1 ml). The final product was titurated from this solution and filtered off by the addition of a large excess of acetone (~40 ml). This solution was purified over an ion-exchange resion (Bio-Rad

Chelex), dialyzed (100 MWCO) and lyophilized to an off-white powder. Total yield, 242 mg (446 μmols, 50% yield). HR-FAB, m/z 545.1361 (M+H) theoretical 545.1358.

1-(Aminoethyl)-4,7,10-tri(carboxymethyl)-cyclen, terbium salt (5b). This compound was made in a fashion similar to **5a**. Total yield, 325 mg (596 μmols, 80% yield). HR-FAB, m/z 546.1384 (M+H) theoretical 546.1376.

Characterization

The number of water molecules in the inner-coordination sphere (*q*) was indirectly determined by measuring the fluorescent lifetimes of **5b** in H_2O and D_2O (**Figure 13**). The O-H oscillators present on the coordinated water molecule are efficient quenchers of the excited state of **5b**. However O-D oscillators are largely ineffective at quenching fluorescence, therefore it is possible to indirectly determine the number of water molecules in both coordination spheres by measuring the fluorescence lifetimes in D_2O vs. H_2O [67]. Nearby water molecules in the outer coordination sphere also quench the excited state, albeit to a lesser extent because of their relative distance from the metal center. This relationship between the fluorescent lifetimes is modeled in **Equation 17** [68, 69].

$$q = 5\left(k_{H_2O} - k_{D_2O} - 0.06\right) \qquad \textbf{[17]}$$

When the published correction factors for the presence of inner-sphere N-H oscillators were incorporated into **Equation 17**, *q* was 0, which is unreasonable considering the crystallographic evidence to the contrary. The uncorrected lifetime data was used instead, indicating $q = 0.6$. The estimated error of this method is approximately ±0.5. Non-integral

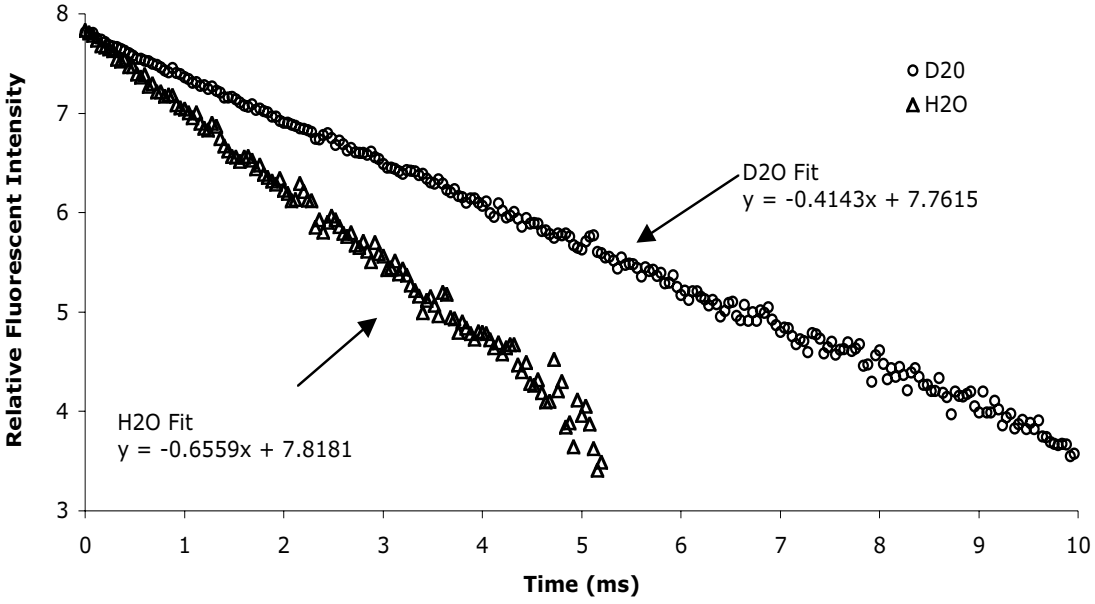

Figure 13: Fluorescent Lifetime Data of AEDO3A-Tb.

results are also indicative of the equilibrium distribution of the complex where there is one or no water molecules bound.

The spin-lattice relaxation times (T_1) of the bulk water were measured in order to estimate the relaxivity (r_1) of **5a**. The relationship between T_1 and r_1 is given in **Equation 18**, where T_1^{OBS} is the half-life of the inversion recovery process. r_1 was estimated by the use of a simplex algorithm.

$$\frac{1}{T_1^{OBS}} = \frac{1}{T_{01}} + r_1[M] \qquad \textbf{[18]}$$

Because relaxivities varies with field strength (**Table 2**), measurements were made at several common field strengths used in both MRI and μMRI applications. The buffer system with phosphate and carbonate anions most closely resembles *in vivo* conditions, while the

Field Strength (MHz)	Relaxivity ($mM^{-1}s^{-1}$)	
	Buffer A	Buffer B
60	2.2	2.6
300	2.6	4.0
500	2.4	4.0
600	2.4	3.1
Composition of buffer	10 mM MOPS 100 mM NaCl 4 mM Na_2CO_3 20 mM Na_3PO_4	10 mM MOPS 100 mM NaCl

Table 2: Relaxivity of 5a. All relaxivities taken at 25° C and pH 7.2, except for the 60MHz data taken at 37° C.

second facilitates comparison with relaxivities of other CAs that were measured in phosphate- and carbonate-free buffer systems [70, 71]. These numbers are typical of a small-molecule CA with a single coordinated water molecule [72].

Using a model for MRI contrast enhancement for T_1 agents it is possible to evaluate the utility of **5a** as the "on" component of a relaxometric probe [63]. Using the r_1 data obtained for **5a**, the relaxivities for the "off" state that will lead to an acceptable signal-to-noise at an intracellular concentration of 1mM were estimated to be 1.6 $mM^{-1}s^{-1}$, 1.9 $mM^{-1}s^{-1}$, 2.2 $mM^{-1}s^{-1}$ or 1.8 $mM^{-1}s^{-1}$ at 60MHz, 300MHz, 500MHz and 600MHz, respectively. These relaxivities represent the smallest-detectable relaxivity change in the *Xenopus* (African horned frog) embryo. Given the relaxivities of other "off" contrast agents [35, 36] and some $q = 0$ complexes [72], it seems reasonable to achieve the desired relaxivity of the "off" component of the relaxometric probe.

Single crystals of **4** and **5a** were obtained by the slow diffusion of acetone into aqueous solutions of the compounds. X-ray crystallography confirmed the structures (**Figure 14**). Compound **5a** crystallized with two conformational isomers (labeled A and B) in the asymmetric unit. The two isomers differed mainly because of an inversion of the ethylene

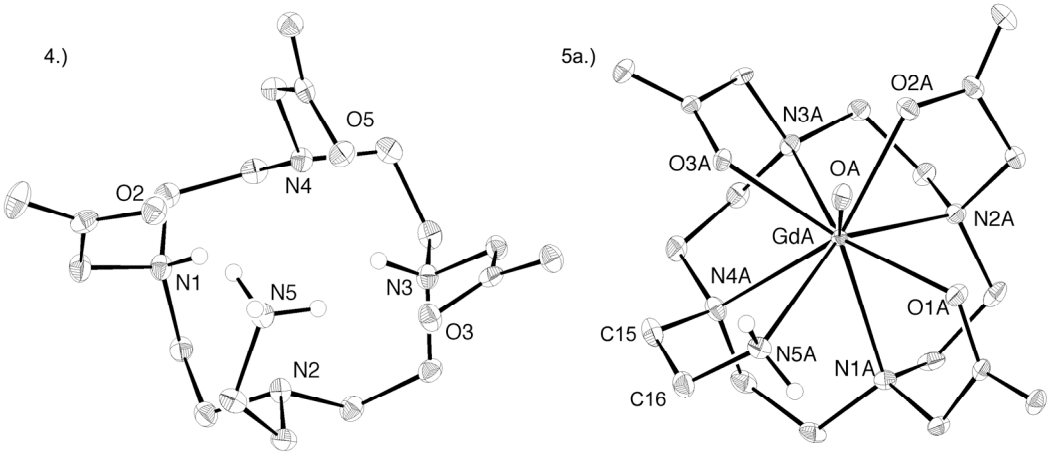

Figure 14. Displacement ellipsoid plots of 4 and 5a with 50% surfaces. Selected bond lengths from 5a: Gd-N5A = 2.597(2) Å, Gd-N5B = 2.560 Å, Gd-N(1-4)(A-B) = 2.637(2) – 2.714(2) Å, Gd-OA 2.471(2) Å, Gd-OB 2.508 Å, Gd-O(1-3)(A-B) = 2.3284(17) – 2.3660(19) Å.

linker to the pendant amine. The torsion angle GdA-N4A-C15A-C16A was 53.8° while GdB-N5B-C15B-C16B was 12.3°. The coordinated atoms are arranged in a monocapped twisted square antiprism, with N1A, N2A, N3A and N4A composing one plane (rms deviation = 0.0170 Å) 1.638 Å below GdA while N5A, O1A, O2A, O3A and N5A line on the second plane (rms deviation = 0.0352 Å) 0.762 Å above GdA. The planes are twisted approximately 37° relative to each other.

Discussion

We succeeded in the synthesis and characterization of gadolinium and terbium complexes of AEDO3A. The relaxation and fluorescent lifetime indicate a potential for the inclusion of AE-DO3A-Gd into a relaxometric probes. The cystallographic data indicate the pendant amine is coordinated to the metal center, a favorable position to serve as an anchor for an effector moiety expected to modulate the inner coordination sphere.

Chapter 5

ASP-DO3A – ATTEMPT AT AN APOPTOSIS-SENSITIVE RELAXOMETRIC PROBE

1-(2-Aspartryl-aminoethyl)-4,7,10-tri(carboxymethyl)-cyclen (Asp-AEDO3A) is evaluated as the second component of an apoptosis-sensitive relaxometric probe system. The synthesis and characterization of the ligand and its Gd and Tb complexes is described. Fluorescence lifetime data of the terbium complex indicate the presence of 0.6 water molecules in the inner coordination sphere. The gadolinium complex has a relaxivity of 1.4 $mM^{-1}s^{-1}$ and 1.7 $mM^{-1}s^{-1}$ at 60Mhz and 500MHz, respectively. Toxicity studies demonstrated *Xenopus* embryos tolerated Asp-AEDO3A•Gd at magnetically useful concentrations as predicted by tissue contrast modeling. X-ray crystallography data are presented for both the ligand and gadolinium complex.

Synthesis

Asp-AEDO3A was synthesized in a manner nearly identical to AEDO3A. All reagents and solvents were purchased from Aldrich, Fluka, or Strem (cyclen) and were used without further purification. Ion exchange resins purchased from Bio-Rad.

Boc-Asp(Ot-Bu)-ethylbromide (6). A 1N solution of sodium hydroxide (65 ml) was added dropwise over 15 minutes to a vigorously stirring biphasic system of bromoethylamine hydrobromide (6.41 g, 32 mmol) in water (50 ml) and N-(Boc-Aspartyloxy)-succinimide t-butyl ester (6.05 g, 16 mmol) in dichloromethane (50 ml). After 2 hours, the layers were separated and the organic layer was washed with 1H HCl (25 ml) twice and a saturated sodium chloride (25 ml) once.

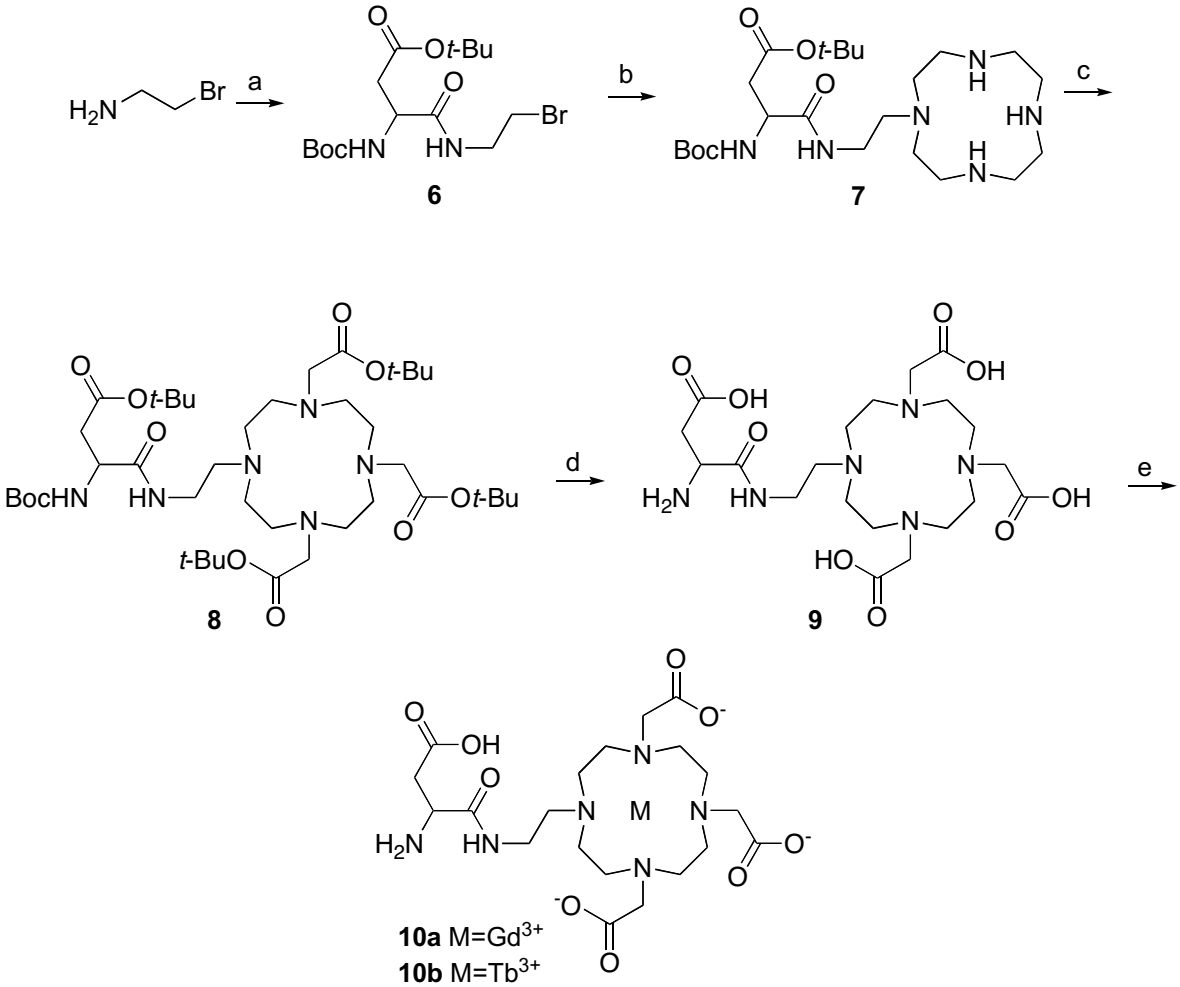

Scheme 2: Synthetic Scheme for Asp-AEDO3A. a) Boc-Asp(O*t*-Bu)-OSu, NaOH, DCM/H_2O, yield 82%; b) cyclen, MePh, yield 53%; c) t-Butyl bromoacetate, Na_2CO_3, yield 54%; d) TFA, Triisopropylsilane, yield 65%; e) MCl_3, LiOH, pH 6-7, H_2O, yield 73%

The organic layer was then dried over sodium sulfate and concentrated in vacuo to a colorless oil. The oil was dissolved in hexanes (5 ml) and placed at –80° C overnight. The white solid that crystallized was filtered and washed with cold hexanes. Total yield, 5.08 grams (12.9 mmol or 82% yield). Total yield, 420 mg (1.1 mmol, 45% yield). ^{13}C NMR ($CDCl_3$, 300 MHz) δ 171.16, 155.58, 81.72, 80.42, 50.68, 41.17, 37.26, 31.63, 28.32, 28.04. ^{1}H NMR ($CDCl_3$,

300 MHz) 7.06 (s, 1H), 6.74 (s, 1H), 4.47 (s, 1H), 3.66 (t, 2H), 4.45 (t, 2H), 2.89-2.61 (m, 2H), 1.45 (s, 18H). HR-FAB, m/z 395.1189 (M+H) theoretical 395.1181.

1-((N-Boc-Aspartyl)aminoethyl)-cyclen t-butyl ester (7). A solution of (N-Boc-aspartyl) aminoethylbromide (5.03 g, 12.9 mmol) and cyclen (15.5 g, 90 mmol) in dichloromethane (250 ml) was stirred at reflux for 48 hours. The mixture was then washed with water (100 ml, 3x). The organic layer was then concentrated in vacuo and resuspended in toluene (100 ml). The product was extracted from toluene solution with water (100 ml, 3x). The combined aqueous layers were washed with toluene (50 ml) followed by dichloromethane (100 ml, 4x). The dichloromethane layers were combined, dried over sodium sulfate and then concentrated in vacuo to a colorless oil. The oil was dissolved in dichloromethane (15 ml), heptane was added until the solution was cloudy and placed at –80°C overnight. The white solid that precipitated was filtered and washed with heptane. Total yield, 3.32 grams (6.8 mmol, 53% yield). ^{13}C NMR ($CDCl_3$, 300 MHz) δ 171.16, 170.59, 155.45, 81.19, 79.94, 51.27, 47.84, 46.39, 45.82, 38.71, 38.20, 37.71, 28.36. ^{1}H NMR ($CDCl_3$, 300 MHz) 5.8 (broad, 1H), 4.4 (broad, 1H), 3.5-2.4 (m, 22H), 1.47 (s, 18H). HR-FAB, m/z 487.3624 (M+H) theoretical 487.3607.

1-((N-Boc-Aspartyl)aminoethyl)-4,7,10-tri(t-butoxycarbonylmethyl)-cyclen (8). A solution of 1-((boc-aspartyl)aminoethyl)-cyclen t-butyl ester (1.35 g, 2.8 mmol), sodium carbonate (2.9 g, 27 mmol) and t–butyl bromoacetate (2.7 ml, 13.9 mmol) in acetonitrile (100 ml) was stirred at 70°C overnight. The following day, the reaction was filtered and washed with heptane (250 ml, 3x). The acetonitrile layer was then concentrated in vacuo to a pale yellow oil. The oil was dissolved in diethyl ether (10 ml), pentane was added until the solution was cloudy

and placed at –80°C overnight. The white solid that precipitated was filtered and washed with pentane. Total yield, 1.22 grams (1.5 mmol, 54% yield). ^{13}C NMR ($CDCl_3$, 500 MHz) δ 173.58, 172.67, 171.35, 170.99, 155.59, 82.86, 82.51, 81.44, 80.13, 55.83 (broad), 53.64, 51.3 (broad), 36.33, 28 (m). ^{1}H NMR ($CDCl_3$, 300 MHz)7.22 (s, 1H), 5.76 (d, 1H), 4.41 (d, 1H), 3.4-2.2 (m, 28H), 1.49-1.43 (m, 45H). HR-FAB, m/z 829.5684 (M+H) theoretical 829.5649.

1-Aspartylaminoethyl-4,7,10-tri(carboxymethyl)-cyclen (9). A solution of 1-((Boc-aspartyl) aminoethyl)-4,7,10-tri(t-butoxycarbonylmethyl)-cyclen t-butyl ester (685 mg, 826 μmol) in triisopropylsilane (500 μl) and trifluoroacetic acid (50 ml) was stirred overnight at room temperature. The following day the solution had turned orange and the solvent was removed in vacuo until approximately 1 ml remained. The remained solution was added dropwise to cold diethyl ether. The pale orange solid that formed immediately was filtered, and then resuspended in a minimal amount of water (~1 ml). The product was titurated and filtered off by the addition of a large excess of acetone (~100 ml). Total yield, 269 mg (533 μmol, 65% yield). ^{13}C NMR ($CDCl_3$, 500 MHz) δ 175.60, 174.18, 172.66, 170.49, 57.35, 52.71, 52.33, 50.71, 50.63, 50.36, 48.46, 48.23, 36.37, 34.62. ^{1}H NMR ($CDCl_3$, 300 MHz) 4.2-2.4 (m). HR-FAB, m/z 505.2623 (M+H) theoretical 505.2621.

1-Aspartylaminoethyl-4,7,10-tri(carboxymethyl)-cyclen, gadolinium salt (10a). A solution of 1-(aspartylaminoethyl)-4,7,10-tri(carboxymethyl)-cyclen (167 mg, 331 μmols) and gadolium chloride (120 mg, 457 μmols) was stirred at 80° C overnight. The pH was periodically checked and adjusted to 6.0 ~ 7.0 using a solution of lithium hydroxide (1M) as needed. After 12 hours, lithium hydroxide was added to bring the pH to ~12 and reaction was syringed through a nylon .2 μm filter. The filtrate was then lypohilized to a white powder that

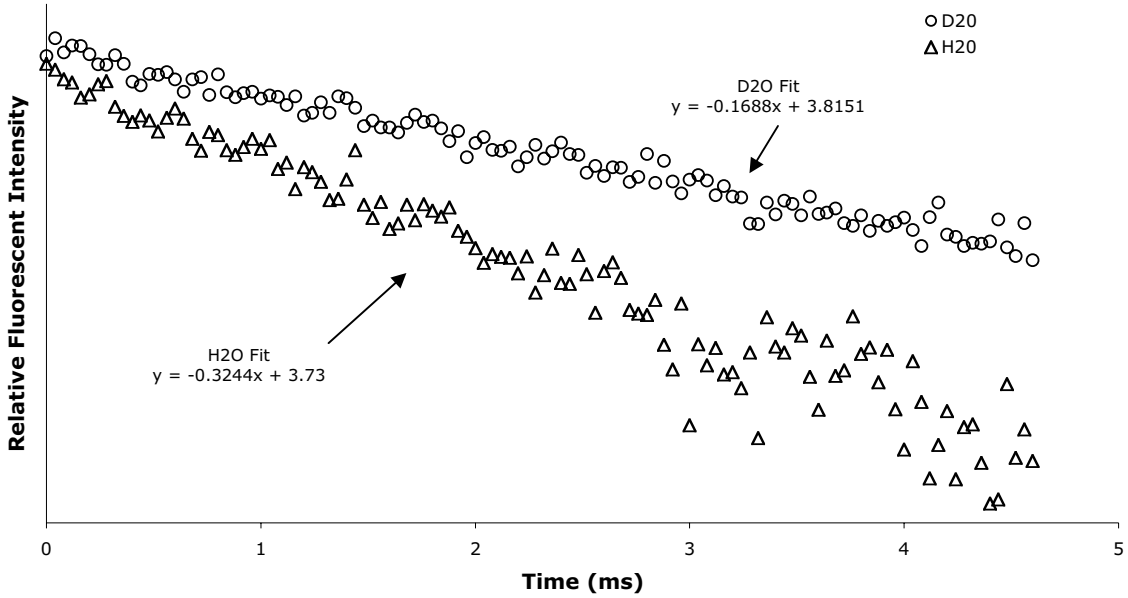

Figure 15: Fluorescent Lifetime Data of Asp-AEDO3A-Tb.

was resuspended in a minimal amount of methanol (~1 ml). The final product was precipitated from this solution by the addition of a large excess of acetone (~40 ml) and filtered off. The precipitate was collected as resuspended in water. This solution was purified over an ion-exchange resin (Bio-Rad Chelex), dialyzed (100 MWCO) and lyophilized to an off-white powder. Total yield, 160 mg (243 μmols, 73% yield). HR-FAB, m/z (M+H) theoretical 545.1358.

1-Aspartylaminoethyl-4,7,10-tri(carboxymethyl)-cyclen, terbium salt (10b). This compound was made in a fashion similar to **10a**. Total yield, 160 mg (243 μmols, 73% yield). HR-FAB, m/z (M+H) theoretical 545.1358.

Characterization

The number of water molecules in the inner-coordination sphere (*q*) was estimated for **10b** in a fashion similar to **5b** (**Figure 15**). The uncorrected lifetime data indicated a *q* of 0.45. The relaxivities of **10a** were estimated in a fashion similar to **5a** (**Table 3**).

Field Strength (MHz)	Relaxivity ($mM^{-1}s^{-1}$)	
	Buffer A	Buffer B
60	1.0	1.0
300	1.9	2.0
500	1.1	1.2
600	1.1	1.1
Composition of buffer	10 mM MOPS 100 mM NaCl 4 mM Na_2CO_3 20 mM Na_3PO_4	10 mM MOPS 100 mM NaCl

Table 3: Relaxivity of **10a**. All relaxivities taken at 25° C and pH 7.2, except for the 60MHz data taken at 37° C.

At this point, a preliminary evaluation was made of the utility of **5a** and **10a** as a relaxometric probe system. Tissue contrast modeling [63] indicated the lowest intracellular concentration of this relaxometric probe that would lead to an acceptable signal-to-noise in the *Xenopus* embryo is 0.7 mM. Microinjection experiments confirmed the embryos tolerated intracellular concentrations as great as 4 mM (**Figure 16**), well above the theoretical limit of detection.

Unfortunately, *in vitro* measurement of the enzymatic hydrolysis failed to detect any cleavage of **10a**. The enzyme assays were repeated under numerous conditions of enzyme concentration, temperature, buffer composition and enzyme source, however no cleavage was detected in any experiment. Competitive inhibition assays indicates that **10a** is recognized by and binds to caspase-3 reasonably well (K_m=1.3 mM).

Single crystals of **10a** were obtained by the slow diffusion of acetone into an aqueous solution of the compound. X-ray crystallography confirmed the structures (**Figure 17**). The coordinated atoms are arranged in a monocapped twisted square antiprism, with N1, N2, N3 and N4 composing one plane (rms deviation = 0.0068 Å) 1.665 Å below GdA while N5, O1,

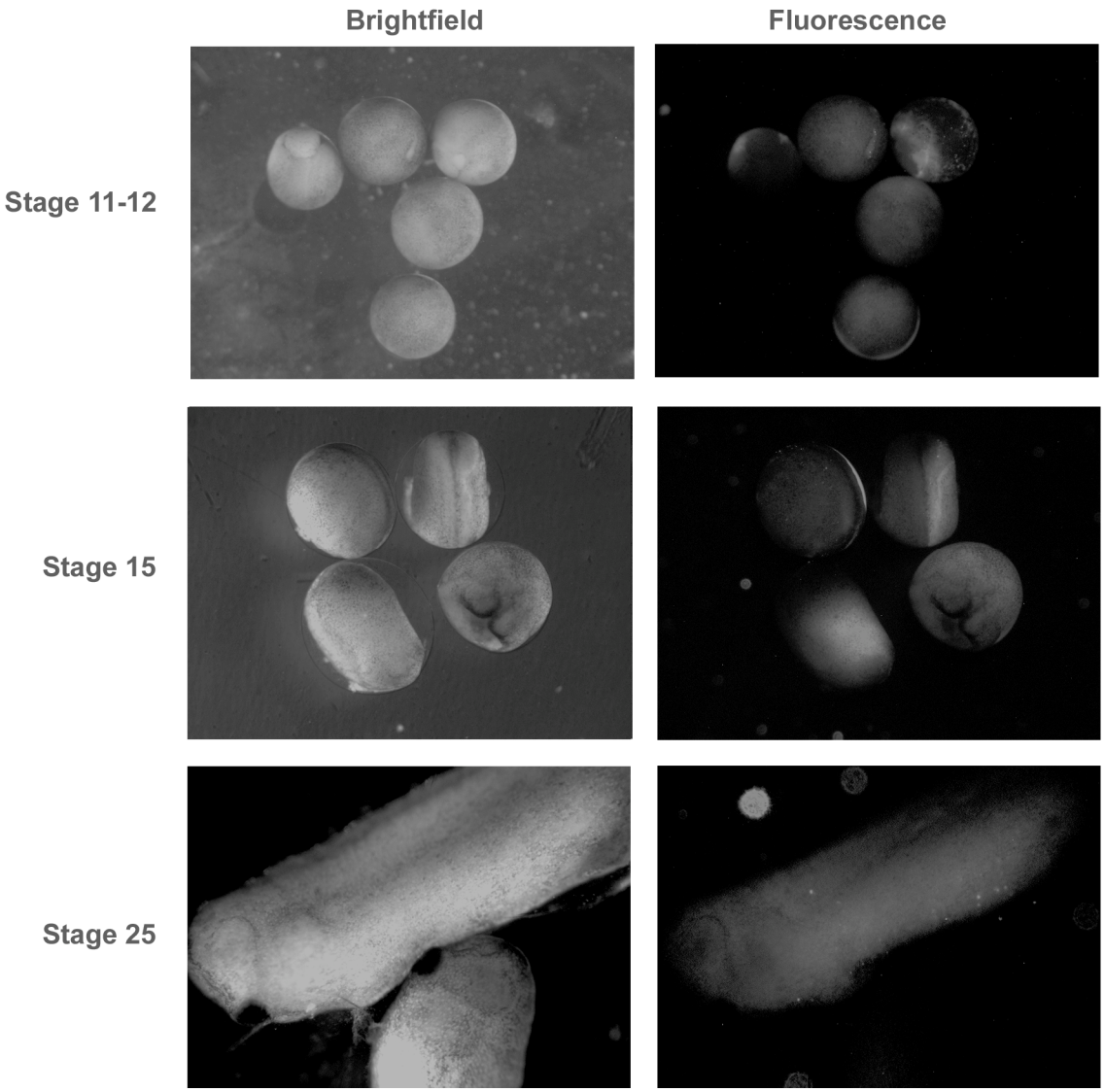

Figure 16. Brightfield and fluorescence images of *Xenopus* embryos with 40nl of a 100 mM solution **10a** with 5mg/ml Rhodamine-Dextran as a fluorescent tracer. All embryos were injected prior to stage 3.

O2, O3 and N5 line on the second plane (rms deviation = 0.0562 A) 0.892 A above GdA. The planes are twisted approximately 23.4 ° relative to each other.

Close inspection of the X-ray structure provided a likely explanation for the negative results in the *in vitro* cleavage assay. The proton on the amide nitrogen has been replaced by the gadolinium ion (**Figure 17**, **Panels B** and **C**). The deprotonation and subsequent coordination

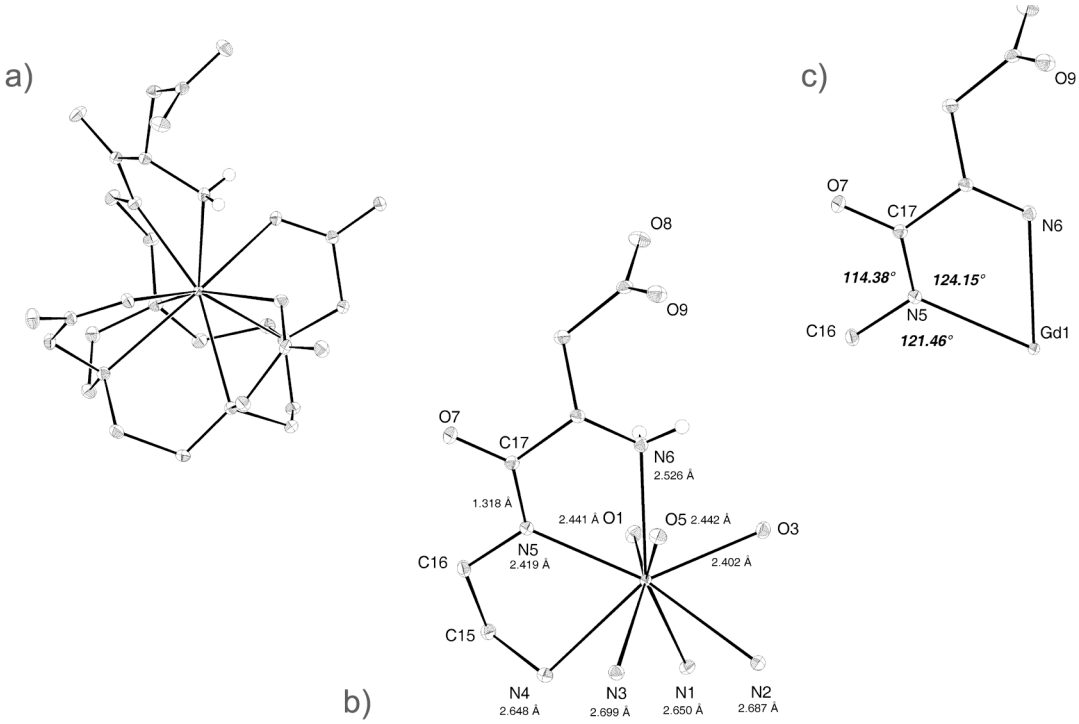

Figure 17. Three displacement ellipsoid plots of **10a** with 50% surfaces. **Panel a**. A perspective overview of the complex. **Panel b.** The non-coordinated atoms from the macrocycle and carboxymethyl arms have been removed for clarity. The distances between the labeled atoms and the gadolinium (center, not labeled) are shown. **Panel c.** The sum of angles (359.99°) among atoms bonded to the amide confirms sp_2 hybridization.

of a carboxamide by a metal ion is a well-studied phenomenon. In fact, in the well-known Biuret assay for proteins a Cu^{2+} ion substitutes for amide protons on the peptide backbone of proteins to form a colored complex, enabling the facile spectrophotometric determination of protein concentration.

Furthermore, the cleavage of N-carboxamido metal complexes at the coordinated amide bonds has also been investigated [73-75]. N-carboxamido metal coordination inhibits the hydrolysis of the amide bond to such a degree that the rate of hydrolysis has never been measured [76]. Although steric effects certainly play some role, this effect is primarily electronic in origin. Cleavage at an amide is preceded by the polarization of the carbonyl,

activatating the carbonyl-carbon for nucleophilic attack. When an amide bond is metalated at a deprotonated amide nitrogen, the carbonyl can no longer be polarized and hence becomes nearly impervious to nucleophilic attack.

Although the stability of this bond in physiological conditions has not been confirmed, there is no question this bond exists in the solid state and was formed in an aqueous solution. As such, this breaks new and exciting ground in multiple ways, overshadowing the failure of this contrast agent to be cleaved by caspase.

Not only will this be the first reported example of any actinide or lanthanide substituting for the proton of a carboxamide in aqueous solution, it will be the first ever-reported N-carboxamido actinide or lanthanide complex. Although this is of general interest to the inorganic chemistry community, the N-carboxamido coordination has the potential to significant impact the future of MRI CA design, perhaps enabling a new generation of CAs with relaxivities an order of magnitude greater than is presently possible. Further work is certainly warranted on the nature of this bond, its formation and interactions with the metal ion.

Discussion

We succeeded in the synthesis and characterization of gadolinium and terbium complexes of Asp-AEDO3A. Although the relaxation, fluorescence lifetime, and toxicity results are all favorable for inclusion into a relaxometric probe, unfortunately caspase never cleaved this bond. However, the disappointment at this failure is tempered by the discovery of a novel coordination chemistry for gadolinium.

Chapter 5

CONCLUSION

A novel and potentially useful contrast agent, AEDO3A•Gd, was synthesized and characterized. This is the first MRI DO3A-derivative containing a pendant amine and may potentially prove useful to other researchers investigating bifunctional contrast-agents or other relaxometric probes. During the course of this investigation, novel methods were developed to reduce the uncertainty in relaxivity estimates, allowing the comparison of relaxivities to be more confidently made.

However the most exciting discovery was the novel coordination chemistry rendering Asp-AEDO3A•Gd resistant to enzymatic hydrolysis. The N-carboxamido coordination of exhibited in Asp-AEDO3A•Gd has the potential to permit the synthesis of a novel class CAs. Attempts to generate high-relaxivity contrast agents eventually come up against τ_m – water exchange rates of gadolinium complexes are simply too long and cannot be increased without decreasing the thermodynamic stability of the CA, which would nullify their utility *in vivo*. Consequently, researchers designing high-relaxivity CAs have focused on exotic oxidation states in metal ions that are normally non-relaxogenic. A most promising example of this is Eu^{2+}. Its complexes have τ_m's two orders of magnitude quicker than most gadolinium complexes and coupling a Eu^{2+}-based CAs to a slowly tumbling macromolecule to increase τ_R, might potentially produce a contrast agent with a relaxivities measured in the hundreds.

Unfortunately, Eu^{2+} is not redox-stable in aqueous solutions and much effort has been devoted to finding a good redox-stabilizing ligand for Eu^{2+} that would also ameliorate its

toxcicity. N-carboxamido metal are excellent π-donors and have been used to stabilize other redox sensitive metal ions. Further research into this area is certainly warranted.

BIBLIOGRAPHY

1. Sanders, E. J. and M. A. Wride, *Programmed cell death in development.* International Reviews in Cytology, 1995. **163**: p. 105-73.
2. Schuchmann, M., P. R. Galle, and S. Kanzler, *Apoptosis in disease.* Medizinische Klinik, 2002. **97**(12): p. 738-46.
3. Hinshaw, W. S., E. R. Andrew, P. A. Bottomley, G. N. Holland, W. S. Moore, and B. S. Worthington, *Internal structural mapping by nuclear magnetic resonance.* Neuroradiology, 1978. **16**: p. 607-9.
4. Reed, J. C., *Mechanisms of apoptosis avoidance in cancer.* Current Opinions in Oncology, 1999. **11**(1): p. 68-75.
5. Kerr, J. F., A. H. Wyllie, and A. R. Currie, *Apoptosis: a basic biological phenomenon with wide-ranging implications in tissue kinetics.* British Journal of Cancer, 1972. **26**(4): p. 239-57.
6. Ellis, R. E., J. Y. Yuan, and H. R. Horvitz, *Mechanisms and functions of cell death.* Annual Reviews in Cell Biology, 1991. **7**: p. 663-98.
7. Kuida, K., J. A. Lippke, G. Ku, M. W. Harding, D. J. Livingston, M. S. Su, and R. A. Flavell, *Altered cytokine export and apoptosis in mice deficient in interleukin-1 beta converting enzyme.* Science, 1995. **267**(5206): p. 2000-3.
8. Li, P., H. Allen, S. Banerjee, S. Franklin, L. Herzog, C. Johnston, J. McDowell, M. Paskind, L. Rodman, J. Salfeld, and et al., *Mice deficient in IL-1 beta-converting enzyme are defective in production of mature IL-1 beta and resistant to endotoxic shock.* Cell, 1995. **80**(3): p. 401-11.

9. Fink, D., H. Schlagbauer-Wadl, E. Selzer, T. Lucas, K. Wolff, H. Pehamberger, H. G. Eichler, and B. Jansen, *Elevated procaspase levels in human melanoma.* Melanoma Research, 2001. **11**(4): p. 385-393.

10. Friedrich, K., T. Wieder, C. Von Haefen, S. Radetzki, R. Janicke, K. Schulze-Osthoff, B. Dorken, and P. T. Daniel, *Overexpression of caspase-3 restores sensitivity for drug-induced apoptosis in breast cancer cell lines with acquired drug resistance.* Oncogene, 2001. **20**(22): p. 2749-60.

11. Lacour, S., A. Hammann, A. Wotawa, L. Corcos, E. Solary, and M. T. Dimanche-Boitrel, *Anticancer agents sensitize tumor cells to tumor necrosis factor-related apoptosis-inducing ligand-mediated caspase-8 activation and apoptosis.* Cancer Research, 2001. **61**(4): p. 1645-51.

12. Gu, Y., K. Kuida, H. Tsutsui, G. Ku, K. Hsiao, M. A. Fleming, N. Hayashi, K. Higashino, H. Okamura, K. Nakanishi, M. Kurimoto, T. Tanimoto, R. A. Flavell, V. Sato, M. W. Harding, D. J. Livingston, and M. S. Su, *Activation of interferon-gamma inducing factor mediated by interleukin-1beta converting enzyme.* Science, 1997. **275**(5297): p. 206-9.

13. Chandra, J., B. Zhivotovsky, S. Zaitsev, L. Juntti-Berggren, P. O. Berggren, and S. Orrenius, *Role of apoptosis in pancreatic beta-cell death in diabetes.* Diabetes, 2001. **50 Suppl 1**: p. S44-7.

14. Gill, R., M. Soriano, K. Blomgren, H. Hagberg, R. Wybrecht, M. T. Miss, S. Hoefer, G. Adam, O. Niederhauser, J. A. Kemp, and H. Loetscher, *Role of caspase-3 activation in cerebral ischemia-induced neurodegeneration in adult and neonatal brain.* Journal of Cerebral Blood Flow and Metabolism, 2002. **22**(4): p. 420-30.

15. Northington, F. J., D. M. Ferriero, D. L. Flock, and L. J. Martin, *Delayed neurodegeneration in neonatal rat thalamus after hypoxia-ischemia is apoptosis.* Journal of Neuroscience, 2001. **21**(6): p. 1931-8.

16. Hsieh, C. C., M. H. Yen, C. H. Yen, and Y. T. Lau, *Oxidized low density lipoprotein induces apoptosis via generation of reactive oxygen species in vascular smooth muscle cells.* Cardiovascular Research, 2001. **49**(1): p. 135-45.

17. Hutchison, J. S., R. E. Derrane, D. L. Johnston, N. Gendron, D. Barnes, H. Fliss, W. J. King, I. Rasquinha, J. MacManus, G. S. Robertson, and A. E. MacKenzie, *Neuronal apoptosis inhibitory protein expression after traumatic brain injury in the mouse.* Journal of Neurotrauma, 2001. **18**(12): p. 1333-1347.

18. Beer, R., G. Franz, S. Krajewski, B. R. Pike, R. L. Hayes, J. C. Reed, K. K. Wang, C. Klimmer, E. Schmutzhard, W. Poewe, and A. Kampfl, *Temporal and spatial profile of caspase 8 expression and proteolysis after experimental traumatic brain injury.* Journal of Neurochemistry, 2001. **78**(4): p. 862-73.

19. Pollack, M., S. Phaneuf, A. Dirks, and C. Leeuwenburgh, *The role of apoptosis in the normal aging brain, skeletal muscle, and heart.* Annals of the New York Academy of Sciences, 2002. **959**: p. 93-107.

20. Dirks, A. and C. Leeuwenburgh, *Apoptosis in skeletal muscle with aging.* American Journal of Physiology - Regulatory, Integrative and Comparative Physiology, 2002. **282**(2): p. R519-27.

21. Gervais, F. G., R. Singaraja, S. Xanthoudakis, C. A. Gutekunst, B. R. Leavitt, M. Metzler, A. S. Hackam, J. Tam, J. P. Vaillancourt, V. Houtzager, D. M. Rasper, S. Roy, M. R. Hayden, and D. W. Nicholson, *Recruitment and activation of caspase-8 by the*

Huntingtin-interacting protein Hip-1 and a novel partner Hippi. Nature: Cell Biology, 2002. **4**(2): p. 95-105.

22. Ellis, H. M. and H. R. Horvitz, *Genetic control of programmed cell death in the nematode C. elegans.* Cell, 1986. **44**(6): p. 817-29.

23. Yuan, J., S. Shaham, S. Ledoux, H. M. Ellis, and H. R. Horvitz, *The C. elegans cell death gene ced-3 encodes a protein similar to mammalian interleukin-1 beta-converting enzyme.* Cell, 1993. **75**(4): p. 641-52.

24. Aime, S., M. Botta, S. G. Crich, G. Giovenzana, G. Palmisano, and M. Sisti, *A macromolecular Gd(III) complex as pH-responsive relaxometric probe for MRI applications.* Chemical Communications, 1999(16): p. 1577-1578.

25. Lowe, M. P., D. Parker, O. Reany, S. Aime, M. Botta, G. Castellano, E. Gianolio, and R. Pagliarin, *pH-dependent modulation of relaxivity and luminescence in macrocyclic gadolinium and europium complexes based on reversible intramolecular sulfonamide ligation.* Journal of the American Chemical Society, 2001. **123**(31): p. 7601-9.

26. Aime, S., M. Botta, E. Gianolio, and E. Terreno, *A pO_2-Responsive MRI Contrast Agent Based on the Redox Switch of Manganese(II / III) - Porphyrin Complexes.* Angewandte Chemie-International Edition, 2000. **39**(4): p. 747-750.

27. Aime, S., G. Digilio, M. Fasano, S. Paoletti, A. Arnelli, and P. Ascenzi, *Metal complexes as allosteric effectors of human hemoglobin: an NMR study of the interaction of the gadolinium(III) bis(m-boroxyphenylamide)diethylenetriaminepentaacetic acid complex with human oxygenated and deoxygenated hemoglobin.* Biophysics Journal, 1999. **76**(5): p. 2735-43.

28. Anelli, P. L., I. Bertini, M. Fragai, L. Lattuada, C. Luchinat, and G. Parigi, *Sulfonamide-functionalized gadolinium DTPA complexes as possible contrast agents for MRI: A relaxometric investigation.* European Journal of Inorganic Chemistry, 2000(4): p. 625-630.

29. De Leon-Rodriguez, L. M., A. Ortiz, A. L. Weiner, S. Zhang, Z. Kovacs, T. Kodadek, and A. D. Sherry, *Magnetic resonance imaging detects a specific peptide-protein binding event.* Journal of the American Chemical Society, 2002. **124**(14): p. 3514-5.

30. Fossheim, S. L., K. A. Il'yasov, J. Hennig, and A. Bjornerud, *Thermosensitive paramagnetic liposomes for temperature control during MR imaging-guided hyperthermia: in vitro feasibility studies.* Academy of Radiology, 2000. **7**(12): p. 1107-15.

31. Tatham, A. T., H. Nakamura, E. C. Wiener, and Y. Yamamoto, *Relaxation properties of a dual-labeled probe for MRI and neutron capture therapy.* Magnetic Resonance in Medicine, 1999. **42**(1): p. 32-6.

32. Li, W. H., S. E. Fraser, and T. J. Meade, *A calcium-sensitive magnetic resonance imaging contrast agent.* Journal of the American Chemical Society, 1999. **121**(6): p. 1413-1414.

33. Hanaoka, K., K. Kikuchi, Y. Urano, M. Narazaki, T. Yokawa, S. Sakamoto, K. Yamaguchi, and T. Nagano, *Design and synthesis of a novel magnetic resonance imaging contrast agent for selective sensing of zinc ion.* Chemical Biology, 2002. **9**(9): p. 1027-32.

34. Nivorozhkin, A. L., A. F. Kolodziej, P. Caravan, M. T. Greenfield, R. B. Lauffer, and T. J. McMurry, *Enzyme-activated Gd(III) MRI contrast agents with a prominent receptor-induced magnetization enhancement.* Angewandte Chemie-International Edition in English, 2001. **40**(15): p. 2903-2906.

35. Louie, A. Y., M. M. Huber, E. T. Ahrens, U. Rothbacher, R. Moats, R. E. Jacobs, S. E. Fraser, and T. J. Meade, *In vivo visualization of gene expression using magnetic resonance imaging.* Nature Biotechnology, 2000. **18**(3): p. 321-325.

36. Moats, R. A., S. E. Fraser, and T. J. Meade, *A "smart" magnetic resonance imaging agent that reports on specific enzymatic activity.* Angewandte Chemie-International Edition in English, 1997. **36**(7): p. 726-728.

37. Bogdanov, A., L. Matuszewski, C. Bremer, A. Petrovsky, and R. Weissleder, *Oligomerization of paramagnetic substrates result in signal amplification and can be used for MR imaging of molecular targets.* Molecular Imaging, 2002. **1**(1): p. 16-23.

38. Bloembergen, N., *Proton Relaxation Times in Paramagnetic Solutions.* Journal of Chemical Physics, 1957. **27**(2): p. 572-573.

39. Solomon, I., *Relaxation Processes in a System of 2 Spins.* Physical Review, 1955. **99**(2): p. 559-565.

40. Hwang, L. P. and J. H. Freed, *Generalized einstein relations for rotational and translational diffusion of molecules including spin.* Journal of Chemical Physics, 1975. **63**(1): p. 118-130.

41. Hwang, L. P. and J. H. Freed, *Dynamic effects of pair correlation-functions on spin relaxation by translational diffusion in liquids.* Journal of Chemical Physics, 1975. **63**(9): p. 4017-4025.

42. Curtet, C., C. Tellier, J. Bohy, M. L. Conti, J. C. Saccavini, P. Thedrez, J. Y. Douillard, J. F. Chatal, and H. Koprowski, *Selective modification of NMR relaxation time in human colorectal carcinoma by using gadolinium-diethylenetriaminepentaacetic acid conjugated with monoclonal antibody 19-9.* Proceedings of the National Academy of Sciences of the United States of America, 1986. **83**(12): p. 4277-81.

43. Curtet, C., C. Bourgoin, J. Bohy, J. C. Saccavini, P. Thedrez, S. Akoka, C. Tellier, and J. F. Chatal, *Gd-25 DTPA-MAb, a potential NMR contrast agent for MRI in the xenografted nude mouse: preliminary studies.* International Journal of Cancer, 1988. **2**: p. 126-32.

44. Saccavini, J. C., C. Curtet, J. Bohy, C. Tellier, C. Bourgoin, and J. M. Lhoste, *Magnetic resonance imaging studies on nude mice grafted with colorectal adenocarcinoma using gadolinium-labeled monoclonal antibody.* Investigational Radiology, 1988. **23 Suppl 1**: p. S292-3.

45. Kayyem, J. F., R. M. Kumar, S. E. Fraser, and T. J. Meade, *Receptor-targeted co-transport of DNA and magnetic resonance contrast agents.* Chemical Biology, 1995. **2**(9): p. 615-20.

46. Reimer, P., R. Weissleder, J. Wittenberg, and T. J. Brady, *Receptor-directed contrast agents for MR imaging: preclinical evaluation with affinity assays*. Radiology, 1992. **182**(2): p. 565-9.

47. Weissleder, R., G. Elizondo, J. Wittenberg, A. S. Lee, L. Josephson, and T. J. Brady, *Ultrasmall superparamagnetic iron oxide: an intravenous contrast agent for assessing lymph nodes with MR imaging*. Radiology, 1990. **175**(2): p. 494-8.

48. Vera, D. R., M. H. Buonocore, E. R. Wisner, R. W. Katzberg, and R. C. Stadalnik, *A molecular receptor-binding contrast agent for magnetic resonance imaging of the liver*. Academy of Radiology, 1995. **2**(6): p. 497-506.

49. Muhler, A., J. Platzek, B. Raduchel, T. Frenzel, and H. J. Weinmann, *Characterization of a gadolinium-labeled cholesterol derivative as an organ-specific contrast agent for adrenal MR imaging*. Journal of Magnetic Resonance in Imaging, 1995. **5**(1): p. 7-10.

50. Perez, J. M., T. O'Loughin, F. J. Simeone, R. Weissleder, and L. Josephson, *DNA-based magnetic nanoparticle assembly acts as a magnetic relaxation nanoswitch allowing screening of DNA-cleaving agents*. Journal of the American Chemical Society, 2002. **124**(12): p. 2856-7.

51. Josephson, L., J. M. Perez, and R. Weissleder, *Magnetic nanosensors for the detection of oligonucleotide sequences*. Angewandte Chemie-International Edition, 2001. **40**(17): p. 3204-+.

52. Zhang, S. R., L. Michaudet, S. Burgess, and A. D. Sherry, *The amide protons of an ytterbium(III) dota tetraamide complex act as efficient antennae for transfer of magnetization to bulk water*. Angewandte Chemie-International Edition, 2002. **41**(11): p. 1919-+.

53. Ward, K. M., A. H. Aletras, and R. S. Balaban, *A new class of contrast agents for MRI based on proton chemical exchange dependent saturation transfer (CEST)*. Journal of Magnetic Resonance, 2000. **143**(1): p. 79-87.

54. Aime, S., A. Barge, D. Delli Castelli, F. Fedeli, A. Mortillaro, F. U. Nielsen, and E. Terreno, *Paramagnetic lanthanide(III) complexes as pH-sensitive chemical exchange saturation transfer (CEST) contrast agents for MRI applications.* Magnetic Resonance in Medicine, 2002. **47**(4): p. 639-48.

55. Aime, S., D. Delli Castelli, F. Fedeli, and E. Terreno, *A paramagnetic MRI-CEST agent responsive to lactate concentration.* Journal of the American Chemical Society, 2002. **124**(32): p. 9364-5.

56. Goldstein, J. C., R. M. Kluck, and D. R. Green, *A single cell analysis of apoptosis. Ordering the apoptotic phenotype.* Annals of the New York Academy of Sciences, 2000. **926**: p. 132-41.

57. Garcia-Calvo, M., E. P. Peterson, D. M. Rasper, J. P. Vaillancourt, R. Zamboni, D. W. Nicholson, and N. A. Thornberry, *Purification and catalytic properties of human caspase family members.* Cell Death and Differentiation, 1999. **6**(4): p. 362-369.

58. Hug, H., M. Los, W. Hirt, and K. M. Debatin, *Rhodamine 110-linked amino acids and peptides as substrates to measure caspase activity upon apoptosis induction in intact cells.* Biochemistry, 1999. **38**(42): p. 13906-11.

59. Li, M. and C. F. Meares, *Synthesis, metal chelate stability studies, and enzyme digestion of a peptide-linked DOTA derivative and its corresponding radiolabeled immunoconjugates.* Bioconjugate Chemistry, 1993. **4**(4): p. 275-283.

60. McCall, M. J., H. Diril, and C. F. Meares, *Simplified method for conjugating macrocyclic bifunctional chelating agents to antibodies via 2-iminothiolane*. Bioconjugate Chemistry, 1990. **1**(3): p. 222-226.

61. Peterson, J. J., R. H. Pak, and C. F. Meares, *Total solid-phase synthesis of 1,4,7,10-tetraazacyclododecane- N,N ',N '',N '''-tetraacetic acid-functionalized peptides for radioimmunotherapy*. Bioconjugate Chemistry, 1999. **10**(2): p. 316-320.

62. Mishra, A. K. and J. F. Chatal, *Synthesis of macrocyclic bifunctional chelating agents: 1,4,7-tris(carboxymethyl)-10-(2-aminoethyl)-1,4,7,10- tetraazacyclododecane and 1,4,8-tris(carboxymethyl)-11-(2- aminoethyl)-1,4,8,11-tetraazacyclotetradecane*. New Journal of Chemistry, 2001. **25**(2): p. 336-339.

63. Ahrens, E. T., U. Rothbacher, R. E. Jacobs, and S. E. Fraser, *A model for MRI contrast enhancement using T_1 agents*. Proceedings of the National Academy of Sciences of the United States of America, 1998. **95**(15): p. 8443-8448.

64. Franklin, S. J. and K. N. Raymond, *Solution Structure and Dynamics of Lanthanide Complexes of the Macrocyclic Polyamino Carboxylate Dtpa-Dien - Nmr-Study and Crystal-Structures of the Lanthanum(Iii) and Europium(Iii) Complexes*. Inorganic Chemistry, 1994. **33**(25): p. 5794-5804.

65. Shukla, R., M. Fernandez, R. K. Pillai, R. Ranganathan, P. C. Ratsep, X. Zhang, and M. F. Tweedle, *Design of conformationally rigid dimeric MRI agents*. Magnetic Resonance in Medicine, 1996. **35**(6): p. 928-931.

66. Taylor, J. R., *An introduction to error analysis*. 1982, Mill Valley: University Science Books. 270.

67. Horrocks, W. D. and D. R. Sudnick, *Lanthanide ion probes of structure in biology - laser-induced luminescence decay constants provide a direct measure of the number of metal-coordinated water molecules*. Journal of the American Chemical Society, 1979. **101**(2): p. 334-340.

68. Beeby, A., I. M. Clarkson, R. S. Dickins, S. Faulkner, D. Parker, L. Royle, A. S. de Sousa, J. A. G. Williams, and M. Woods, *Non-radiative deactivation of the excited states of*

europium, terbium and ytterbium complexes by proximate energy-matched OH, NH and CH oscillators: an improved luminescence method for establishing solution hydration states. Journal of the Chemical Society-Perkin Transactions 2, 1999(3): p. 493-503.

69. Beeby, A., L. M. Bushby, D. Maffeo, and J. A. G. Williams, *Intramolecular sensitisation of lanthanide(III) luminescence by acetophenone-containing ligands: the critical effect of para- substituents and solvent*. Journal of the Chemical Society-Dalton Transactions, 2002(1): p. 48-54.

70. Burai, L., V. Hietapelto, R. Kiraly, E. Toth, and E. Brucher, *Stability constants and ^{1}H relaxation effects of ternary complexes formed between Gd-DTPA, Gd-DTPA-BMA, Gd-DOTA, and Gd- EDTA and citrate, phosphate, and carbonate ions.* Magnetic Resonance in Medicine, 1997. **38**(1): p. 146-150.

71. Supkowski, R. M. and W. D. Horrocks, *Displacement of inner-sphere water molecules from Eu^{3+} analogues of Gd^{3+} MRI contrast agents by carbonate and phosphate anions: Dissociation constants from luminescence data in the rapid-exchange limit*. Inorganic Chemistry, 1999. **38**(24): p. 5616-5619.

72. Caravan, P., J. J. Ellison, T. J. McMurry, and R. B. Lauffer, *Gadolinium(III) chelates as MRI contrast agents: Structure, dynamics, and applications*. Chemical Reviews, 1999. **99**(9): p. 2293-2352.

73. Martin, R. B., *Amide nitrogen is unlikely to be a proton acceptor*. Nature, 1978. **271**(5640): p. 94-94.

74. Andreatt, R., H. C. Freeman, A. Robertso, and R. L. Sinclair, *Selective cleavage of peptides by alkali in presence of transition-metal ions*. Chemical Communications, 1967(4): p. 203-&.

75. Jones, M. M., T. J. Cook, and S. Brammer, *Effect of co-ordination to copper(II) on basic hydrolysis of glycylglycine*. Journal of Inorganic & Nuclear Chemistry, 1966. **28**(5): p. 1265-&.

76. Sigel, H. and R. B. Martin, *Coordinating Properties of the Amide Bond - Stability and Structure of Metal-Ion Complexes of Peptides and Related Ligands*. Chemical Reviews, 1982. **82**(4): p. 385-426.

APPENDIX

Crystal Structure Analysis of AEDO3A

Crystallographic data have been deposited with the CCDC as supplementary publication CCDC 175662. These data can be obtained free of charge via http://www.ccdc.cam.ac.uk/ conts/retrieving.html (or from CCDC, 12 Union Road, Cambridge CB2 1EZ, UK; fax: +44 1223 335033; or deposit@ccdc.cam.ac.uk). Structure factors are available from the author via email: xray@caltech.edu.

Table A.1.1. Crystal data and structure refinement for AEDO3A.

Empirical formula	$C_{16}H_{31}N_5O_6 \cdot 5(H_2O)$	
Formula weight	479.54	
Crystallization Solvent	Water	
Crystal Habit	Block	
Crystal size	0.33 x 0.22 x 0.22 mm^3	
Crystal color	Colorless	
	Data Collection	
Preliminary Photos	Rotation	
Type of diffractometer	Bruker SMART 1000	
Wavelength	0.71073 Å MoKα	
Data Collection Temperature	98(2) K	
θ range for 15223 reflections used in lattice determination	2.29 to 28.09°	
Unit cell dimensions	a = 7.7997(5) Å	
	b = 16.6844(11) Å	β= 92.1710(10)°
	c = 17.7687(12) Å	
Volume	2310.6(3) $Å^3$	
Z	4	
Crystal system	Monoclinic	
Space group	$P2_1/c$	
Density (calculated)	1.378 Mg/m^3	
F(000)	1040	
Data collection program	Bruker SMART v5.054	
θ range for data collection	1.67 to 28.19°	
Completeness to θ = 28.19°	95.7 %	
Index ranges	$-10 \le h \le 10$, $-22 \le k \le 22$, $-23 \le l \le 23$	
Data collection scan type	ω scans at 7 φ settings	
Data reduction program	Bruker SAINT v6.22	
Reflections collected	46047	

Table A.1.1. Crystal data and structure refinement for AEDO3A.

Independent reflections	5450 [R_{int} = 0.0610]
Absorption coefficient	0.115 mm^{-1}
Absorption correction	None
Max. and min. transmission	0.9749 and 0.9627

Structure solution and Refinement

Structure solution program	SHELXS-97 (Sheldrick, 1990)
Primary solution method	Direct methods
Secondary solution method	Difference Fourier map
Hydrogen placement	Difference Fourier map
Structure refinement program	SHELXL-97 (Sheldrick, 1997)
Refinement method	Full matrix least-squares on F^2
Data / restraints / parameters	5450 / 0 / 453
Treatment of hydrogen atoms	Unrestrained
Goodness-of-fit on F^2	1.749
Final R indices [I>2σ(I), 3978 reflections]	R1 = 0.0390, ωR2 = 0.0584
R indices (all data)	R1 = 0.0577, ωR2 = 0.0597
Type of weighting scheme used	Sigma
Weighting scheme used	$w=1/\sigma^2(Fo^2)$
Max shift/error	0.000
Average shift/error	0.000
Largest diff. peak and hole	0.362 and -0.274 e.$Å^{-3}$

Special Refinement Details

Refinement of F^2 against ALL reflections. The weighted R-factor (*w*R) and goodness of fit (S) are based on F^2, conventional R-factors (R) are based on F, with F set to zero for negative F^2. The threshold expression of $F^2 > 2\sigma(F^2)$ is used only for calculating R-factors(gt) etc. and is not relevant to the choice of reflections for refinement. R-factors based on F^2 are statistically about twice as large as those based on F, and R-factors based on ALL data will be even larger.

All esds (except the esd in the dihedral angle between two l.s. planes) are estimated using the full covariance matrix. The cell esds are taken into account individually in the estimation of esds in distances, angles and torsion angles; correlations between esds in cell parameters are only used when they are defined by crystal symmetry. An approximate (isotropic) treatment of cell esds is used for estimating esds involving l.s. planes.

Table A.1.2. Atomic coordinates (x 10^4) and equivalent isotropic displacement parameters ($Å^2$ x 10^3) for AEDO3A. U_{eq} is defined as the trace of the orthogonalized U^{ij} tensor.

	x	y	z	U_{eq}
O(1)	1923(1)	-2606(1)	2211(1)	25(1)
O(2)	3685(1)	-1658(1)	2695(1)	19(1)
O(3)	7023(1)	-69(1)	4607(1)	18(1)
O(4)	7691(1)	1222(1)	4741(1)	18(1)
O(5)	5369(1)	84(1)	2969(1)	17(1)
O(6)	3382(1)	489(1)	2109(1)	18(1)
N(1)	6496(1)	-2319(1)	2140(1)	15(1)
N(2)	8075(1)	-1988(1)	3667(1)	14(1)
N(3)	9008(1)	-264(1)	3362(1)	14(1)
N(4)	7280(1)	-655(1)	1908(1)	15(1)
N(5)	4761(2)	-1263(1)	4161(1)	16(1)
C(1)	8048(2)	-2747(1)	2463(1)	16(1)
C(2)	8018(2)	-2787(1)	3311(1)	16(1)
C(3)	9855(2)	-1691(1)	3684(1)	16(1)
C(4)	10016(2)	-812(1)	3886(1)	16(1)
C(5)	9861(2)	-202(1)	2614(1)	17(1)
C(6)	8551(2)	-4(1)	1997(1)	17(1)
C(7)	7888(2)	-1259(1)	1378(1)	17(1)
C(8)	6785(2)	-2004(1)	1362(1)	17(1)
C(9)	4895(2)	-2815(1)	2152(1)	19(1)
C(10)	3364(2)	-2309(1)	2369(1)	17(1)
C(11)	7436(2)	-2052(1)	4434(1)	17(1)
C(12)	5501(2)	-2037(1)	4449(1)	19(1)
C(13)	8836(2)	551(1)	3711(1)	15(1)
C(14)	7748(2)	561(1)	4404(1)	15(1)
C(15)	5605(2)	-325(1)	1681(1)	16(1)
C(16)	4726(2)	113(1)	2310(1)	15(1)
O(21)	2050(1)	449(1)	663(1)	24(1)
O(22)	3129(1)	817(1)	3947(1)	23(1)
O(23)	9172(1)	2612(1)	4280(1)	26(1)
O(24)	4955(2)	-1222(1)	-84(1)	32(1)
O(25)	1239(1)	-993(1)	-82(1)	27(1)

Table A.1.3. Bond lengths [Å] for AEDO3A.

O(1)-C(10)	1.2501(15)	C(5)-C(6)	1.5073(18)
O(2)-C(10)	1.2520(15)	C(5)-H(5A)	1.007(12)
O(3)-C(14)	1.2521(15)	C(5)-H(5B)	0.987(13)
O(4)-C(14)	1.2560(15)	C(6)-H(6A)	1.006(12)
O(5)-C(16)	1.2570(14)	C(6)-H(6B)	0.986(13)
O(6)-C(16)	1.2616(14)	C(7)-C(8)	1.5121(19)
N(1)-C(9)	1.4996(17)	C(7)-H(7A)	0.997(13)
N(1)-C(1)	1.5006(16)	C(7)-H(7B)	1.000(12)
N(1)-C(8)	1.5042(17)	C(8)-H(8A)	0.996(12)
N(1)-H(1)	0.917(14)	C(8)-H(8B)	0.970(13)
N(2)-C(11)	1.4721(16)	C(9)-C(10)	1.5239(18)
N(2)-C(3)	1.4738(16)	C(9)-H(9A)	0.964(13)
N(2)-C(2)	1.4756(16)	C(9)-H(9B)	0.983(13)
N(3)-C(13)	1.5027(16)	C(11)-C(12)	1.5109(19)
N(3)-C(4)	1.5052(16)	C(11)-H(11A)	1.001(12)
N(3)-C(5)	1.5116(16)	C(11)-H(11B)	0.967(13)
N(3)-H(3)	0.938(13)	C(12)-H(12A)	0.978(13)
N(4)-C(15)	1.4597(16)	C(12)-H(12B)	0.985(12)
N(4)-C(7)	1.4690(16)	C(13)-C(14)	1.5221(18)
N(4)-C(6)	1.4748(16)	C(13)-H(13A)	0.939(12)
N(5)-C(12)	1.4960(17)	C(13)-H(13B)	0.979(13)
N(5)-H(5C)	0.948(15)	C(15)-C(16)	1.5208(18)
N(5)-H(5D)	0.928(14)	C(15)-H(15A)	0.952(12)
N(5)-H(5E)	0.984(16)	C(15)-H(15B)	1.008(12)
C(1)-C(2)	1.5095(18)	O(21)-H(21A)	0.849(17)
C(1)-H(1A)	0.981(12)	O(21)-H(21B)	0.874(18)
C(1)-H(1B)	0.997(11)	O(22)-H(22A)	0.905(17)
C(2)-H(2A)	1.004(12)	O(22)-H(22B)	0.867(17)
C(2)-H(2B)	0.998(12)	O(23)-H(23A)	0.856(19)
C(3)-C(4)	1.5141(18)	O(23)-H(23B)	0.885(18)
C(3)-H(3A)	1.029(13)	O(24)-H(24A)	1.01(2)
C(3)-H(3B)	0.965(12)	O(24)-H(24B)	0.95(2)
C(4)-H(4A)	0.964(12)	O(25)-H(25A)	0.864(17)
C(4)-H(4B)	0.997(12)	O(25)-H(25B)	0.833(17)

Table A.1.4. Bond Angles [°] for AEDO3A.

C(9)-N(1)-C(1)	113.07(11)	C(5)-C(6)-H(6B)	107.8(7)
C(9)-N(1)-C(8)	111.04(11)	H(6A)-C(6)-H(6B)	107.6(10)
C(1)-N(1)-C(8)	111.76(10)	N(4)-C(7)-C(8)	112.32(11)
C(9)-N(1)-H(1)	106.3(8)	N(4)-C(7)-H(7A)	112.2(7)
C(1)-N(1)-H(1)	109.1(8)	C(8)-C(7)-H(7A)	107.9(7)
C(8)-N(1)-H(1)	105.1(8)	N(4)-C(7)-H(7B)	108.5(7)
C(11)-N(2)-C(3)	110.96(10)	C(8)-C(7)-H(7B)	109.4(7)
C(11)-N(2)-C(2)	109.03(10)	H(7A)-C(7)-H(7B)	106.2(10)
C(3)-N(2)-C(2)	109.01(10)	N(1)-C(8)-C(7)	111.95(11)
C(13)-N(3)-C(4)	110.30(10)	N(1)-C(8)-H(8A)	107.4(7)
C(13)-N(3)-C(5)	110.50(10)	C(7)-C(8)-H(8A)	110.2(7)
C(4)-N(3)-C(5)	110.36(10)	N(1)-C(8)-H(8B)	107.5(8)
C(13)-N(3)-H(3)	107.3(8)	C(7)-C(8)-H(8B)	110.9(7)
C(4)-N(3)-H(3)	110.6(8)	H(8A)-C(8)-H(8B)	108.8(10)
C(5)-N(3)-H(3)	107.6(8)	N(1)-C(9)-C(10)	110.98(11)
C(15)-N(4)-C(7)	112.87(10)	N(1)-C(9)-H(9A)	107.9(7)
C(15)-N(4)-C(6)	110.08(10)	C(10)-C(9)-H(9A)	108.3(7)
C(7)-N(4)-C(6)	109.99(10)	N(1)-C(9)-H(9B)	107.2(8)
C(12)-N(5)-H(5C)	111.4(8)	C(10)-C(9)-H(9B)	112.9(7)
C(12)-N(5)-H(5D)	112.3(8)	H(9A)-C(9)-H(9B)	109.4(10)
H(5C)-N(5)-H(5D)	109.3(12)	O(1)-C(10)-O(2)	127.55(12)
C(12)-N(5)-H(5E)	107.8(8)	O(1)-C(10)-C(9)	115.46(12)
H(5C)-N(5)-H(5E)	109.9(12)	O(2)-C(10)-C(9)	116.98(11)
H(5D)-N(5)-H(5E)	106.0(12)	N(2)-C(11)-C(12)	112.86(11)
N(1)-C(1)-C(2)	111.12(11)	N(2)-C(11)-H(11A)	109.5(7)
N(1)-C(1)-H(1A)	105.6(7)	C(12)-C(11)-H(11A)	108.0(7)
C(2)-C(1)-H(1A)	112.2(7)	N(2)-C(11)-H(11B)	109.7(8)
N(1)-C(1)-H(1B)	108.1(6)	C(12)-C(11)-H(11B)	109.0(7)
C(2)-C(1)-H(1B)	111.7(6)	H(11A)-C(11)-H(11B)	107.7(10)
H(1A)-C(1)-H(1B)	107.9(9)	N(5)-C(12)-C(11)	112.38(12)
N(2)-C(2)-C(1)	112.73(11)	N(5)-C(12)-H(12A)	106.3(7)
N(2)-C(2)-H(2A)	109.0(7)	C(11)-C(12)-H(12A)	108.1(7)
C(1)-C(2)-H(2A)	110.9(7)	N(5)-C(12)-H(12B)	107.0(7)
N(2)-C(2)-H(2B)	110.4(7)	C(11)-C(12)-H(12B)	112.5(7)
C(1)-C(2)-H(2B)	108.1(7)	H(12A)-C(12)-H(12B)	110.5(11)
H(2A)-C(2)-H(2B)	105.4(9)	N(3)-C(13)-C(14)	113.86(11)
N(2)-C(3)-C(4)	113.60(11)	N(3)-C(13)-H(13A)	108.9(7)
N(2)-C(3)-H(3A)	109.8(7)	C(14)-C(13)-H(13A)	108.3(8)
C(4)-C(3)-H(3A)	107.8(7)	N(3)-C(13)-H(13B)	107.9(7)
N(2)-C(3)-H(3B)	107.7(7)	C(14)-C(13)-H(13B)	109.2(7)
C(4)-C(3)-H(3B)	111.2(7)	H(13A)-C(13)-H(13B)	108.6(10)
H(3A)-C(3)-H(3B)	106.5(10)	O(3)-C(14)-O(4)	125.16(12)
N(3)-C(4)-C(3)	113.91(11)	O(3)-C(14)-C(13)	119.68(12)
N(3)-C(4)-H(4A)	105.3(7)	O(4)-C(14)-C(13)	115.14(11)
C(3)-C(4)-H(4A)	109.6(7)	N(4)-C(15)-C(16)	113.67(11)
N(3)-C(4)-H(4B)	105.4(7)	N(4)-C(15)-H(15A)	109.1(7)
C(3)-C(4)-H(4B)	111.3(7)	C(16)-C(15)-H(15A)	105.6(8)
H(4A)-C(4)-H(4B)	111.0(10)	N(4)-C(15)-H(15B)	112.2(7)
C(6)-C(5)-N(3)	110.25(11)	C(16)-C(15)-H(15B)	109.0(7)
C(6)-C(5)-H(5A)	111.4(7)	H(15A)-C(15)-H(15B)	106.8(10)
N(3)-C(5)-H(5A)	106.6(7)	O(5)-C(16)-O(6)	125.54(12)
C(6)-C(5)-H(5B)	112.9(7)	O(5)-C(16)-C(15)	119.43(11)
N(3)-C(5)-H(5B)	107.7(7)	O(6)-C(16)-C(15)	115.03(11)

Table A.1.4. Bond Angles [°] for AEDO3A.

H(5A)-C(5)-H(5B)	107.8(10)	H(21A)-O(21)-H(21B)	111.6(16)
N(4)-C(6)-C(5)	110.56(11)	H(22A)-O(22)-H(22B)	103.2(14)
N(4)-C(6)-H(6A)	107.7(7)	H(23A)-O(23)-H(23B)	106.2(16)
C(5)-C(6)-H(6A)	110.8(7)	H(24A)-O(24)-H(24B)	111.5(16)
N(4)-C(6)-H(6B)	112.3(7)	H(25A)-O(25)-H(25B)	104.5(15

Table A.1.5. Anisotropic displacement parameters ($Å^2$ x 10^4) for AEDO3A. The anisotropic displacement factor exponent takes the form: $-2\pi^2[h^2 a^{*2}U^{11} + ... + 2 h k a^* b^* U^{12}]$

	U^{11}	U^{22}	U^{33}	U^{23}	U^{13}	U^{12}
O(1)	131(5)	363(6)	266(6)	-95(5)	8(4)	-38(5)
O(2)	189(5)	197(5)	186(5)	-33(4)	7(4)	6(4)
O(3)	201(5)	159(5)	189(5)	5(4)	31(4)	-37(4)
O(4)	209(5)	150(5)	183(5)	-27(4)	37(4)	-7(4)
O(5)	169(5)	204(5)	147(5)	-15(4)	7(4)	11(4)
O(6)	145(5)	180(5)	204(5)	5(4)	7(4)	29(4)
N(1)	135(6)	145(6)	181(7)	-32(5)	11(5)	2(5)
N(2)	140(6)	144(6)	146(6)	-14(5)	20(5)	-8(5)
N(3)	126(6)	151(6)	157(6)	-7(5)	14(5)	-7(5)
N(4)	139(6)	142(6)	158(6)	-16(5)	13(5)	8(5)
N(5)	153(6)	160(7)	161(7)	-3(5)	20(5)	-5(5)
C(1)	115(7)	148(8)	207(8)	-17(6)	4(6)	16(6)
C(2)	160(8)	139(8)	189(8)	5(6)	8(6)	3(6)
C(3)	139(7)	180(8)	170(8)	-12(6)	-1(6)	11(6)
C(4)	124(7)	189(8)	174(8)	8(6)	-21(6)	6(6)
C(5)	163(7)	172(8)	175(8)	-7(6)	56(6)	-17(6)
C(6)	189(7)	171(8)	164(8)	13(6)	55(6)	11(6)
C(7)	175(8)	194(8)	150(8)	-7(6)	24(6)	26(6)
C(8)	178(8)	189(8)	148(8)	-21(6)	1(6)	29(6)
C(9)	152(7)	174(8)	228(9)	-25(7)	-3(6)	-23(6)
C(10)	166(8)	247(8)	102(7)	22(6)	14(6)	10(6)
C(11)	196(8)	157(8)	151(8)	13(6)	-3(6)	26(6)
C(12)	211(8)	163(8)	184(8)	27(7)	28(6)	15(6)
C(13)	160(8)	126(7)	166(8)	-14(6)	4(6)	-4(6)
C(14)	121(7)	183(8)	143(7)	16(6)	-28(6)	20(6)
C(15)	170(7)	167(8)	154(8)	16(6)	-2(6)	16(6)
C(16)	158(7)	119(7)	180(8)	8(6)	25(6)	-34(6)
O(21)	276(6)	227(6)	206(6)	-8(5)	-34(5)	-1(5)
O(22)	229(6)	270(6)	202(6)	23(5)	44(5)	61(5)
O(23)	303(6)	212(6)	248(7)	17(5)	3(5)	-70(5)
O(24)	309(7)	284(6)	352(7)	56(5)	-8(5)	11(6)
O(25)	247(7)	240(7)	304(7)	40(5)	-18(5)	9(5)

Table A.1.6. Hydrogen coordinates (x 10^4) and isotropic displacement parameters ($Å^2$ x 10^3) for AEDO3A.

	x	y	z	U_{iso}
H(1)	6294(17)	-1873(8)	2426(8)	26(4)
H(1A)	8023(14)	-3280(8)	2232(7)	10(3)
H(1B)	9087(15)	-2462(7)	2292(6)	5(3)
H(2A)	6972(15)	-3080(7)	3476(7)	13(3)
H(2B)	9013(15)	-3119(7)	3496(6)	12(3)
H(3)	7896(18)	-463(8)	3268(7)	27(4)
H(3A)	10591(16)	-2011(7)	4071(7)	21(4)
H(3B)	10318(15)	-1799(7)	3198(7)	10(3)
H(4A)	11194(16)	-645(7)	3853(6)	12(3)
H(4B)	9583(15)	-703(7)	4397(7)	10(3)
H(5A)	10420(15)	-736(7)	2525(7)	15(3)
H(5B)	10778(16)	204(8)	2668(7)	18(4)
H(5C)	4428(17)	-1299(8)	3643(9)	29(4)
H(5D)	5515(18)	-837(8)	4232(8)	30(4)
H(5E)	3757(19)	-1136(8)	4458(8)	36(4)
H(6A)	7914(15)	501(7)	2117(6)	11(3)
H(6B)	9171(16)	93(7)	1532(7)	22(4)
H(7A)	7924(15)	-1049(7)	854(7)	16(4)
H(7B)	9094(15)	-1405(7)	1531(7)	12(3)
H(8A)	7351(15)	-2438(7)	1077(7)	12(3)
H(8B)	5668(17)	-1897(7)	1124(7)	20(4)
H(9A)	5071(15)	-3228(8)	2526(7)	21(4)
H(9B)	4737(16)	-3063(7)	1652(7)	21(4)
H(11A)	7889(14)	-1593(7)	4746(7)	12(3)
H(11B)	7851(15)	-2542(8)	4667(7)	19(4)
H(12A)	5176(16)	-2080(7)	4974(8)	20(4)
H(12B)	4964(16)	-2468(8)	4144(7)	19(4)
H(13A)	8337(16)	902(7)	3352(7)	14(4)
H(13B)	9990(17)	745(7)	3850(7)	14(3)
H(15A)	4854(16)	-753(7)	1536(7)	18(4)
H(15B)	5667(15)	42(7)	1232(7)	14(3)
H(21A)	1860(20)	-19(10)	491(9)	47(6)
H(21B)	2450(20)	434(11)	1129(11)	64(6)
H(22A)	3830(20)	571(9)	3623(9)	51(5)
H(22B)	3320(20)	557(10)	4364(10)	52(6)
H(23A)	8810(20)	2179(11)	4476(10)	65(7)
H(23B)	8850(20)	2592(10)	3797(11)	61(6)
H(24A)	5890(30)	-877(12)	-301(12)	99(8)
H(24B)	3850(30)	-1018(12)	-212(12)	93(8)
H(25A)	250(20)	-908(9)	-303(9)	47(6)
H(25B)	1130(20)	-1431(10)	136(9)	48(6)

Table A.1.7. Hydrogen bonds for AEDO3A [Å and °].

D-H…A	d(D-H)	d(H…A)	d(D…A)	<(DHA)
N(1)-H(1)…O(2)	0.917(14)	2.139(13)	2.6756(14)	116.4(10)
N(1)-H(1)…N(4)	0.917(14)	2.372(13)	2.8759(15)	114.5(10)
N(3)-H(3)…O(5)	0.938(13)	2.218(13)	2.9544(14)	134.8(11)
N(3)-H(3)…N(4)	0.938(13)	2.468(13)	2.9422(15)	111.4(10)
N(5)-H(5C)…O(2)	0.948(15)	1.860(15)	2.7849(16)	164.5(12)
N(5)-H(5D)…O(3)	0.928(14)	1.846(15)	2.7571(15)	166.5(13)
N(5)-H(5E)…O(4)#1	0.984(16)	1.856(16)	2.7851(15)	156.3(12)
O(21)-H(21A)…O(25)	0.849(17)	1.968(17)	2.8061(16)	169.0(16)
O(21)-H(21B)…O(6)	0.874(18)	1.862(19)	2.7346(14)	175.1(18)
O(22)-H(22A)…O(5)	0.905(17)	1.887(18)	2.7921(14)	177.4(15)
O(22)-H(22B)…O(3)#1	0.867(17)	2.030(18)	2.8643(14)	161.2(16)
O(23)-H(23A)…O(4)	0.856(19)	1.887(19)	2.7309(14)	168.4(17)
O(23)-H(23B)…O(1)#2	0.885(18)	1.898(19)	2.7766(15)	171.8(17)
O(24)-H(24A)…O(21)#3	1.01(2)	1.90(2)	2.8917(16)	166.5(17)
O(24)-H(24B)…O(25)	0.95(2)	2.06(2)	2.9233(17)	151.3(18)
O(25)-H(25A)…O(21)#4	0.864(17)	2.032(17)	2.8763(16)	165.4(15)
O(25)-H(25B)…O(23)#5	0.833(17)	1.924(18)	2.7542(16)	174.7(16)

Symmetry transformations used to generate equivalent atoms:

#1 -x+1,-y,-z+1
#2 -x+1,y+1/2,-z+1/2
#3 -x+1,-y,-z
#4 -x,-y,-z
#5 -x+1,y-1/2,-z+1/2

Crystal Structure Analysis of AEDO3A-Gd

Crystallographic data have been deposited with the CCDC as supplementary publication CCDC 204982. These data can be obtained free of charge via http://www.ccdc.cam.ac.uk/ conts/retrieving.html (or from CCDC, 12 Union Road, Cambridge CB2 1EZ, UK; fax: +44 1223 335033; or deposit@ccdc.cam.ac.uk). Structure factors are available from the author via email: xray@caltech.edu.

Table A.2.1. Crystal data and structure refinement for AEDO3A-Gd.

Empirical formula	$C_{16}H_{31}N_5O_6 \cdot 5(H_2O)$	
Formula weight	479.54	
Crystallization Solvent	Water	
Crystal Habit	Block	
Crystal size	0.33 x 0.22 x 0.22 mm^3	
Crystal color	Colorless	
	Data Collection	
Preliminary Photos	Rotation	
Type of diffractometer	Bruker SMART 1000	
Wavelength	0.71073 Å Mo Kα	
Data Collection Temperature	98(2) K	
θ range for 15223 reflections used in lattice determination	2.42 to 28.19°	
Unit cell dimensions	a = 10.2547(5) Å	α = 69.1670(10)°
	b = 15.5284(8) Å	β = 76.6460(10)°
	c = 17.3478(9) Å	γ = 87.8020(10)°
Volume	2509.1(2) $Å^3$	
Z	4	
Crystal system	Triclinic	
Space group	P-1	
Density (calculated)	1.773 Mg/m^3	
F(000)	1364	
Data collection program	Bruker SMART v5.054	
θ range for data collection	1.53 to 28.36°	
Completeness to θ = 28.19°	91.5 %	
Index ranges	$-13 \le h \le 13$, $-20 \le k \le 20$, $-23 \le l \le 22$	
Data collection scan type	ω scans at 7 ϕ settings	

Table A.2.1. Crystal data and structure refinement for AEDO3A-Gd.

Data reduction program	Bruker SAINT v6.022
Reflections collected	51532
Independent Reflections	11495 [R_{int}= 0.0531]
Absorption coefficient	2.715 mm^{-1}
Absorption correction	None

Structure solution and Refinement

Structure solution program	SHELXS-97 (Sheldrick, 1990)
Primary solution method	Direct methods
Secondary solution method	Difference Fourier map
Hydrogen placement	Geometric positions
Structure refinement program	SHELXL-97 (Sheldrick, 1997)
Refinement method	Full matrix least-squares on F^2
Data / restraints / parameters	11495 / 38 / 717
Treatment of hydrogen atoms	Riding
Goodness-of-fit on F^2	1.234
Final R indices [I>2σ(I), 3978 reflections]	R1 = 0.0247, ωR2 = 0.0469
R indices (all data)	R1 = 0.0380, ωR2 = 0.0490
Type of weighting scheme used	Sigma
Weighting scheme used	$\omega=1/\sigma^2(Fo^2)$
Max shift/error	0.006
Average shift/error	0.000
Largest diff. peak and hole	1.211 and -0.666 e.$Å^{-3}$

Special Refinement Details

Restraints were placed on the geometry of all water molecules or ligands. All O-H and H-H distances were set to refine to a common target (within a reasonable esd). All distances and angles are listed in Tables A.2.3 and A.2.4 and hydrogen bonds distances and angles are listed in Table A.2.7.

Refinement of F^2 against ALL reflections. The weighted R-factor (ωR) and goodness of fit (S) are based on F^2, conventional R-factors (R) are based on F, with F set to zero for negative F2. The threshold expression of $F^2 > 2\sigma(F^2)$ is used only for calculating R-factors (gt) etc. and is not relevant to the choice of reflections for refinement. R-factors based on F^2 are statistically about twice as large as those based on F, and R-factors based on ALL data will be even larger.

All esds (except the esd in the dihedral angle between two l.s. planes) are estimated using the full covariance matrix. The cell esds are taken into account individually in the estimation of esds in distances, angles and torsion angles; correlations between esds in cell parameters are only used when they are defined by crystal symmetry. An approximate (isotropic) treatment of cell esds is used for estimating esds involving l.s. planes.

Table A.2.2. Atomic coordinates (x 10^4) and equivalent isotropic displacement parameters ($Å^2$x 10^3) for AEDO3A-Gd. U_{eq} is defined as the trace of the orthogonalized U^{ij} tensor.

	x	y	z	U_{eq}
Gd(A)	8153(1)	2985(1)	4434(1)	8(1)
O(1A)	7942(2)	4510(1)	4358(1)	14(1)
O(2A)	6623(2)	3324(1)	3544(1)	14(1)
O(3A)	9109(2)	2047(1)	3675(1)	12(1)
O(4A)	8252(2)	5677(1)	4763(1)	15(1)
O(5A)	4591(2)	3634(1)	3290(1)	23(1)
O(6A)	9138(2)	772(1)	3370(1)	15(1)
O(A)	9335(2)	3967(1)	2988(1)	14(1)
N(1A)	7977(2)	3193(1)	5919(2)	11(1)
N(2A)	5611(2)	3071(1)	5232(2)	12(1)
N(3A)	6696(2)	1440(1)	4867(2)	11(1)
N(4A)	9128(2)	1557(2)	5509(2)	14(1)
N(5A)	10658(2)	3212(2)	4414(2)	15(1)
C(1A)	6576(3)	2978(2)	6436(2)	15(1)
C(2A)	5558(3)	3428(2)	5933(2)	15(1)
C(3A)	4860(3)	2162(2)	5601(2)	14(1)
C(4A)	5236(3)	1579(2)	5053(2)	13(1)
C(5A)	7030(3)	729(2)	5624(2)	14(1)
C(6A)	8511(3)	673(2)	5583(2)	16(1)
C(7A)	8859(3)	1611(2)	6369(2)	16(1)
C(8A)	8900(3)	2578(2)	6391(2)	16(1)
C(9A)	8348(3)	4168(2)	5743(2)	13(1)
C(10A)	8148(3)	4838(2)	4896(2)	11(1)
C(11A)	4994(3)	3714(2)	4570(2)	15(1)
C(12A)	5413(3)	3541(2)	3733(2)	13(1)
C(13A)	7064(3)	1136(2)	4134(2)	12(1)
C(14A)	8553(3)	1317(2)	3697(2)	10(1)
C(15A)	10588(3)	1537(2)	5137(2)	17(1)
C(16A)	11356(3)	2424(2)	4906(2)	17(1)
Gd(B)	1882(1)	6946(1)	10590(1)	8(1)
O(1B)	864(2)	7907(1)	11317(1)	11(1)
O(2B)	3364(2)	6813(1)	11477(1)	13(1)
O(3B)	2169(2)	5396(1)	10717(1)	13(1)
O(4B)	756(2)	9177(1)	11636(1)	15(1)
O(5B)	5337(2)	6470(1)	11819(1)	18(1)
O(6B)	1774(2)	4170(1)	10403(1)	16(1)
O(B)	764(2)	5930(1)	12070(1)	13(1)
N(1B)	3212(2)	8552(1)	10109(1)	11(1)
N(2B)	4417(2)	6886(2)	9846(2)	11(1)
N(3B)	2164(2)	6619(2)	9125(1)	12(1)
N(4B)	873(2)	8256(2)	9419(2)	15(1)
N(5B)	-589(2)	6634(2)	10670(2)	13(1)
C(1B)	4689(3)	8464(2)	9903(2)	13(1)
C(2B)	5094(3)	7824(2)	9413(2)	14(1)
C(3B)	4554(3)	6427(2)	9212(2)	16(1)
C(4B)	3595(3)	6792(2)	8643(2)	17(1)
C(5B)	1310(3)	7225(2)	8579(2)	17(1)
C(6B)	1370(3)	8195(2)	8563(2)	19(1)
C(7B)	1311(3)	9166(2)	9399(2)	17(1)

Table A.2.2. Atomic coordinates (x 10^4) and equivalent isotropic displacement parameters ($Å^2$x 10^3) for AEDO3A-Gd. U_{eq} is defined as the trace of the orthogonalized U^{ij} tensor.

	x	y	z	U_{eq}
C(8B)	2813(3)	9229(2)	9358(2)	15(1)
C(9B)	2839(3)	8882(2)	10828(2)	13(1)
C(10B)	1370(3)	8652(2)	11289(2)	12(1)
C(11B)	5040(3)	6326(2)	10548(2)	15(1)
C(12B)	4560(3)	6560(2)	11342(2)	13(1)
C(13B)	1749(3)	5645(2)	9355(2)	14(1)
C(14B)	1933(3)	5024(2)	10220(2)	12(1)
C(15B)	-635(3)	8161(2)	9627(2)	22(1)
C(16B)	-1257(3)	7513(2)	10503(2)	20(1)
O(1)	2453(2)	510(1)	1672(2)	20(1)
O(2)	1759(2)	1560(1)	2632(2)	17(1)
O(3)	3907(3)	1845(2)	3270(2)	26(1)
O(4)	1560(2)	3424(1)	2108(1)	18(1)
O(5)	2533(3)	4671(2)	2703(2)	22(1)
O(6)	7395(2)	5418(1)	2330(2)	19(1)
O(7)	6062(2)	8262(2)	1744(2)	24(1)
O(8)	8511(2)	6486(1)	3031(2)	19(1)
O(9)	8216(2)	8349(1)	2458(2)	18(1)
O(10)	7332(2)	9545(2)	3311(2)	23(1)
O(11)	4435(2)	9277(1)	7398(1)	21(1)
O(12)	4306(2)	9378(1)	2327(2)	21(1)

Table A.2.3. Bond lengths [Å] for AEDO3A-Gd.

Gd(A)-O(1A)	2.3284(17)	Gd(B)-O(1B)	2.3480(18)
Gd(A)-O(3A)	2.3408(18)	Gd(B)-O(3B)	2.3500(17)
Gd(A)-O(2A)	2.3660(19)	Gd(B)-O(2B)	2.3564(19)
Gd(A)-OA	2.471(2)	Gd(B)-OB	2.508(2)
Gd(A)-N(5A)	2.597(2)	Gd(B)-N(5B)	2.560(2)
Gd(A)-N(3A)	2.650(2)	Gd(B)-N(2B)	2.637(2)
Gd(A)-N(1A)	2.672(2)	Gd(B)-N(1B)	2.652(2)
Gd(A)-N(4A)	2.672(2)	Gd(B)-N(4B)	2.684(2)
Gd(A)-N(2A)	2.677(2)	Gd(B)-N(3B)	2.715(2)
O(1A)-C(10A)	1.270(3)	O(1B)-C(10B)	1.268(3)
O(2A)-C(12A)	1.272(3)	O(2B)-C(12B)	1.268(3)
O(3A)-C(14A)	1.273(3)	O(3B)-C(14B)	1.264(3)
O(4A)-C(10A)	1.244(3)	O(4B)-C(10B)	1.248(3)
O(5A)-C(12A)	1.238(3)	O(5B)-C(12B)	1.246(3)
O(6A)-C(14A)	1.242(3)	O(6B)-C(14B)	1.257(3)
OA-HA1	0.70(3)	OB-HB1	0.83(3)
OA-HA2	0.73(3)	OB-HB2	0.71(3)
N(1A)-C(9A)	1.481(3)	N(1B)-C(9B)	1.479(3)
N(1A)-C(1A)	1.487(4)	N(1B)-C(8B)	1.485(3)
N(1A)-C(8A)	1.487(3)	N(1B)-C(1B)	1.487(3)
N(2A)-C(11A)	1.480(3)	N(2B)-C(11B)	1.487(3)
N(2A)-C(3A)	1.486(3)	N(2B)-C(3B)	1.488(4)
N(2A)-C(2A)	1.495(4)	N(2B)-C(2B)	1.492(3)
N(3A)-C(13A)	1.475(3)	N(3B)-C(13B)	1.474(3)
N(3A)-C(4A)	1.481(3)	N(3B)-C(4B)	1.493(4)
N(3A)-C(5A)	1.486(3)	N(3B)-C(5B)	1.495(3)
N(4A)-C(6A)	1.485(4)	N(4B)-C(7B)	1.486(4)
N(4A)-C(7A)	1.486(4)	N(4B)-C(6B)	1.491(4)
N(4A)-C(15A)	1.491(4)	N(4B)-C(15B)	1.505(4)
N(5A)-C(16A)	1.487(3)	N(5B)-C(16B)	1.469(3)
N(5A)-H(5A1)	0.9200	N(5B)-H(5B1)	0.9200
N(5A)-H(5A2)	0.9200	N(5B)-H(5B2)	0.9200
C(1A)-C(2A)	1.506(4)	C(1B)-C(2B)	1.513(4)
C(1A)-H(1A1)	0.9900	C(1B)-H(1B1)	0.9900
C(1A)-H(1A2)	0.9900	C(1B)-H(1B2)	0.9900
C(2A)-H(2A1)	0.9900	C(2B)-H(2B1)	0.9900
C(2A)-H(2A2)	0.9900	C(2B)-H(2B2)	0.9900
C(3A)-C(4A)	1.514(4)	C(3B)-C(4B)	1.507(4)
C(3A)-H(3A1)	0.9900	C(3B)-H(3B1)	0.9900
C(3A)-H(3A2)	0.9900	C(3B)-H(3B2)	0.9900
C(4A)-H(4A1)	0.9900	C(4B)-H(4B1)	0.9900
C(4A)-H(4A2)	0.9900	C(4B)-H(4B2)	0.9900
C(5A)-C(6A)	1.504(4)	C(5B)-C(6B)	1.501(4)
C(5A)-H(5A3)	0.9900	C(5B)-H(5B3)	0.9900
C(5A)-H(5A4)	0.9900	C(5B)-H(5B4)	0.9900
C(6A)-H(6A1)	0.9900	C(6B)-H(6B1)	0.9900
C(6A)-H(6A2)	0.9900	C(6B)-H(6B2)	0.9900
C(7A)-C(8A)	1.518(4)	C(7B)-C(8B)	1.530(4)
C(7A)-H(7A1)	0.9900	C(7B)-H(7B1)	0.9900

Table A.2.3. Bond lengths [Å] for AEDO3A-Gd.

C(7A)-H(7A2)	0.9900	C(7B)-H(7B2)	0.9900
C(8A)-H(8A1)	0.9900	C(8B)-H(8B1)	0.9900
C(8A)-H(8A2)	0.9900	C(8B)-H(8B2)	0.9900
C(9A)-C(10A)	1.522(4)	C(9B)-C(10B)	1.522(4)
C(9A)-H(9A1)	0.9900	C(9B)-H(9B1)	0.9900
C(9A)-H(9A2)	0.9900	C(9B)-H(9B2)	0.9900
C(11A)-C(12A)	1.531(4)	C(11B)-C(12B)	1.516(4)
C(11A)-H(11A)	0.9900	C(11B)-H(11C)	0.9900
C(11A)-H(11B)	0.9900	C(11B)-H(11D)	0.9900
C(13A)-C(14A)	1.527(4)	C(13B)-C(14B)	1.518(4)
C(13A)-H(13A)	0.9900	C(13B)-H(13C)	0.9900
C(13A)-H(13B)	0.9900	C(13B)-H(13D)	0.9900
C(15A)-C(16A)	1.491(4)	C(15B)-C(16B)	1.498(4)
C(15A)-H(15A)	0.9900	C(15B)-H(15C)	0.9900
C(15A)-H(15B)	0.9900	C(15B)-H(15D)	0.9900
C(16A)-H(16A)	0.9900	C(16B)-H(16C)	0.9900
C(16A)-H(16B)	0.9900	C(16B)-H(16D)	0.9900
O(1)-H(1E)	0.89(3)	O(7)-H(7E)	0.78(3)
O(1)-H(1F)	0.80(3)	O(7)-H(7F)	0.79(3)
O(2)-H(2E)	0.81(3)	O(8)-H(8E)	0.75(3)
O(2)-H(2F)	0.84(3)	O(8)-H(8F)	0.73(3)
O(3)-H(3E)	0.75(3)	O(9)-H(9E)	0.86(3)
O(3)-H(3F)	0.81(3)	O(9)-H(9F)	0.81(3)
O(4)-H(4E)	0.74(3)	O(10)-H(10E)	0.75(3)
O(4)-H(4F)	0.80(3)	O(10)-H(10F)	0.94(3)
O(5)-H(5E)	0.75(3)	O(11)-H(11E)	0.99(3)
O(5)-H(5F)	0.71(3)	O(11)-H(11F)	0.98(3)
O(6)-H(6E)	0.77(3)	O(12)-H(12E)	0.75(3)
O(6)-H(6F)	0.71(3)	O(12)-H(12F)	0.88(3)

Table A.2.4. Bond Angles [°] for AEDO3A-Gd.

O(1A)-Gd(A)-O(3A)	143.67(7)	O(1B)-Gd(B)-O(3B)	143.49(7)
O(1A)-Gd(A)-O(2A)	85.38(7)	O(1B)-Gd(B)-O(2B)	80.26(6)
O(3A)-Gd(A)-O(2A)	84.65(6)	O(3B)-Gd(B)-O(2B)	90.12(6)
O(1A)-Gd(A)-OA	73.00(7)	O(1B)-Gd(B)-OB	72.42(6)
O(3A)-Gd(A)-OA	70.71(6)	O(3B)-Gd(B)-OB	71.13(7)
O(2A)-Gd(A)-OA	71.27(7)	O(2B)-Gd(B)-OB	71.34(7)
O(1A)-Gd(A)-N(5A)	86.28(7)	O(1B)-Gd(B)-N(5B)	79.88(7)
O(3A)-Gd(A)-N(5A)	80.66(7)	O(3B)-Gd(B)-N(5B)	86.16(7)
O(2A)-Gd(A)-N(5A)	142.29(7)	O(2B)-Gd(B)-N(5B)	140.78(7)
OA-Gd(A)-N(5A)	71.12(7)	OB-Gd(B)-N(5B)	70.54(7)
O(1A)-Gd(A)-N(3A)	141.34(7)	O(1B)-Gd(B)-N(2B)	130.08(7)
O(3A)-Gd(A)-N(3A)	67.30(7)	O(3B)-Gd(B)-N(2B)	74.98(7)
O(2A)-Gd(A)-N(3A)	73.75(7)	O(2B)-Gd(B)-N(2B)	66.54(7)
OA-Gd(A)-N(3A)	126.84(7)	OB-Gd(B)-N(2B)	124.85(7)
N(5A)-Gd(A)-N(3A)	129.58(7)	N(5B)-Gd(B)-N(2B)	147.64(7)
O(1A)-Gd(A)-N(1A)	66.59(7)	O(1B)-Gd(B)-N(1B)	66.37(7)
O(3A)-Gd(A)-N(1A)	141.04(6)	O(3B)-Gd(B)-N(1B)	142.72(7)
O(2A)-Gd(A)-N(1A)	130.55(7)	O(2B)-Gd(B)-N(1B)	71.07(7)
OA-Gd(A)-N(1A)	130.06(7)	OB-Gd(B)-N(1B)	127.60(7)
N(5A)-Gd(A)-N(1A)	78.06(7)	N(5B)-Gd(B)-N(1B)	128.73(7)
N(3A)-Gd(A)-N(1A)	103.10(7)	N(2B)-Gd(B)-N(1B)	68.08(7)
O(1A)-Gd(A)-N(4A)	130.66(7)	O(1B)-Gd(B)-N(4B)	76.82(7)
O(3A)-Gd(A)-N(4A)	73.18(7)	O(3B)-Gd(B)-N(4B)	127.29(7)
O(2A)-Gd(A)-N(4A)	141.16(7)	O(2B)-Gd(B)-N(4B)	139.49(7)
OA-Gd(A)-N(4A)	126.81(7)	OB-Gd(B)-N(4B)	130.17(7)
N(5A)-Gd(A)-N(4A)	65.52(7)	N(5B)-Gd(B)-N(4B)	66.14(7)
N(3A)-Gd(A)-N(4A)	68.41(7)	N(2B)-Gd(B)-N(4B)	104.96(7)
N(1A)-Gd(A)-N(4A)	68.38(7)	N(1B)-Gd(B)-N(4B)	69.25(7)
O(1A)-Gd(A)-N(2A)	74.87(7)	O(1B)-Gd(B)-N(3B)	143.19(6)
O(3A)-Gd(A)-N(2A)	130.83(7)	O(3B)-Gd(B)-N(3B)	65.07(7)
O(2A)-Gd(A)-N(2A)	66.02(7)	O(2B)-Gd(B)-N(3B)	132.00(7)
OA-Gd(A)-N(2A)	127.72(7)	OB-Gd(B)-N(3B)	128.58(7)
N(5A)-Gd(A)-N(2A)	145.17(8)	N(5B)-Gd(B)-N(3B)	80.77(7)
N(3A)-Gd(A)-N(2A)	67.02(7)	N(2B)-Gd(B)-N(3B)	67.54(7)
N(1A)-Gd(A)-N(2A)	67.67(7)	N(1B)-Gd(B)-N(3B)	103.70(7)
N(4A)-Gd(A)-N(2A)	105.42(7)	N(4B)-Gd(B)-N(3B)	66.75(7)
C(10A)-O(1A)-Gd(A)	126.53(17)	C(10B)-O(1B)-Gd(B)	126.35(19)
C(12A)-O(2A)-Gd(A)	126.09(18)	C(12B)-O(2B)-Gd(B)	124.83(19)
C(14A)-O(3A)-Gd(A)	125.37(19)	C(14B)-O(3B)-Gd(B)	126.48(17)
Gd(A)-OA-HA1	121(3)	Gd(B)-OB-HB1	114(2)
Gd(A)-OA-HA2	122(3)	Gd(B)-OB-HB2	108(3)
HA1-OA-HA2	113(4)	HB1-OB-HB2	109(3)
C(9A)-N(1A)-C(1A)	108.9(2)	C(9B)-N(1B)-C(8B)	109.3(2)
C(9A)-N(1A)-C(8A)	109.8(2)	C(9B)-N(1B)-C(1B)	109.1(2)
C(1A)-N(1A)-C(8A)	109.7(2)	C(8B)-N(1B)-C(1B)	109.3(2)
C(9A)-N(1A)-Gd(A)	107.94(16)	C(9B)-N(1B)-Gd(B)	106.68(16)
C(1A)-N(1A)-Gd(A)	109.90(16)	C(8B)-N(1B)-Gd(B)	110.34(17)
C(8A)-N(1A)-Gd(A)	110.57(16)	C(1B)-N(1B)-Gd(B)	112.05(15)
C(11A)-N(2A)-C(3A)	109.6(2)	C(11B)-N(2B)-C(3B)	109.7(2)

Table A.2.4. Bond Angles [°] for AEDO3A-Gd.

C(11A)-N(2A)-C(2A)	110.7(2)	C(11B)-N(2B)-C(2B)	110.5(2)
C(3A)-N(2A)-C(2A)	108.0(2)	C(3B)-N(2B)-C(2B)	108.6(2)
C(11A)-N(2A)-Gd(A)	104.83(17)	C(11B)-N(2B)-Gd(B)	104.44(17)
C(3A)-N(2A)-Gd(A)	112.88(16)	C(3B)-N(2B)-Gd(B)	111.54(17)
C(2A)-N(2A)-Gd(A)	110.83(17)	C(2B)-N(2B)-Gd(B)	112.09(16)
C(13A)-N(3A)-C(4A)	109.5(2)	C(13B)-N(3B)-C(4B)	109.9(2)
C(13A)-N(3A)-C(5A)	109.9(2)	C(13B)-N(3B)-C(5B)	109.6(2)
C(4A)-N(3A)-C(5A)	109.0(2)	C(4B)-N(3B)-C(5B)	108.8(2)
C(13A)-N(3A)-Gd(A)	105.91(16)	C(13B)-N(3B)-Gd(B)	107.34(16)
C(4A)-N(3A)-Gd(A)	112.46(15)	C(4B)-N(3B)-Gd(B)	109.89(16)
C(5A)-N(3A)-Gd(A)	110.00(17)	C(5B)-N(3B)-Gd(B)	111.35(17)
C(6A)-N(4A)-C(7A)	108.1(2)	C(7B)-N(4B)-C(6B)	109.2(2)
C(6A)-N(4A)-C(15A)	106.1(2)	C(7B)-N(4B)-C(15B)	110.1(2)
C(7A)-N(4A)-C(15A)	112.6(2)	C(6B)-N(4B)-C(15B)	107.3(2)
C(6A)-N(4A)-Gd(A)	110.60(16)	C(7B)-N(4B)-Gd(B)	107.71(17)
C(7A)-N(4A)-Gd(A)	111.46(16)	C(6B)-N(4B)-Gd(B)	111.28(16)
C(15A)-N(4A)-Gd(A)	107.81(15)	C(15B)-N(4B)-Gd(B)	111.20(16)
C(16A)-N(5A)-Gd(A)	119.27(17)	C(16B)-N(5B)-Gd(B)	108.28(16)
C(16A)-N(5A)-H(5A1)	107.5	C(16B)-N(5B)-H(5B1)	110.0
Gd(A)-N(5A)-H(5A1)	107.5	Gd(B)-N(5B)-H(5B1)	110.0
C(16A)-N(5A)-H(5A2)	107.5	C(16B)-N(5B)-H(5B2)	110.0
Gd(A)-N(5A)-H(5A2)	107.5	Gd(B)-N(5B)-H(5B2)	110.0
H(5A1)-N(5A)-H(5A2)	107.0	H(5B1)-N(5B)-H(5B2)	108.4
N(1A)-C(1A)-C(2A)	112.5(2)	N(1B)-C(1B)-C(2B)	112.0(2)
N(1A)-C(1A)-H(1A1)	109.1	N(1B)-C(1B)-H(1B1)	109.2
C(2A)-C(1A)-H(1A1)	109.1	C(2B)-C(1B)-H(1B1)	109.2
N(1A)-C(1A)-H(1A2)	109.1	N(1B)-C(1B)-H(1B2)	109.2
C(2A)-C(1A)-H(1A2)	109.1	C(2B)-C(1B)-H(1B2)	109.2
H(1A1)-C(1A)-H(1A2)	107.8	H(1B1)-C(1B)-H(1B2)	107.9
N(2A)-C(2A)-C(1A)	110.6(2)	N(2B)-C(2B)-C(1B)	113.7(2)
N(2A)-C(2A)-H(2A1)	109.5	N(2B)-C(2B)-H(2B1)	108.8
C(1A)-C(2A)-H(2A1)	109.5	C(1B)-C(2B)-H(2B1)	108.8
N(2A)-C(2A)-H(2A2)	109.5	N(2B)-C(2B)-H(2B2)	108.8
C(1A)-C(2A)-H(2A2)	109.5	C(1B)-C(2B)-H(2B2)	108.8
H(2A1)-C(2A)-H(2A2)	108.1	H(2B1)-C(2B)-H(2B2)	107.7
N(2A)-C(3A)-C(4A)	112.9(2)	N(2B)-C(3B)-C(4B)	111.4(2)
N(2A)-C(3A)-H(3A1)	109.0	N(2B)-C(3B)-H(3B1)	109.3
C(4A)-C(3A)-H(3A1)	109.0	C(4B)-C(3B)-H(3B1)	109.3
N(2A)-C(3A)-H(3A2)	109.0	N(2B)-C(3B)-H(3B2)	109.3
C(4A)-C(3A)-H(3A2)	109.0	C(4B)-C(3B)-H(3B2)	109.3
H(3A1)-C(3A)-H(3A2)	107.8	H(3B1)-C(3B)-H(3B2)	108.0
N(3A)-C(4A)-C(3A)	112.1(2)	N(3B)-C(4B)-C(3B)	112.3(2)
N(3A)-C(4A)-H(4A1)	109.2	N(3B)-C(4B)-H(4B1)	109.1
C(3A)-C(4A)-H(4A1)	109.2	C(3B)-C(4B)-H(4B1)	109.1
N(3A)-C(4A)-H(4A2)	109.2	N(3B)-C(4B)-H(4B2)	109.1
C(3A)-C(4A)-H(4A2)	109.2	C(3B)-C(4B)-H(4B2)	109.1
H(4A1)-C(4A)-H(4A2)	107.9	H(4B1)-C(4B)-H(4B2)	107.9
N(3A)-C(5A)-C(6A)	113.7(2)	N(3B)-C(5B)-C(6B)	111.3(2)
N(3A)-C(5A)-H(5A3)	108.8	N(3B)-C(5B)-H(5B3)	109.4
C(6A)-C(5A)-H(5A3)	108.8	C(6B)-C(5B)-H(5B3)	109.4
N(3A)-C(5A)-H(5A4)	108.8	N(3B)-C(5B)-H(5B4)	109.4

Table A.2.4. Bond Angles [°] for AEDO3A-Gd.

C(6A)-C(5A)-H(5A4)	108.8	C(6B)-C(5B)-H(5B4)	109.4
H(5A3)-C(5A)-H(5A4)	107.7	H(5B3)-C(5B)-H(5B4)	108.0
N(4A)-C(6A)-C(5A)	112.2(2)	N(4B)-C(6B)-C(5B)	112.6(2)
N(4A)-C(6A)-H(6A1)	109.2	N(4B)-C(6B)-H(6B1)	109.1
C(5A)-C(6A)-H(6A1)	109.2	C(5B)-C(6B)-H(6B1)	109.1
N(4A)-C(6A)-H(6A2)	109.2	N(4B)-C(6B)-H(6B2)	109.1
C(5A)-C(6A)-H(6A2)	109.2	C(5B)-C(6B)-H(6B2)	109.1
H(6A1)-C(6A)-H(6A2)	107.9	H(6B1)-C(6B)-H(6B2)	107.8
N(4A)-C(7A)-C(8A)	115.3(2)	N(4B)-C(7B)-C(8B)	112.3(2)
N(4A)-C(7A)-H(7A1)	108.5	N(4B)-C(7B)-H(7B1)	109.2
C(8A)-C(7A)-H(7A1)	108.5	C(8B)-C(7B)-H(7B1)	109.2
N(4A)-C(7A)-H(7A2)	108.5	N(4B)-C(7B)-H(7B2)	109.2
C(8A)-C(7A)-H(7A2)	108.5	C(8B)-C(7B)-H(7B2)	109.2
H(7A1)-C(7A)-H(7A2)	107.5	H(7B1)-C(7B)-H(7B2)	107.9
N(1A)-C(8A)-C(7A)	112.7(2)	N(1B)-C(8B)-C(7B)	113.4(2)
N(1A)-C(8A)-H(8A1)	109.1	N(1B)-C(8B)-H(8B1)	108.9
C(7A)-C(8A)-H(8A1)	109.1	C(7B)-C(8B)-H(8B1)	108.9
N(1A)-C(8A)-H(8A2)	109.1	N(1B)-C(8B)-H(8B2)	108.9
C(7A)-C(8A)-H(8A2)	109.1	C(7B)-C(8B)-H(8B2)	108.9
H(8A1)-C(8A)-H(8A2)	107.8	H(8B1)-C(8B)-H(8B2)	107.7
N(1A)-C(9A)-C(10A)	114.4(2)	N(1B)-C(9B)-C(10B)	112.2(2)
N(1A)-C(9A)-H(9A1)	108.7	N(1B)-C(9B)-H(9B1)	109.2
C(10A)-C(9A)-H(9A1)	108.7	C(10B)-C(9B)-H(9B1)	109.2
N(1A)-C(9A)-H(9A2)	108.7	N(1B)-C(9B)-H(9B2)	109.2
C(10A)-C(9A)-H(9A2)	108.7	C(10B)-C(9B)-H(9B2)	109.2
H(9A1)-C(9A)-H(9A2)	107.6	H(9B1)-C(9B)-H(9B2)	107.9
O(4A)-C(10A)-O(1A)	124.1(3)	O(4B)-C(10B)-O(1B)	124.2(3)
O(4A)-C(10A)-C(9A)	117.6(3)	O(4B)-C(10B)-C(9B)	119.3(2)
O(1A)-C(10A)-C(9A)	118.3(2)	O(1B)-C(10B)-C(9B)	116.5(2)
N(2A)-C(11A)-C(12A)	111.8(2)	N(2B)-C(11B)-C(12B)	112.7(2)
N(2A)-C(11A)-H(11A)	109.2	N(2B)-C(11B)-H(11C)	109.0
C(12A)-C(11A)-H(11A)	109.2	C(12B)-C(11B)-H(11C)	109.0
N(2A)-C(11A)-H(11B)	109.2	N(2B)-C(11B)-H(11D)	109.0
C(12A)-C(11A)-H(11B)	109.2	C(12B)-C(11B)-H(11D)	109.0
H(11A)-C(11A)-H(11B)	107.9	H(11C)-C(11B)-H(11D)	107.8
O(5A)-C(12A)-O(2A)	125.2(3)	O(5B)-C(12B)-O(2B)	125.0(3)
O(5A)-C(12A)-C(11A)	119.4(3)	O(5B)-C(12B)-C(11B)	118.7(3)
O(2A)-C(12A)-C(11A)	115.4(3)	O(2B)-C(12B)-C(11B)	116.3(3)
N(3A)-C(13A)-C(14A)	112.7(2)	N(3B)-C(13B)-C(14B)	113.9(2)
N(3A)-C(13A)-H(13A)	109.0	N(3B)-C(13B)-H(13C)	108.8
C(14A)-C(13A)-H(13A)	109.0	C(14B)-C(13B)-H(13C)	108.8
N(3A)-C(13A)-H(13B)	109.0	N(3B)-C(13B)-H(13D)	108.8
C(14A)-C(13A)-H(13B)	109.0	C(14B)-C(13B)-H(13D)	108.8
H(13A)-C(13A)-H(13B)	107.8	H(13C)-C(13B)-H(13D)	107.7
O(6A)-C(14A)-O(3A)	124.0(3)	O(6B)-C(14B)-O(3B)	124.7(3)
O(6A)-C(14A)-C(13A)	119.4(2)	O(6B)-C(14B)-C(13B)	116.8(3)
O(3A)-C(14A)-C(13A)	116.5(2)	O(3B)-C(14B)-C(13B)	118.4(2)
C(16A)-C(15A)-N(4A)	114.1(2)	C(16B)-C(15B)-N(4B)	114.7(2)
C(16A)-C(15A)-H(15A)	108.7	C(16B)-C(15B)-H(15C)	108.6
N(4A)-C(15A)-H(15A)	108.7	N(4B)-C(15B)-H(15C)	108.6
C(16A)-C(15A)-H(15B)	108.7	C(16B)-C(15B)-H(15D)	108.6

Table A.2.4. Bond Angles [°] for AEDO3A-Gd.

N(4A)-C(15A)-H(15B)	108.7	N(4B)-C(15B)-H(15D)	108.6
H(15A)-C(15A)-H(15B)	107.6	H(15C)-C(15B)-H(15D)	107.6
N(5A)-C(16A)-C(15A)	110.6(2)	N(5B)-C(16B)-C(15B)	109.7(2)
N(5A)-C(16A)-H(16A)	109.5	N(5B)-C(16B)-H(16C)	109.7
C(15A)-C(16A)-H(16A)	109.5	C(15B)-C(16B)-H(16C)	109.7
N(5A)-C(16A)-H(16B)	109.5	N(5B)-C(16B)-H(16D)	109.7
C(15A)-C(16A)-H(16B)	109.5	C(15B)-C(16B)-H(16D)	109.7
H(16A)-C(16A)-H(16B)	108.1	H(16C)-C(16B)-H(16D)	108.2
H(1E)-O(1)-H(1F)	108(3)	H(7E)-O(7)-H(7F)	104(3)
H(2E)-O(2)-H(2F)	101(3)	H(8E)-O(8)-H(8F)	111(4)
H(3E)-O(3)-H(3F)	101(3)	H(9E)-O(9)-H(9F)	116(3)
H(4E)-O(4)-H(4F)	113(3)	H(10E)-O(10)-H(10F)	101(3)
H(5E)-O(5)-H(5F)	106(4)	H(11E)-O(11)-H(11F)	110(2)
H(6E)-O(6)-H(6F)	104(4)	H(12E)-O(12)-H(12F)	103(3)

Table A.2.5. Anisotropic displacement parameters ($Å^2 x\ 10^4$) for AEDO3A-Gd. The anisotropic displacement factor exponent takes the form: The anisotropic displacement factor exponent takes the form:

$-2\pi^2[\ h^2\ a^{*2}U^{11} + \ldots + 2\ h\ k\ a^*\ b^*\ U^{12}\ ]$

	U^{11}	U^{22}	U^{33}	U^{23}	U^{13}	U^{12}
O(1A)	177(12)	115(9)	125(11)	-51(8)	-33(9)	4(8)
O(2A)	122(12)	183(10)	119(11)	-50(8)	-35(9)	21(8)
O(3A)	137(12)	85(9)	118(11)	-32(8)	-19(9)	11(8)
O(4A)	159(12)	100(9)	206(12)	-74(8)	-24(9)	0(8)
O(5A)	184(13)	274(11)	272(13)	-105(10)	-140(10)	80(10)
O(6A)	177(12)	136(9)	130(11)	-70(8)	-9(9)	14(8)
O(A)	158(13)	99(9)	145(12)	-34(9)	-9(10)	10(9)
N(1A)	106(13)	111(11)	114(13)	-34(10)	-17(10)	-32(9)
N(2A)	131(14)	110(11)	111(13)	-39(10)	-32(11)	8(10)
N(3A)	116(14)	101(11)	114(13)	-42(10)	-11(11)	-10(10)
N(4A)	126(13)	142(11)	117(13)	-14(10)	-32(10)	24(10)
N(5A)	143(14)	150(11)	137(14)	-40(10)	-41(11)	-3(10)
C(1A)	146(16)	215(14)	121(16)	-99(12)	-12(13)	-36(12)
C(2A)	152(17)	147(13)	164(16)	-99(12)	30(13)	-24(12)
C(3A)	122(17)	147(14)	153(17)	-74(12)	-2(14)	-17(12)
C(4A)	98(16)	139(13)	150(17)	-57(12)	-17(13)	-25(12)
C(5A)	177(17)	90(12)	136(16)	-20(12)	-18(13)	-14(11)
C(6A)	249(18)	78(12)	120(15)	-1(11)	-68(13)	46(12)
C(7A)	184(17)	141(13)	137(16)	1(12)	-76(13)	-6(12)
C(8A)	199(17)	181(14)	88(15)	-15(12)	-85(13)	10(12)
C(9A)	144(16)	145(13)	138(16)	-83(12)	-46(13)	5(12)
C(10A)	53(15)	117(13)	176(16)	-87(12)	5(12)	-13(11)
C(11A)	118(16)	158(13)	174(16)	-69(12)	-50(13)	34(12)
C(12A)	121(16)	102(13)	168(16)	-17(12)	-61(13)	-5(11)
C(13A)	137(16)	115(13)	114(16)	-62(11)	-25(13)	-22(11)
C(14A)	163(17)	78(12)	75(15)	-16(11)	-57(13)	15(11)
C(15A)	141(15)	178(14)	166(16)	-36(12)	-37(13)	47(12)
C(16A)	137(15)	190(14)	176(16)	-70(13)	-36(13)	43(12)
Gd(B)	80(1)	85(1)	81(1)	-31(1)	-25(1)	-2(1)
O(1B)	110(11)	103(9)	111(11)	-37(8)	-7(9)	-17(8)
O(2B)	106(11)	141(9)	138(11)	-46(8)	-47(9)	7(8)
O(3B)	172(12)	118(9)	119(11)	-54(8)	-31(9)	-4(8)
O(4B)	173(12)	124(9)	164(12)	-72(9)	-34(10)	32(8)
O(5B)	153(12)	199(10)	238(12)	-88(9)	-114(10)	40(9)
O(6B)	183(12)	125(9)	201(12)	-96(9)	-40(9)	-16(8)
O(B)	126(13)	137(10)	129(12)	-45(9)	-43(9)	31(8)
N(1B)	96(14)	122(11)	98(13)	-48(10)	-4(11)	-4(10)
N(2B)	86(13)	125(11)	128(13)	-66(10)	-13(11)	-14(10)
N(3B)	130(13)	157(11)	82(12)	-32(10)	-32(10)	-33(10)
N(4B)	127(14)	141(11)	150(14)	4(10)	-35(11)	-6(10)
N(5B)	150(14)	125(11)	99(13)	-28(10)	-19(11)	-21(10)
C(1B)	112(16)	124(13)	139(16)	-51(12)	0(13)	-21(12)

Table A.2.5. Anisotropic displacement parameters ($Å^2 x\ 10^4$) for AEDO3A-Gd. The anisotropic displacement factor exponent takes the form: The anisotropic displacement factor exponent takes the form:

$-2\pi^2[\ h^2\ a^{*2}U^{11} + \ldots + 2\ h\ k\ a^*\ b^*\ U^{12}\ ]$

	U^{11}	U^{22}	U^{33}	U^{23}	U^{13}	U^{12}
C(2B)	112(17)	134(13)	147(17)	-30(12)	0(13)	-51(12)
C(3B)	138(16)	173(14)	175(16)	-104(12)	30(13)	-18(12)
C(4B)	171(17)	231(15)	95(15)	-71(12)	42(13)	-72(13)
C(5B)	199(17)	196(14)	100(15)	-11(12)	-58(13)	-69(12)
C(6B)	267(19)	194(14)	79(15)	4(12)	-78(13)	-29(13)
C(7B)	231(18)	156(14)	103(15)	-20(12)	-42(13)	73(13)
C(8B)	231(18)	92(13)	127(16)	-30(12)	-43(14)	2(12)
C(9B)	163(17)	107(13)	147(16)	-66(12)	-35(14)	-9(12)
C(10B)	142(17)	126(13)	73(15)	-16(11)	-49(13)	31(12)
C(11B)	104(16)	138(13)	211(17)	-62(12)	-51(13)	37(12)
C(12B)	171(18)	70(12)	152(16)	-18(11)	-53(13)	10(12)
C(13B)	146(16)	148(13)	145(16)	-83(12)	-25(13)	-41(12)
C(14B)	64(15)	174(14)	126(15)	-59(12)	-3(12)	10(11)
C(15B)	166(16)	238(16)	226(17)	-34(14)	-89(14)	76(13)
C(16B)	118(15)	215(15)	271(18)	-99(14)	-27(14)	8(12)
O(1)	217(13)	159(11)	226(13)	-81(10)	-63(11)	12(9)
O(2)	139(13)	171(11)	220(13)	-105(9)	-1(10)	1(9)
O(3)	285(16)	254(12)	345(15)	-165(12)	-170(12)	63(11)
O(4)	245(13)	106(10)	172(12)	-36(9)	-28(11)	-5(9)
O(5)	277(15)	192(11)	301(15)	-131(10)	-214(12)	100(10)
O(6)	159(13)	151(10)	233(13)	-8(10)	-89(11)	18(10)
O(7)	229(15)	210(11)	362(15)	-156(11)	-144(12)	52(11)
O(8)	204(13)	174(11)	176(12)	-62(10)	-36(11)	-28(9)
O(9)	170(13)	135(10)	249(14)	-83(10)	-34(10)	-7(9)
O(10)	240(14)	185(11)	290(14)	-166(10)	3(11)	-16(10)
O(11)	217(13)	239(11)	179(13)	-84(10)	-49(10)	21(10)
O(12)	209(14)	183(11)	240(13)	-86(10)	-9(11)	-15(9)

Table A.2.6. Hydrogen coordinates (x 10^4) and isotropic displacement parameters ($Å^2$ x 10^3) for AEDO3A-Gd.

	x	y	z	U_{iso}
H(A1)	9370(30)	4450(20)	2860(20)	17
H(A2)	9860(30)	3790(20)	2720(20)	17
H(5A1)	11131	3404	3857	17
H(5A2)	10723	3689	4603	17
H(1A1)	6475	3189	6921	18
H(1A2)	6396	2301	6667	18
H(2A1)	4649	3301	6312	18
H(2A2)	5743	4105	5691	18
H(3A1)	3887	2263	5681	17
H(3A2)	5038	1822	6166	17
H(4A1)	4745	971	5346	15
H(4A2)	4958	1883	4513	15
H(5A3)	6667	120	5686	17
H(5A4)	6582	866	6134	17
H(6A1)	8657	179	6100	19
H(6A2)	8958	506	5088	19
H(7A1)	9528	1250	6667	19
H(7A2)	7963	1314	6690	19
H(8A1)	8654	2542	6988	19
H(8A2)	9828	2849	6142	19
H(9A1)	9302	4214	5756	16
H(9A2)	7805	4358	6202	16
H(11A)	5266	4356	4473	17
H(11B)	4005	3642	4769	17
H(13A)	6528	1463	3719	14
H(13B)	6836	467	4327	14
H(15A)	10980	1044	5549	20
H(15B)	10694	1378	4622	20
H(16A)	11452	2512	5429	20
H(16B)	12266	2402	4565	20
H(B1)	320(30)	6210(20)	12360(20)	16
H(B2)	1270(30)	5700(20)	12270(20)	16
H(5B1)	-656	6381	10274	15
H(5B2)	-990	6224	11199	15
H(1B1)	5003	8226	10436	15
H(1B2)	5133	9081	9564	15
H(2B1)	4882	8105	8850	17
H(2B2)	6077	7762	9320	17
H(3B1)	4375	5754	9511	19
H(3B2)	5485	6531	8862	19
H(4B1)	3782	7464	8340	21
H(4B2)	3745	6494	8213	21
H(5B3)	369	6975	8798	21
H(5B4)	1619	7225	7994	21
H(6B1)	2310	8447	8332	22
H(6B2)	824	8581	8178	22
H(7B1)	798	9273	9912	21
H(7B2)	1107	9657	8898	21

Table A.2.6. Hydrogen coordinates (x 10^4) and isotropic displacement parameters ($Å^2$ x 10^3) for AEDO3A-Gd.

H(8B1)	3323	9127	8841	18
H(8B2)	3061	9859	9310	18
H(9B1)	3012	9559	10616	16
H(9B2)	3409	8596	11233	16
H(11C)	6027	6430	10357	18
H(11D)	4827	5664	10685	18
H(13C)	2274	5412	8921	17
H(13D)	791	5607	9346	17
H(15C)	-996	8778	9557	26
H(15D)	-910	7945	9213	26
H(16C)	-1167	7788	10924	24
H(16D)	-2225	7405	10558	24
H(1E)	3090(30)	170(20)	1890(20)	23
H(1F)	1890(30)	170(20)	1670(20)	23
H(2E)	1010(30)	1340(20)	2900(20)	21
H(2F)	2010(30)	1200(20)	2370(20)	21
H(3E)	4050(40)	2350(20)	3120(20)	32
H(3F)	3300(40)	1820(20)	3050(20)	32
H(4E)	1610(30)	3650(20)	1650(20)	22
H(4F)	1490(30)	2880(20)	2260(20)	22
H(5E)	3110(30)	4500(20)	2910(20)	27
H(5F)	2480(40)	4390(20)	2470(20)	27
H(6E)	6710(30)	5580(20)	2240(20)	23
H(6F)	7290(30)	4930(20)	2550(20)	23
H(7E)	5910(30)	7750(20)	1830(20)	29
H(7F)	6710(30)	8260(20)	1910(20)	29
H(8E)	8470(30)	6280(20)	3500(20)	22
H(8F)	8100(30)	6210(20)	2900(20)	22
H(9E)	8960(30)	8630(20)	2140(20)	22
H(9F)	8230(30)	7790(20)	2680(20)	22
H(10E)	7660(30)	9230(20)	3090(20)	27
H(10F)	8090(30)	9890(20)	3280(20)	27
H(11E)	5020(30)	8990(20)	7027(19)	25
H(11F)	3830(30)	9690(20)	7090(20)	25
H(12E)	4760(30)	9710(20)	2370(20)	26
H(12F)	4860(30)	9020(20)	2130(20)	26

Table A.2.7. Hydrogen bonds for AEDO3A-Gd [Å and °].

D-H…A	d(D-H)	d(H…A)	d(D…A)	<(DHA)
N(5A)-H(5A1)…O(5)#1	0.92	2.46	3.248(4)	144.4
N(5A)-H(5A2)…O(4A)#2	0.92	2.16	2.984(3)	148.4
N(5B)-H(5B1)…O(6B)#3	0.92	2.20	3.052(3)	153.7
N(5B)-H(5B2)…O(6)#4	0.92	2.25	3.133(3)	160.1
O(1)-H(1E)…O(12)#5	0.89(3)	1.82(3)	2.704(3)	175(3)
O(1)-H(1F)…O(4B)#6	0.80(3)	1.99(3)	2.781(3)	170(3)
O(2)-H(2E)…O(6A)#7	0.81(3)	2.01(3)	2.812(3)	170(3)
O(2)-H(2E)…O(3A)#7	0.81(3)	2.55(3)	3.126(3)	129(3)
O(2)-H(2F)…O(1)	0.84(3)	1.86(3)	2.690(3)	173(3)
O(3)-H(3E)…O(5A)	0.75(3)	2.22(3)	2.904(3)	153(4)
O(3)-H(3F)…O(2)	0.81(3)	1.99(3)	2.796(3)	171(3)
O(4)-H(4E)…O(6B)#8	0.74(3)	1.99(3)	2.725(3)	175(4)
O(4)-H(4E)…O(3B)#8	0.74(3)	2.62(3)	3.128(3)	128(3)
O(4)-H(4F)…O(2)	0.80(3)	1.94(3)	2.723(3)	166(3)
O(5)-H(5E)…O(5A)	0.75(3)	2.06(3)	2.767(3)	157(3)
O(5)-H(5F)…O(4)	0.71(3)	2.14(3)	2.803(3)	157(4)
O(6)-H(6E)…O(5B)#8	0.77(3)	2.01(3)	2.734(3)	158(3)
O(6)-H(6F)…O(2A)	0.71(3)	2.49(3)	3.193(3)	168(4)
O(7)-H(7E)…O(5B)#8	0.78(3)	2.09(3)	2.859(3)	168(3)
O(7)-H(7F)…O(9)	0.79(3)	2.02(3)	2.799(3)	172(4)
O(8)-H(8E)…O(4A)	0.75(3)	2.02(3)	2.765(3)	176(4)
O(8)-H(8E)…O(1A)	0.75(3)	2.62(3)	3.090(3)	122(3)
O(8)-H(8F)…O(6)	0.73(3)	2.07(3)	2.785(3)	165(4)
O(9)-H(9E)…O(4B)#9	0.86(3)	1.93(3)	2.776(3)	167(3)
O(9)-H(9E)…O(1B)#9	0.86(3)	2.61(3)	3.179(3)	125(2)
O(9)-H(9F)…O(8)	0.81(3)	1.93(3)	2.735(3)	170(3)
O(10)-H(10E)…O(9)	0.75(3)	2.02(3)	2.768(3)	170(4)
O(10)-H(10F)…O(6A)#10	0.94(3)	1.84(3)	2.751(3)	161(3)
O(11)-H(11E)…O(3)#11	0.99(3)	1.80(3)	2.751(3)	159(3)
O(11)-H(11F)…O(10)#12	0.98(3)	1.73(3)	2.706(3)	171(3)
O(12)-H(12E)…O(11)#12	0.75(3)	2.00(3)	2.731(3)	166(4)
O(12)-H(12F)…O(7)	0.88(3)	1.85(3)	2.727(3)	179(3)

Symmetry transformations used to generate equivalent atoms:
#1 x+1,y,z
#2 -x+2,-y+1,-z+1
#3 -x,-y+1,-z+2
#4 x-1,y,z+1
#5 x,y-1,z
#6 x,y-1,z-1
#7 x-1,y,z
#8 x,y,z-1
#9 x+1,y,z-1
#10 x,y+1,z
#11 -x+1,-y+1,-z+1
#12 -x+1,-y+2,-z+1

Crystal Structure Analysis of Asp-AEDO3A-Gd

Crystallographic data have been deposited with the CCDC as supplementary publication CCDC 204982. These data can be obtained free of charge via http://www.ccdc.cam.ac.uk/ conts/retrieving.html (or from CCDC, 12 Union Road, Cambridge CB2 1EZ, UK; fax: +44 1223 335033; or deposit@ccdc.cam.ac.uk). Structure factors are available from the author via email: xray@caltech.edu.

Table A.2.1. Crystal data and structure refinement for Asp-AEDO3A-Gd.

Empirical formula	[C20H31N6O9Gd]-2 · Li+(H2O)4 · Li+(H2O)2 · H2O
Formula weight	796.75
Crystallization Solvent	Acetone/water
Crystal Habit	Plates
Crystal size	0.47 x 0.44 x 0.04 mm^3
Crystal color	Colorless
	Data Collection
Preliminary Photos	Rotation
Type of diffractometer	Bruker SMART 1000
Wavelength	0.71073 Å Mo Kα
Data Collection Temperature	98(2) K
θ range for 15223 reflections used in lattice determination	2.20 to 46.27°
Unit cell dimensions	a = 9.0229(3) Å b = 18.2905(6) Å β = 95.2850(10)° c = 9.2813(3) Å
Volume	1525.21(9) $Å^3$
Z	2
Crystal system	Monoclinic
Space group	$P2_1$
Density (calculated)	1.735 Mg/m^3
F(000)	810
Data collection program	Bruker SMART v5.054
θ range for data collection	2.20 to 46.17°
Completeness to θ = 28.19°	99.0 %
Index ranges	$-18 \le h \le 18$, $-36 \le k \le 35$, $-18 \le l \le 18$
Data collection scan type	ω scans at 7 ϕ settings each for 2 settings of 2θ
Data reduction program	Bruker SAINT v6.022

Table A.2.1. Crystal data and structure refinement for Asp-AEDO3A-Gd.

Reflections collected	88027
Independent reflections	25434 [R_{int} = 0.0419]
Absorption coefficient	2.255 mm^{-1}
Absorption correction	SADABS
Max. and min. transmission	1.0000 and 0.7853

Structure solution and Refinement

Structure solution program	SHELXS-97 (Sheldrick, 1990)
Primary solution method	Direct methods
Secondary solution method	Difference Fourier map
Hydrogen placement	Difference Fourier map
Structure refinement program	SHELXL-97 (Sheldrick, 1997)
Refinement method	Full matrix least-squares on F^2
Data / restraints / parameters	25434 / 1 / 586
Treatment of hydrogen atoms	Unrestrained
Goodness-of-fit on F^2	1.136
Final R indices [I>2σ(I), 23032 reflections]	R1 = 0.0236, ωR2 = 0.0407
R indices (all data)	R1 = 0.0281, ωR2 = 0.0412
Type of weighting scheme used	Sigma
Weighting scheme used	$\omega=1/\sigma^2(Fo^2)$
Max shift/error	0.001
Average shift/error	0.000
Absolute structure parameter	0.001(3)
Largest diff. peak and hole	2.470 and -1.470 e.A^{-3}

Special Refinement Details

The top twenty peaks in the difference Fourier map were all within one angstrom of the metal center and arise presumably incomplete absorption correction. All non-hydrogen atoms were refined anisotropically and all hydrogen atoms were refined isotropically without any restraints whatsoever.

Refinement of F^2 against ALL reflections. The weighted R-factor (ωR) and goodness of fit (S) are based on F^2, conventional R-factors (R) are based on F, with F set to zero for negative F^2. The threshold expression of $F^2 > 2\sigma(F^2)$ is used only for calculating R-factors(gt) etc. and is not relevant to the choice of reflections for refinement. R-factors based on F^2 are statistically about twice as large as those based on F, and R-factors based on ALL data will be even larger. All esds (except the esd in the dihedral angle between two l.s. planes) are estimated using the full covariance matrix. The cell esds are taken into account individually in the estimation of esds in distances, angles and torsion angles; correlations between esds in cell parameters are only used when they are defined by crystal symmetry. An approximate (isotropic) treatment of cell esds is used for estimating esds involving l.s. planes.

Table A.3.2. Atomic coordinates (x 10^4) and equivalent isotropic displacement parameters ($Å^2$x 10^3) for Asp-AEDO3A-Gd. U_{eq} is defined as the trace of the orthogonalized U^{ij} tensor.

	x	y	z	U_{eq}
Gd(1)	1827(1)	2498(1)	882(1)	5(1)
O(1)	4165(1)	2798(1)	-110(1)	9(1)
O(2)	4989(1)	3590(1)	-1696(1)	11(1)
O(3)	919(1)	3047(1)	-1379(1)	10(1)
O(4)	-979(1)	3467(1)	-2873(1)	12(1)
O(5)	-280(1)	1663(1)	452(1)	9(1)
O(6)	-1848(1)	829(1)	1218(1)	14(1)
O(7)	3945(1)	227(1)	1035(1)	13(1)
O(8)	2917(1)	470(1)	-4456(1)	13(1)
O(9)	775(1)	342(1)	-3447(1)	13(1)
N(1)	2880(1)	3833(1)	1413(1)	8(1)
N(2)	-328(1)	3506(1)	976(1)	8(1)
N(3)	89(1)	2284(1)	3060(1)	9(1)
N(4)	3287(1)	2593(1)	3485(1)	9(1)
N(5)	3337(1)	1429(1)	1485(1)	8(1)
N(6)	2197(1)	1646(1)	-1196(1)	8(1)
C(1)	3501(1)	4062(1)	70(1)	10(1)
C(2)	4292(1)	3436(1)	-633(1)	8(1)
C(3)	1733(1)	4367(1)	1786(1)	10(1)
C(4)	287(1)	4259(1)	844(1)	10(1)
C(5)	4102(1)	3805(1)	2607(1)	11(1)
C(6)	3683(1)	3363(1)	3889(1)	10(1)
C(7)	-1326(1)	3358(1)	-345(1)	11(1)
C(8)	-395(1)	3287(1)	-1641(1)	9(1)
C(9)	-1123(1)	3468(1)	2300(1)	10(1)
C(10)	-1344(1)	2687(1)	2796(1)	10(1)
C(11)	-262(1)	1493(1)	2990(1)	10(1)
C(12)	-853(1)	1301(1)	1444(1)	9(1)
C(13)	831(1)	2489(1)	4496(1)	10(1)
C(14)	2460(1)	2265(1)	4643(1)	11(1)
C(15)	4680(1)	2171(1)	3353(1)	10(1)
C(16)	4373(1)	1402(1)	2794(1)	10(1)
C(17)	3292(1)	826(1)	704(1)	8(1)
C(18)	2362(1)	872(1)	-762(1)	8(1)
C(19)	3049(1)	401(1)	-1884(1)	9(1)
C(20)	2175(1)	411(1)	-3371(1)	9(1)
Li	6726(3)	1532(1)	7228(3)	14(1)
O(11)	5904(1)	769(1)	5946(1)	13(1)
O(12)	6014(1)	1551(1)	9163(1)	16(1)
O(13)	6426(1)	2557(1)	6715(1)	14(1)
O(14)	8839(1)	1363(1)	7561(1)	14(1)
Li(2)	4823(2)	-413(1)	2484(2)	12(1)
O(20)	6788(1)	3(1)	3306(1)	11(1)
O(21)	3464(1)	-680(1)	3889(1)	14(1)
O(22)	-692(1)	-623(1)	-5409(1)	13(1)

Table A.2.3. Bond lengths [Å] for Asp-AEDO3A-Gd.

Gd(1)-O(3)	2.4023(8)	C(1)-H(1B)	0.865(17)
Gd(1)-N(5)	2.4187(9)	C(3)-C(4)	1.5150(17)
Gd(1)-O(1)	2.4406(8)	C(3)-H(3A)	0.952(15)
Gd(1)-O(5)	2.4422(8)	C(3)-H(3B)	0.938(19)
Gd(1)-N(6)	2.5261(10)	C(4)-H(4A)	0.913(18)
Gd(1)-N(4)	2.6479(9)	C(4)-H(4B)	0.894(17)
Gd(1)-N(1)	2.6497(9)	C(5)-C(6)	1.5146(18)
Gd(1)-N(2)	2.6868(10)	C(5)-H(5A)	0.952(19)
Gd(1)-N(3)	2.6989(10)	C(5)-H(5B)	0.965(17)
O(1)-C(2)	1.2739(13)	C(6)-H(6C)	0.982(18)
O(2)-C(2)	1.2505(14)	C(6)-H(6D)	0.926(18)
O(2)-Li(2)#1	1.977(2)	C(7)-C(8)	1.5346(16)
O(3)-C(8)	1.2668(13)	C(7)-H(7A)	0.980(18)
O(4)-C(8)	1.2579(15)	C(7)-H(7B)	0.979(18)
O(5)-C(12)	1.2813(14)	C(9)-C(10)	1.5192(16)
O(6)-C(12)	1.2492(14)	C(9)-H(9A)	0.957(16)
O(7)-C(17)	1.2679(14)	C(9)-H(9B)	0.980(18)
O(7)-Li(2)	1.900(2)	C(10)-H(10A)	1.021(16)
O(8)-C(20)	1.2639(14)	C(10)-H(10B)	0.900(18)
O(9)-C(20)	1.2649(14)	C(11)-C(12)	1.5256(17)
N(1)-C(1)	1.4737(15)	C(11)-H(11A)	0.924(19)
N(1)-C(3)	1.4863(14)	C(11)-H(11B)	0.870(17)
N(1)-C(5)	1.4904(16)	C(13)-C(14)	1.5202(16)
N(2)-C(7)	1.4782(15)	C(13)-H(13A)	0.940(19)
N(2)-C(9)	1.4807(15)	C(13)-H(13B)	0.905(18)
N(2)-C(4)	1.4950(15)	C(14)-H(14A)	0.923(15)
N(3)-C(11)	1.4808(15)	C(14)-H(14B)	0.971(16)
N(3)-C(13)	1.4838(14)	C(15)-C(16)	1.5157(17)
N(3)-C(10)	1.4885(15)	C(15)-H(15A)	0.942(17)
N(4)-C(15)	1.4896(14)	C(15)-H(15B)	0.986(17)
N(4)-C(14)	1.4896(15)	C(16)-H(16A)	1.067(17)
N(4)-C(6)	1.4931(14)	C(16)-H(16B)	0.940(19)
N(5)-C(17)	1.3184(14)	C(17)-C(18)	1.5344(16)
N(5)-C(16)	1.4638(15)	C(18)-C(19)	1.5261(16)
N(6)-C(18)	1.4745(14)	C(18)-H(18)	1.020(15)
N(6)-H(6A)	0.882(19)	C(19)-C(20)	1.5255(16)
N(6)-H(6B)	0.746(18)	C(19)-H(19A)	0.941(19)
C(1)-C(2)	1.5264(16)	C(19)-H(19B)	0.946(18)
C(1)-H(1A)	0.956(19)		
Li-O(14)	1.928(3)	O(14)-H(14C)	0.75(2)
Li-O(11)	1.936(3)	O(14)-H(14D)	0.54(3)
Li-O(13)	1.947(3)	Li(2)-O(21)	1.933(3)
Li-O(12)	1.963(3)	Li(2)-O(2)#2	1.977(2)
Li-H(13C)	2.33(2)	Li(2)-O(20)	2.014(2)
Li-H(14D)	2.07(3)	Li(2)-H(21D)	2.29(2)
O(11)-H(11C)	0.70(2)	O(20)-H(20C)	0.76(2)
O(11)-H(11D)	0.74(2)	O(20)-H(20D)	0.76(2)
O(12)-H(12C)	0.85(2)	O(21)-H(21C)	0.81(2)

Table A.2.3. Bond lengths [Å] for Asp-AEDO3A-Gd.

O(12)-H(12D)	0.79(2)	O(21)-H(21D)	0.75(2)
O(13)-H(13C)	0.73(2)	O(22)-H(22A)	0.70(2)
O(13)-H(13D)	0.75(2)	O(22)-H(22B)	0.79(2)

Table A.2.4. Bond Angles [°] for Asp-AEDO3A-Gd.

O(3)-Gd(1)-N(5)	132.83(3)	C(5)-N(1)-Gd(1)	109.53(7)
O(3)-Gd(1)-O(1)	79.24(3)	C(7)-N(2)-C(9)	112.01(9)
N(5)-Gd(1)-O(1)	77.36(3)	C(7)-N(2)-C(4)	107.65(9)
O(3)-Gd(1)-O(5)	85.46(3)	C(9)-N(2)-C(4)	108.88(9)
N(5)-Gd(1)-O(5)	86.89(3)	C(7)-N(2)-Gd(1)	103.61(7)
O(1)-Gd(1)-O(5)	139.95(3)	C(9)-N(2)-Gd(1)	113.69(7)
O(3)-Gd(1)-N(6)	69.47(3)	C(4)-N(2)-Gd(1)	110.79(7)
N(5)-Gd(1)-N(6)	64.32(3)	C(11)-N(3)-C(13)	111.27(12)
O(1)-Gd(1)-N(6)	70.78(3)	C(11)-N(3)-C(10)	107.35(9)
O(5)-Gd(1)-N(6)	69.20(3)	C(13)-N(3)-C(10)	109.66(10)
O(3)-Gd(1)-N(4)	150.51(3)	C(11)-N(3)-Gd(1)	104.21(7)
N(5)-Gd(1)-N(4)	67.67(3)	C(13)-N(3)-Gd(1)	112.98(6)
O(1)-Gd(1)-N(4)	87.43(3)	C(10)-N(3)-Gd(1)	111.13(7)
O(5)-Gd(1)-N(4)	120.29(3)	C(15)-N(4)-C(14)	109.43(9)
N(6)-Gd(1)-N(4)	130.36(3)	C(15)-N(4)-C(6)	109.01(9)
O(3)-Gd(1)-N(1)	82.20(3)	C(14)-N(4)-C(6)	108.85(9)
N(5)-Gd(1)-N(1)	121.17(3)	C(15)-N(4)-Gd(1)	104.10(6)
O(1)-Gd(1)-N(1)	63.62(3)	C(14)-N(4)-Gd(1)	113.05(7)
O(5)-Gd(1)-N(1)	150.08(3)	C(6)-N(4)-Gd(1)	112.23(7)
N(6)-Gd(1)-N(1)	129.81(3)	C(17)-N(5)-C(16)	114.38(9)
N(4)-Gd(1)-N(1)	68.31(3)	C(17)-N(5)-Gd(1)	124.15(7)
O(3)-Gd(1)-N(2)	63.34(3)	C(16)-N(5)-Gd(1)	121.46(7)
N(5)-Gd(1)-N(2)	160.22(3)	C(18)-N(6)-Gd(1)	113.60(7)
O(1)-Gd(1)-N(2)	120.74(3)	C(18)-N(6)-H(6A)	114.0(12)
O(5)-Gd(1)-N(2)	83.07(3)	Gd(1)-N(6)-H(6A)	110.3(12)
N(6)-Gd(1)-N(2)	126.50(3)	C(18)-N(6)-H(6B)	109.2(14)
N(4)-Gd(1)-N(2)	103.07(3)	Gd(1)-N(6)-H(6B)	105.1(15)
N(1)-Gd(1)-N(2)	67.03(3)	H(6A)-N(6)-H(6B)	103.8(19)
O(3)-Gd(1)-N(3)	122.68(3)	N(1)-C(1)-C(2)	112.20(9)
N(5)-Gd(1)-N(3)	93.63(3)	N(1)-C(1)-H(1A)	110.5(12)
O(1)-Gd(1)-N(3)	153.84(3)	C(2)-C(1)-H(1A)	108.9(12)
O(5)-Gd(1)-N(3)	62.24(3)	N(1)-C(1)-H(1B)	107.2(12)
N(6)-Gd(1)-N(3)	127.52(3)	C(2)-C(1)-H(1B)	107.5(12)
N(4)-Gd(1)-N(3)	66.49(3)	H(1A)-C(1)-H(1B)	110.5(16)
N(1)-Gd(1)-N(3)	102.58(3)	O(2)-C(2)-O(1)	125.23(10)
O(5)-Gd(1)-N(3)	62.24(3)	O(2)-C(2)-C(1)	117.21(10)
N(6)-Gd(1)-N(3)	127.52(3)	O(1)-C(2)-C(1)	117.54(10)
N(4)-Gd(1)-N(3)	66.49(3)	N(1)-C(3)-C(4)	111.20(9)
N(1)-Gd(1)-N(3)	102.58(3)	N(1)-C(3)-H(3A)	111.6(9)
N(2)-Gd(1)-N(3)	66.61(3)	C(4)-C(3)-H(3A)	110.2(9)
C(2)-O(1)-Gd(1)	117.44(7)	N(1)-C(3)-H(3B)	108.6(11)
C(2)-O(2)-Li(2)#1	124.50(10)	C(4)-C(3)-H(3B)	103.2(11)
C(8)-O(3)-Gd(1)	123.41(7)	H(3A)-C(3)-H(3B)	111.8(15)
C(12)-O(5)-Gd(1)	124.45(7)	N(2)-C(4)-C(3)	112.23(9)
C(17)-O(7)-Li(2)	149.07(11)	N(2)-C(4)-H(4A)	110.0(11)
C(1)-N(1)-C(3)	109.72(9)	C(3)-C(4)-H(4A)	108.6(11)
C(1)-N(1)-C(5)	109.02(9)	N(2)-C(4)-H(4B)	109.3(10)
C(3)-N(1)-C(5)	109.44(9)	C(3)-C(4)-H(4B)	110.0(10)
C(1)-N(1)-Gd(1)	105.20(6)	H(4A)-C(4)-H(4B)	106.5(15)

Table A.2.4. Bond Angles [°] for Asp-AEDO3A-Gd.

C(3)-N(1)-Gd(1)	113.78(7)	N(1)-C(5)-C(6)	112.40(10)
N(1)-C(5)-H(5A)	107.6(11)	C(13)-C(14)-H(14B)	106.5(9)
C(6)-C(5)-H(5A)	109.6(11)	H(14A)-C(14)-H(14B)	108.1(14)
N(1)-C(5)-H(5B)	109.3(10)	N(4)-C(15)-C(16)	112.31(9)
C(6)-C(5)-H(5B)	112.3(10)	N(4)-C(15)-H(15A)	112.1(10)
H(5A)-C(5)-H(5B)	105.3(15)	C(16)-C(15)-H(15A)	110.3(10)
N(4)-C(6)-C(5)	112.16(9)	N(4)-C(15)-H(15B)	107.6(11)
N(4)-C(6)-H(6C)	108.6(11)	C(16)-C(15)-H(15B)	108.2(12)
C(5)-C(6)-H(6C)	110.2(11)	H(15A)-C(15)-H(15B)	106.0(13)
N(4)-C(6)-H(6D)	105.3(12)	N(5)-C(16)-C(15)	109.61(9)
C(5)-C(6)-H(6D)	113.0(12)	N(5)-C(16)-H(16A)	110.2(10)
H(6C)-C(6)-H(6D)	107.3(15)	C(15)-C(16)-H(16A)	110.7(9)
N(2)-C(7)-C(8)	109.25(9)	N(5)-C(16)-H(16B)	107.8(12)
N(2)-C(7)-H(7A)	111.4(11)	C(15)-C(16)-H(16B)	112.2(12)
C(8)-C(7)-H(7A)	113.1(11)	H(16A)-C(16)-H(16B)	106.2(15)
N(2)-C(7)-H(7B)	108.7(12)	O(7)-C(17)-N(5)	126.86(11)
C(8)-C(7)-H(7B)	108.1(12)	O(7)-C(17)-C(18)	117.83(10)
H(7A)-C(7)-H(7B)	106.1(15)	N(5)-C(17)-C(18)	115.31(9)
O(4)-C(8)-O(3)	124.83(11)	N(6)-C(18)-C(19)	113.12(9)
O(4)-C(8)-C(7)	118.49(10)	N(6)-C(18)-C(17)	109.20(9)
O(3)-C(8)-C(7)	116.68(10)	C(19)-C(18)-C(17)	110.50(9)
N(2)-C(9)-C(10)	112.52(9)	N(6)-C(18)-H(18)	105.8(8)
N(2)-C(9)-H(9A)	108.6(10)	C(19)-C(18)-H(18)	112.2(8)
C(10)-C(9)-H(9A)	108.4(10)	C(17)-C(18)-H(18)	105.6(9)
N(2)-C(9)-H(9B)	107.4(11)	C(20)-C(19)-C(18)	113.70(9)
C(10)-C(9)-H(9B)	108.2(10)	C(20)-C(19)-H(19A)	110.2(11)
H(9A)-C(9)-H(9B)	111.7(14)	C(18)-C(19)-H(19A)	109.0(12)
N(3)-C(10)-C(9)	112.30(9)	C(20)-C(19)-H(19B)	108.1(11)
N(3)-C(10)-H(10A)	108.0(9)	C(18)-C(19)-H(19B)	111.6(11)
C(9)-C(10)-H(10A)	110.3(9)	H(19A)-C(19)-H(19B)	103.7(15)
N(3)-C(10)-H(10B)	113.2(15)	O(8)-C(20)-O(9)	124.26(11)
C(9)-C(10)-H(10B)	103.7(17)	O(8)-C(20)-C(19)	117.05(10)
H(10A)-C(10)-H(10B)	109.4(13)	O(9)-C(20)-C(19)	118.66(10)
N(3)-C(11)-C(12)	108.70(9)	O(14)-Li-O(11)	107.47(12)
N(3)-C(11)-H(11A)	110.2(12)	O(14)-Li-O(13)	107.86(12)
C(12)-C(11)-H(11A)	111.8(11)	O(11)-Li-O(13)	120.46(13)
N(3)-C(11)-H(11B)	112.1(11)	O(14)-Li-O(12)	104.96(12)
C(12)-C(11)-H(11B)	106.3(11)	O(11)-Li-O(12)	115.87(13)
H(11A)-C(11)-H(11B)	107.7(15)	O(13)-Li-O(12)	98.99(12)
O(6)-C(12)-O(5)	124.68(11)	O(14)-Li-H(13C)	91.1(6)
O(6)-C(12)-C(11)	120.02(10)	O(11)-Li-H(13C)	128.5(6)
O(5)-C(12)-C(11)	115.29(10)	O(13)-Li-H(13C)	16.8(5)
N(3)-C(13)-C(14)	111.42(10)	O(12)-Li-H(13C)	104.1(6)
N(3)-C(13)-H(13A)	110.5(12)	O(14)-Li-H(14D)	15.1(8)
C(14)-C(13)-H(13A)	108.5(11)	O(11)-Li-H(14D)	117.7(9)
N(3)-C(13)-H(13B)	110.1(11)	O(13)-Li-H(14D)	108.2(8)
C(14)-C(13)-H(13B)	107.5(11)	O(12)-Li-H(14D)	90.1(8)
H(13A)-C(13)-H(13B)	108.8(17)	H(13C)-Li-H(14D)	92.1(10)
N(4)-C(14)-C(13)	111.79(10)	Li-O(11)-H(11C)	126.3(17)
N(4)-C(14)-H(14A)	109.9(10)	Li-O(11)-H(11D)	123.0(16)
C(13)-C(14)-H(14A)	112.6(10)	H(11C)-O(11)-H(11D)	108(2)

Table A.2.4. Bond Angles [°] for Asp-AEDO3A-Gd.

N(4)-C(14)-H(14B)	107.7(10)	Li-O(12)-H(12C)	127.0(15)
Li-O(12)-H(12D)	119.8(16)	O(2)#2-Li(2)-O(20)	112.71(11)
H(12C)-O(12)-H(12D)	108(2)	O(7)-Li(2)-H(21D)	103.4(5)
Li-O(13)-H(13C)	112.8(16)	O(21)-Li(2)-H(21D)	17.9(5)
Li-O(13)-H(13D)	129.0(17)	O(2)#2-Li(2)-H(21D)	84.9(5)
H(13C)-O(13)-H(13D)	101(2)	O(20)-Li(2)-H(21D)	133.1(6)
Li-O(14)-H(14C)	129.2(15)	Li(2)-O(20)-H(20C)	115.2(17)
Li-O(14)-H(14D)	98(3)	Li(2)-O(20)-H(20D)	124.4(17)
H(14C)-O(14)-H(14D)	116(3)	H(20C)-O(20)-H(20D)	110(2)
O(7)-Li(2)-O(21)	112.57(12)	Li(2)-O(21)-H(21C)	119.6(16)
O(7)-Li(2)-O(2)#2	110.53(12)	Li(2)-O(21)-H(21D)	109.6(16)
O(21)-Li(2)-O(2)#2	95.64(10)	H(21C)-O(21)-H(21D)	106(2)
O(7)-Li(2)-O(20)	109.30(11)	H(22A)-O(22)-H(22B)	104(2)
O(21)-Li(2)-O(20)	115.51(12)		

Symmetry transformations used to generate equivalent atoms:
#1 -x+1,y+1/2,-z
#2 -x+1,y-1/2,-z

Table A.3.5. Anisotropic displacement parameters ($Å^2 x\ 10^4$) for Asp.AEDO3A-Gd. The anisotropic displacement factor exponent takes the form: The anisotropic displacement factor exponent takes the form:

$-2\pi^2[\ h^2 a^{*2} U^{11} + ... + 2\ h\ k\ a^*\ b^*\ U^{12}\ ]$

	U^{11}	U^{22}	U^{33}	U^{23}	U^{13}	U^{12}
Gd(1)	54(1)	50(1)	55(1)	2(1)	6(1)	1(1)
O(1)	97(3)	73(3)	114(3)	15(2)	26(3)	-4(2)
O(2)	135(4)	86(3)	125(4)	8(3)	60(3)	-5(2)
O(3)	87(3)	108(3)	100(3)	13(3)	15(3)	26(2)
O(4)	111(4)	155(4)	97(4)	35(3)	-2(3)	18(3)
O(5)	94(3)	105(3)	88(3)	2(3)	23(3)	-17(2)
O(6)	143(4)	135(4)	136(4)	18(3)	0(3)	-60(3)
O(7)	184(4)	83(3)	113(4)	3(3)	-16(3)	46(3)
O(8)	140(4)	151(4)	97(4)	-20(3)	38(3)	-26(3)
O(9)	93(3)	173(4)	118(4)	-34(3)	3(3)	0(3)
N(1)	91(4)	67(4)	92(4)	-5(3)	15(3)	2(3)
N(2)	86(4)	82(4)	82(4)	1(3)	9(3)	4(3)
N(3)	101(4)	81(3)	81(4)	-1(3)	9(3)	-4(3)
N(4)	98(3)	93(6)	80(3)	-11(3)	3(3)	3(3)
N(5)	102(4)	77(4)	71(4)	-6(3)	-6(3)	12(3)
N(6)	88(4)	78(4)	76(4)	6(3)	3(3)	-4(3)
C(1)	118(5)	67(4)	115(5)	7(3)	40(4)	-3(3)
C(2)	66(4)	82(4)	105(4)	-4(3)	14(3)	-11(3)
C(3)	116(5)	80(4)	119(5)	-15(3)	30(4)	9(3)
C(4)	115(5)	75(4)	121(5)	8(3)	32(4)	17(3)
C(5)	91(5)	102(5)	122(5)	-17(4)	8(4)	-15(3)
C(6)	118(4)	91(4)	92(4)	-26(3)	-6(3)	-5(3)
C(7)	90(4)	136(5)	97(4)	15(3)	6(3)	10(3)
C(8)	97(4)	65(4)	104(4)	15(3)	0(3)	-1(3)
C(9)	98(4)	104(4)	111(4)	2(3)	35(4)	24(3)
C(10)	83(4)	120(4)	110(4)	8(3)	28(3)	3(3)
C(11)	121(5)	89(4)	101(4)	16(3)	18(4)	-21(3)
C(12)	83(4)	91(4)	103(4)	11(3)	15(3)	-5(3)
C(13)	118(3)	117(3)	78(3)	-5(7)	18(3)	2(7)
C(14)	125(5)	120(4)	74(4)	8(3)	0(3)	-6(3)
C(15)	90(4)	101(4)	99(4)	-10(3)	-13(3)	15(3)
C(16)	109(5)	92(5)	90(4)	6(3)	-26(4)	12(3)
C(17)	86(4)	76(4)	73(4)	-1(3)	13(3)	5(3)
C(18)	85(4)	75(4)	70(4)	-8(3)	4(3)	-2(3)
C(19)	97(4)	97(4)	86(4)	-14(3)	12(3)	8(3)
C(20)	109(4)	67(4)	88(4)	-19(3)	11(3)	-1(3)
Li	145(10)	139(10)	135(10)	1(8)	11(8)	7(7)
O(11)	109(4)	167(4)	122(4)	-34(3)	7(3)	-11(3)
O(12)	150(4)	200(5)	124(4)	3(3)	28(3)	31(3)
O(13)	144(3)	116(5)	147(3)	-25(4)	7(3)	-1(4)
O(14)	119(4)	179(5)	115(4)	-36(3)	-3(3)	36(3)
Li(2)	127(10)	98(9)	126(10)	10(7)	19(8)	18(7)

Table A.3.5. Anisotropic displacement parameters ($Å^2$x 10^4) for Asp.AEDO3A-Gd. The anisotropic displacement factor exponent takes the form: The anisotropic displacement factor exponent takes the form:

$$-2\pi^2[h^2 a^{*2} U^{11} + ... + 2 h k a^* b^* U^{12}]$$

	U^{11}	U^{22}	U^{33}	U^{23}	U^{13}	U^{12}
O(20)	96(4)	114(4)	130(4)	21(3)	4(3)	6(3)
O(21)	130(4)	152(4)	145(4)	-48(3)	41(3)	-33(3)
O(22)	112(4)	160(4)	129(4)	-29(3)	2(3)	5(3)

Table A.3.6. Hydrogen coordinates (x 10^4) and isotropic displacement parameters ($Å^2$ x 10^3) for Asp.AEDO3A-Gd.

	x	y	z	U_{iso}
H(6A)	1510(20)	1723(10)	-1920(20)	18(5)
H(6B)	2900(20)	1772(10)	-1490(20)	15(4)
H(1A)	4190(20)	4456(10)	260(20)	20(5)
H(1B)	2762(19)	4196(10)	-531(19)	6(4)
H(3A)	2071(17)	4857(9)	1713(18)	3(3)
H(3B)	1470(20)	4260(10)	2720(20)	18(5)
H(4A)	-385(19)	4597(10)	1101(19)	13(4)
H(4B)	425(18)	4348(9)	-82(19)	7(4)
H(5A)	4320(20)	4294(10)	2900(20)	18(5)
H(5B)	4997(19)	3626(9)	2233(19)	6(4)
H(6C)	4510(20)	3357(10)	4650(20)	15(4)
H(6D)	2860(20)	3548(10)	4292(19)	13(4)
H(7A)	-2110(20)	3727(10)	-490(20)	16(4)
H(7B)	-1830(20)	2891(10)	-230(20)	21(5)
H(9A)	-2080(18)	3689(9)	2103(18)	8(4)
H(9B)	-515(19)	3726(10)	3070(20)	7(4)
H(10A)	-1854(17)	2682(8)	3733(18)	10(4)
H(10B)	-1959(16)	2492(16)	2078(16)	15(3)
H(11A)	-940(20)	1377(10)	3650(20)	14(4)
H(11B)	526(18)	1224(9)	3193(18)	6(4)
H(13A)	360(20)	2262(9)	5240(20)	21(5)
H(13B)	796(19)	2979(10)	4620(20)	13(4)
H(14A)	2934(16)	2376(10)	5539(17)	10(4)
H(14B)	2479(17)	1737(9)	4524(18)	5(4)
H(15A)	5295(18)	2158(9)	4230(19)	10(4)
H(15B)	5253(15)	2430(13)	2657(16)	10(4)
H(16A)	5381(19)	1138(9)	2570(20)	7(4)
H(16B)	3950(20)	1106(10)	3470(20)	19(5)
H(18)	1322(17)	700(8)	-577(17)	1(3)
H(19A)	3146(19)	-81(10)	-1540(20)	15(4)
H(19B)	4040(20)	543(10)	-2000(20)	14(4)
H(11C)	6230(20)	625(11)	5350(20)	20(5)
H(11D)	5100(20)	676(11)	5860(20)	24(5)
H(12C)	5600(20)	1908(13)	9560(20)	32(6)
H(12D)	6400(20)	1302(12)	9790(30)	31(6)
H(13C)	7120(20)	2758(11)	6700(20)	28(6)
H(13D)	5950(20)	2835(11)	7040(20)	29(6)
H(14C)	9300(20)	1061(11)	7290(20)	15(4)
H(14D)	8890(30)	1405(16)	8140(30)	53(10)
H(20C)	7200(20)	226(13)	2780(30)	34(6)
H(20D)	7340(20)	-198(13)	3830(30)	29(6)
H(21C)	3120(20)	-365(14)	4370(20)	30(6)
H(21D)	2810(20)	-880(12)	3520(20)	21(5)
H(22A)	-220(20)	-362(12)	-5060(30)	28(6)
H(22B)	-160(20)	-846(12)	-5880(20)	29(5)

Table A.1.7. Hydrogen bonds for Asp-AEDO3A-Gd [Å and °].

D-H…A	d(D-H)	d(H…A)	d(D…A)	<(DHA)
N(6)-H(6A)...O(14)#3	0.882(19)	2.499(19)	3.1831(15)	134.9(16)
N(6)-H(6B)...O(1)	0.746(18)	2.489(19)	2.8773(13)	114.3(17)
O(11)-H(11C)...O(20)	0.70(2)	2.30(2)	2.9937(14)	167(2)
O(11)-H(11D)...O(8)#4	0.74(2)	2.00(2)	2.7421(14)	177(2)
O(12)-H(12C)...O(1)#4	0.85(2)	2.12(2)	2.9396(13)	162(2)
O(12)-H(12D)...O(6)#5	0.79(2)	2.15(2)	2.9033(14)	159(2)
O(13)-H(13C)...O(4)#5	0.73(2)	2.16(2)	2.8701(15)	167(2)
O(13)-H(13D)...O(2)#4	0.75(2)	2.06(2)	2.7890(15)	168(2)
O(14)-H(14C)...O(9)#5	0.75(2)	2.04(2)	2.7783(14)	171.9(19)
O(14)-H(14D)...O(5)#5	0.54(3)	2.25(3)	2.7823(15)	165(4)
O(20)-H(20C)...O(6)#6	0.76(2)	2.07(2)	2.8271(13)	175(2)
O(20)-H(20D)...O(22)#5	0.76(2)	2.01(2)	2.7211(13)	158(2)
O(21)-H(21C)...O(8)#4	0.81(2)	1.89(2)	2.6771(13)	163(2)
O(21)-H(21D)...O(4)#7	0.75(2)	2.09(2)	2.8219(14)	169(2)
O(22)-H(22A)...O(9)	0.70(2)	2.11(2)	2.7816(13)	161(2)
O(22)-H(22B)...O(4)#8	0.79(2)	2.05(2)	2.8324(14)	172(2)

Symmetry transformations used to generate equivalent atoms:
#1 -x+1,y+1/2,-z
#2 -x+1,y-1/2,-z
#3 x-1,y,z-1
#4 x,y,z+1
#5 x+1,y,z+1
#6 x+1,y,z
#7 -x,y-1/2,-z
#8 -x,y-1/2,-z-1

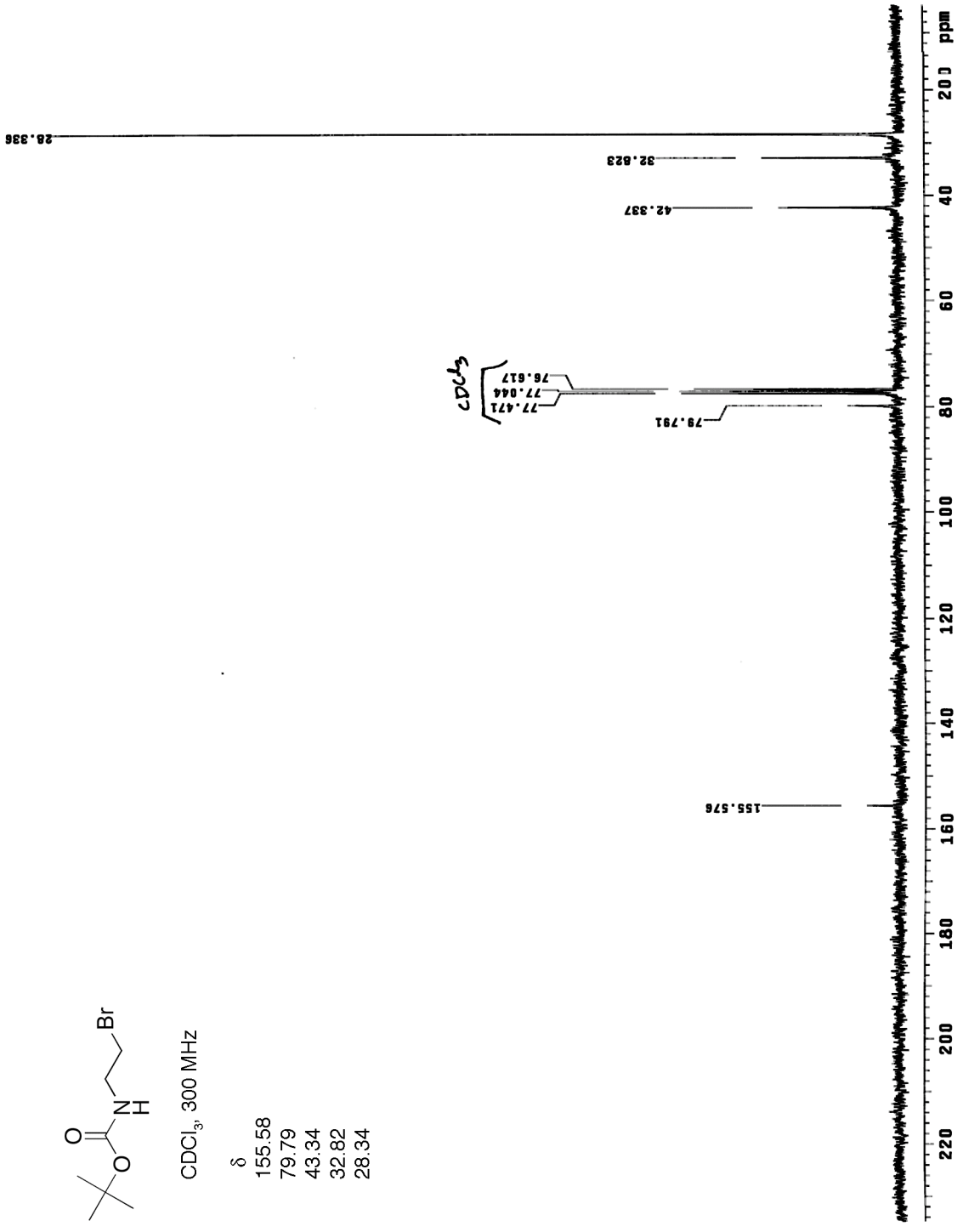
Br
N
H
O
O
O
CDCl3, 300 MHz
δ
155.58
79.79
43.34
32.82
28.34
28.336
32.823
42.337
CDCl3
77.471
77.044
76.617
79.791
155.576
220
200
180
160
140
120
100
80
60
40
20
ppm

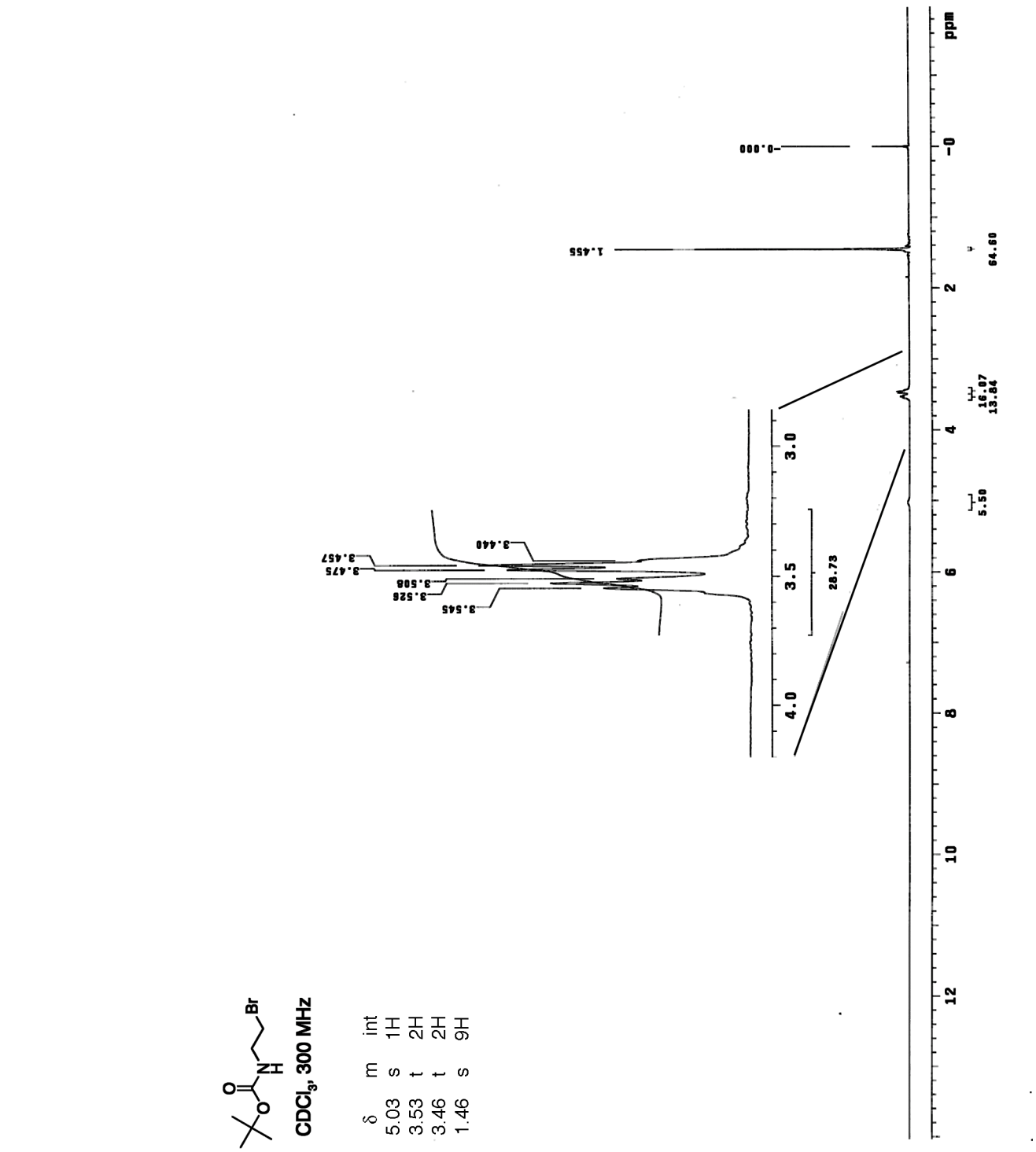
Br
O
N
H
O
O
CDCl3, 300 MHz
δ m int
5.03 s 1H
3.53 t 2H
3.46 t 2H
1.46 s 9H
3.545
3.526
3.508
3.475
3.457
3.440
1.455
0.000
3.0
3.5
4.0
28.73
5.50
16.07
13.84
64.66
ppm

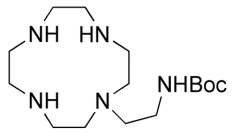

$CDCl_3$, 300 MHz

δ
155.99
81.73
80.43
50.66
41.17
37.17
31.67
28.32
28.04

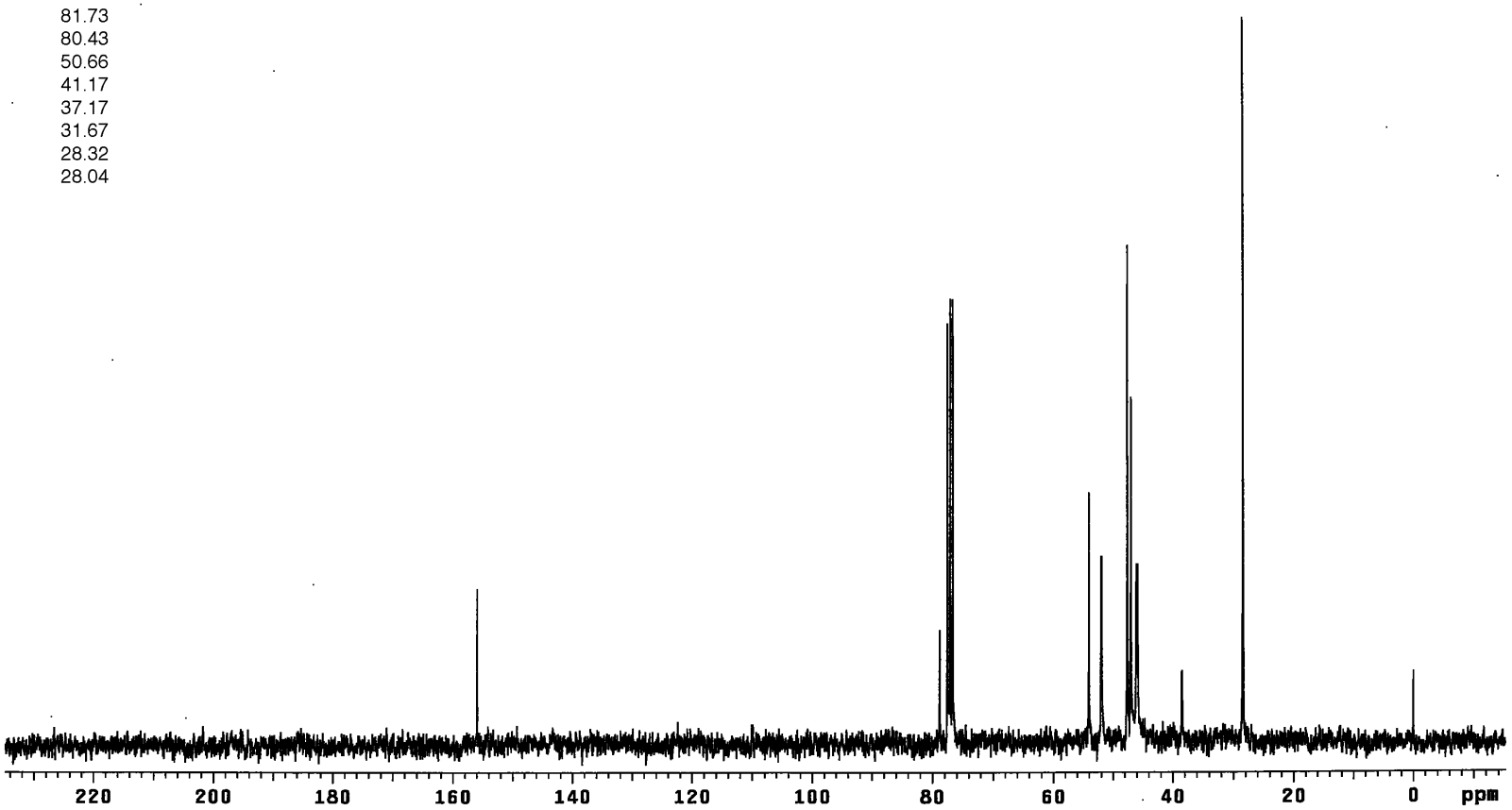

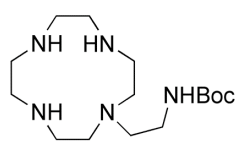

$CDCl_3$, 300 MHz

δ	m	int
5.65	s	1H
3.21	q	2H
2.74-2.48	m	21H
1.44	s	9H

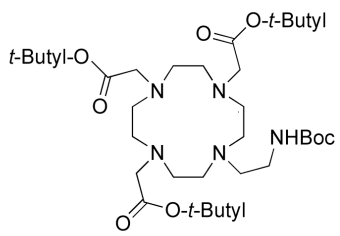

$CDCl_3$, 300 MHz

δ
173.36
172.84
172.58
156.42
82.80
81.42
81.94
79.20
56.51
55.69
53.95
50.34
37.84
28.41
28.01
27.82

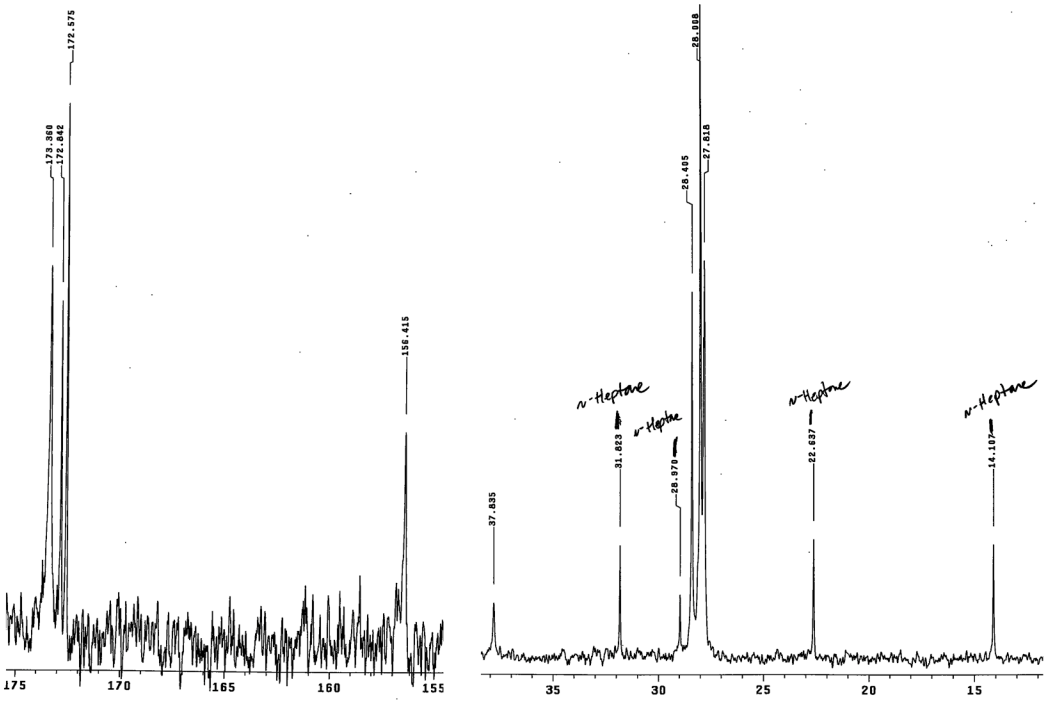
172.575
173.360
172.842
156.415
175
170
165
160
155
28.088
28.495
27.818
n-Heptane
n-Heptane
n-Heptane
n-Heptane
31.823
28.070
22.637
14.107
37.835
35
30
25
20
15

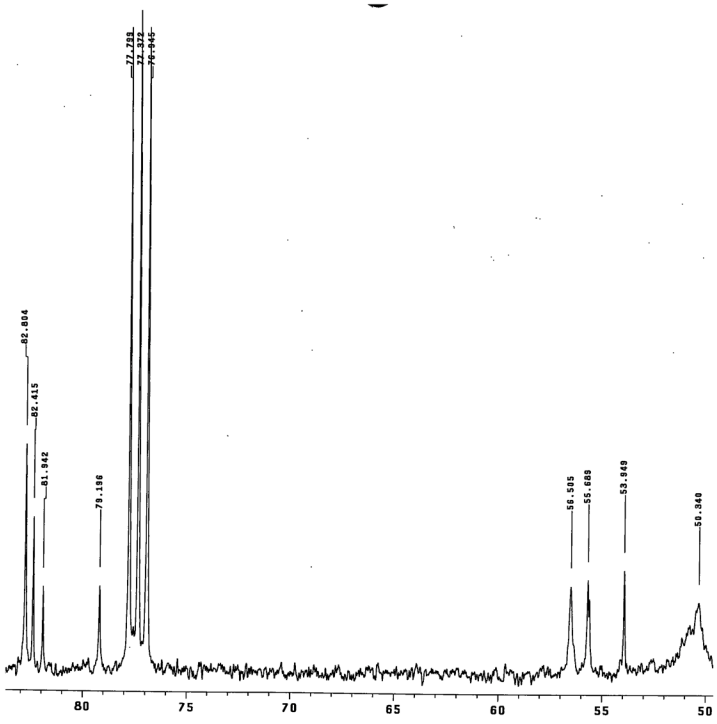
82.804
82.415
81.942
79.186
77.799
77.322
76.946
56.505
55.688
53.949
50.340
80
75
70
65
60
55
50

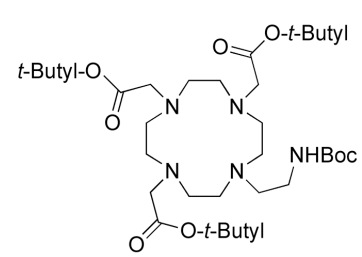

$CDCl_3$, 300 MHz

δ	m	int
5.43	s	1H
3.4-2.2	m	26H
1.6 - 1.4	m	36H

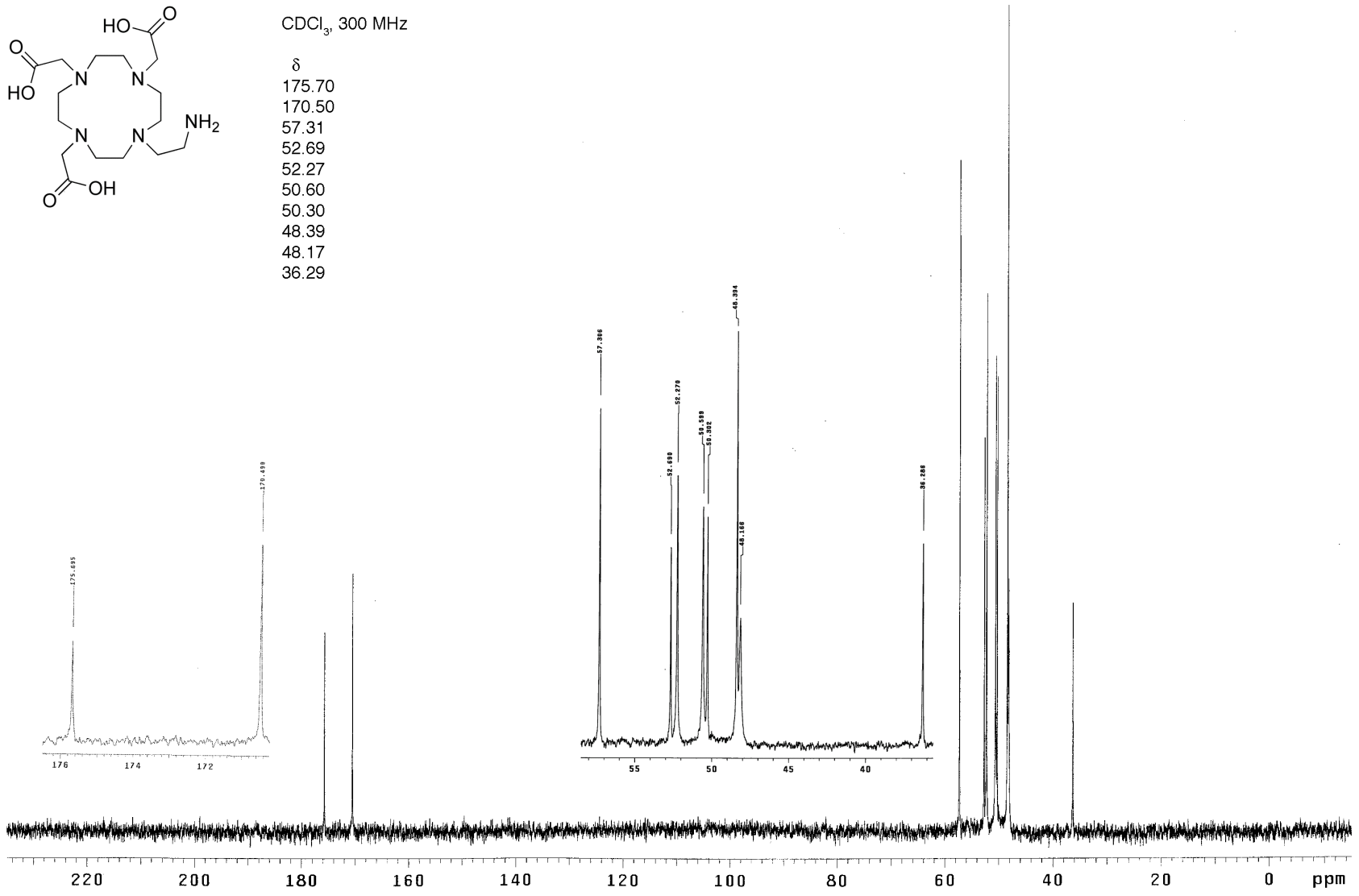
HO
O
O
HO
N
N
N
N
NH2
O
OH
CDCl3, 300 MHz
δ
175.70
170.50
57.31
52.69
52.27
50.60
50.30
48.39
48.17
36.29
220
200
180
160
140
120
100
80
60
40
20
0
ppm

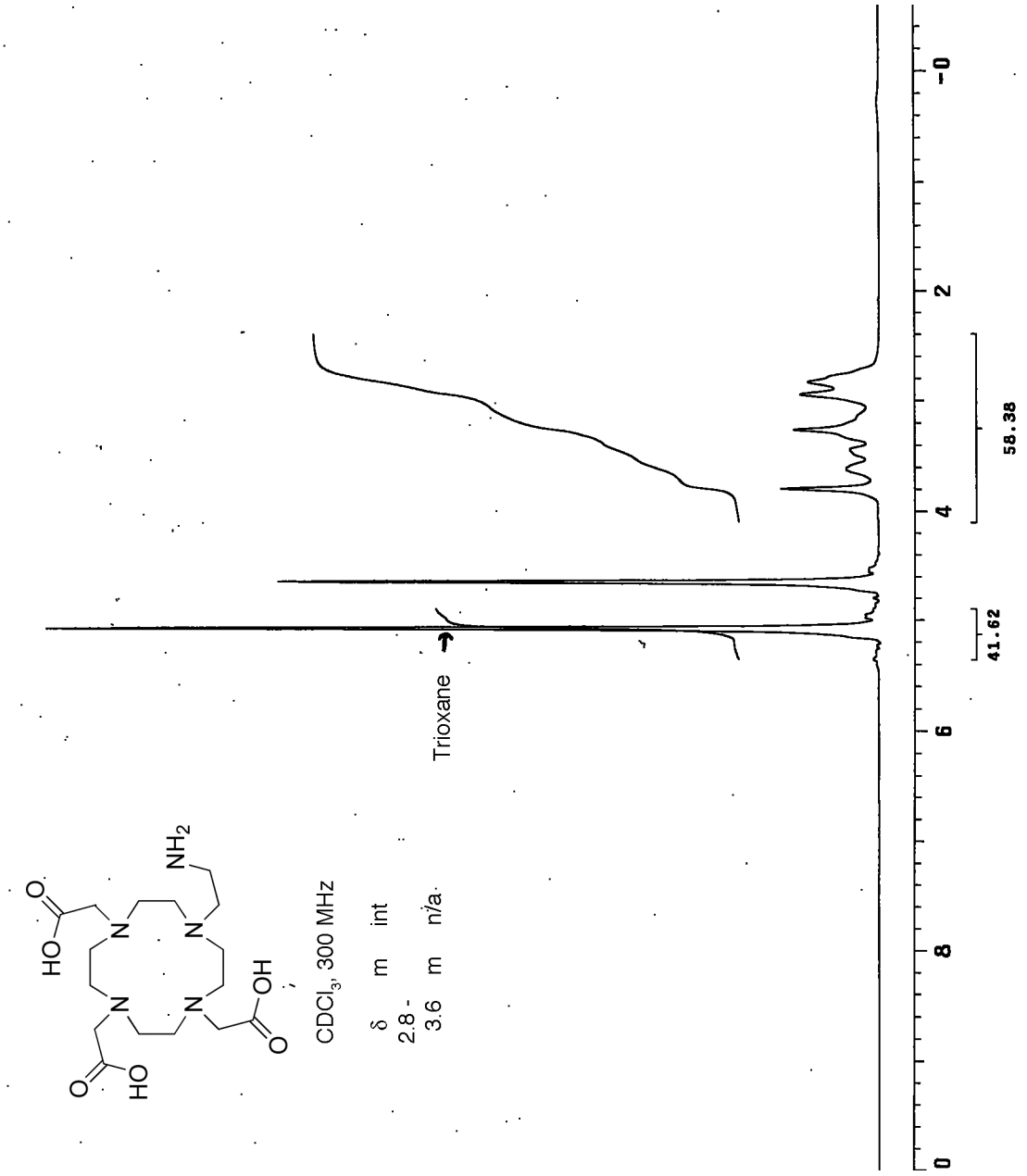
NH2
HO
O
OH
O
HO
CDCl3, 300 MHz
δ m int
2.8 - 3.6 m n/a
Trioxane
41.62
58.38
0
2
4
6
8
-0

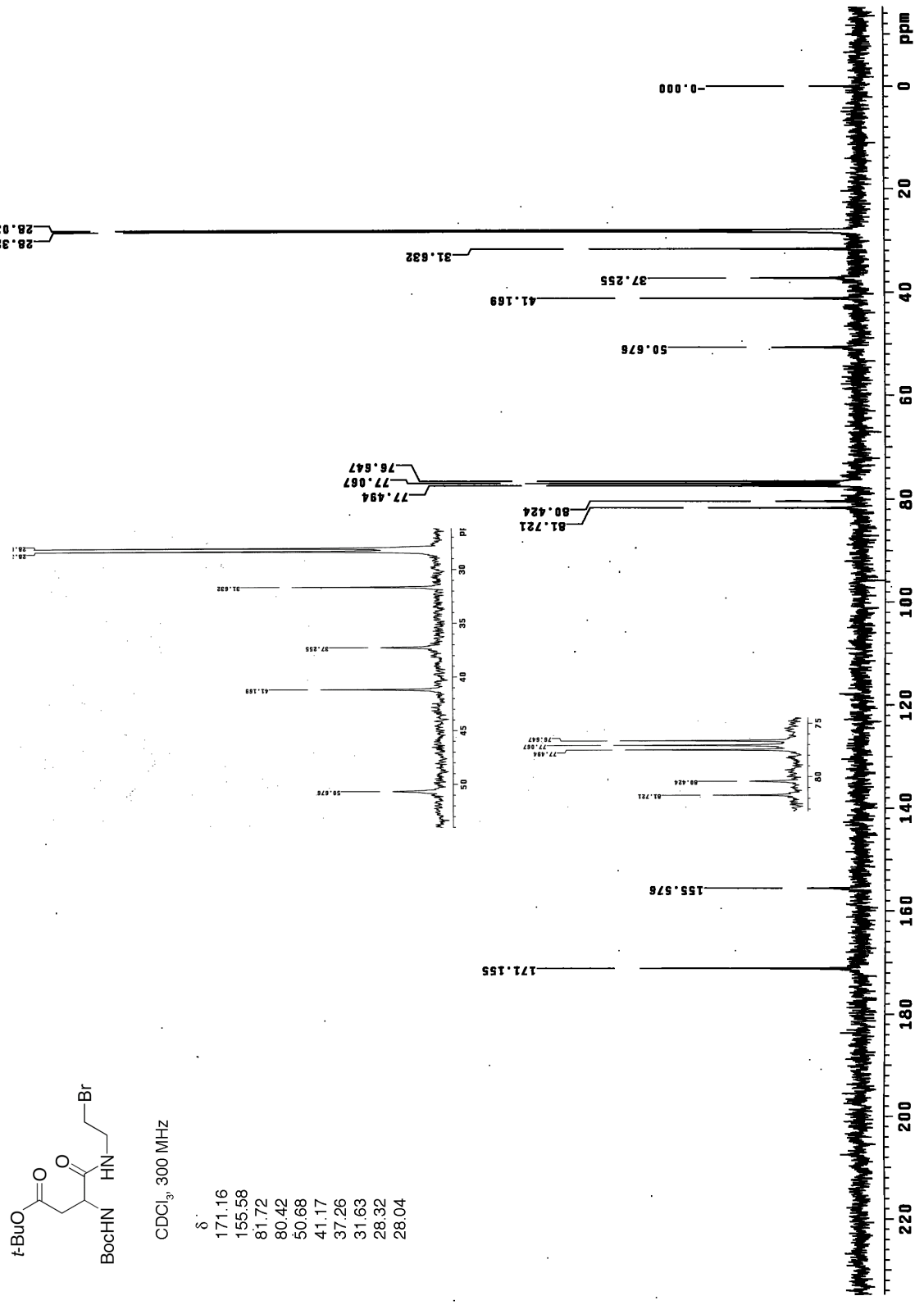
t-BuO
O
O
HN
Br
BocHN
CDCl3, 300 MHz
δ
171.16
155.58
81.72
80.42
50.68
41.17
37.26
31.63
28.32
28.04
155.576
171.155
81.721
80.424
77.494
77.067
76.647
50.676
41.169
37.255
31.632
28.321
28.039
0.000
ppm

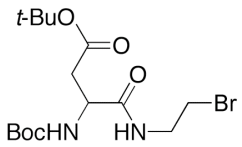

$CDCl_3$, 300 MHz

δ	m	int
7.06	s	1H
6.74	s	1H
4.47	s	1H
3.66	t	2H
4.45	t	2H
2.7	ABX	2H
1.45	s	18H

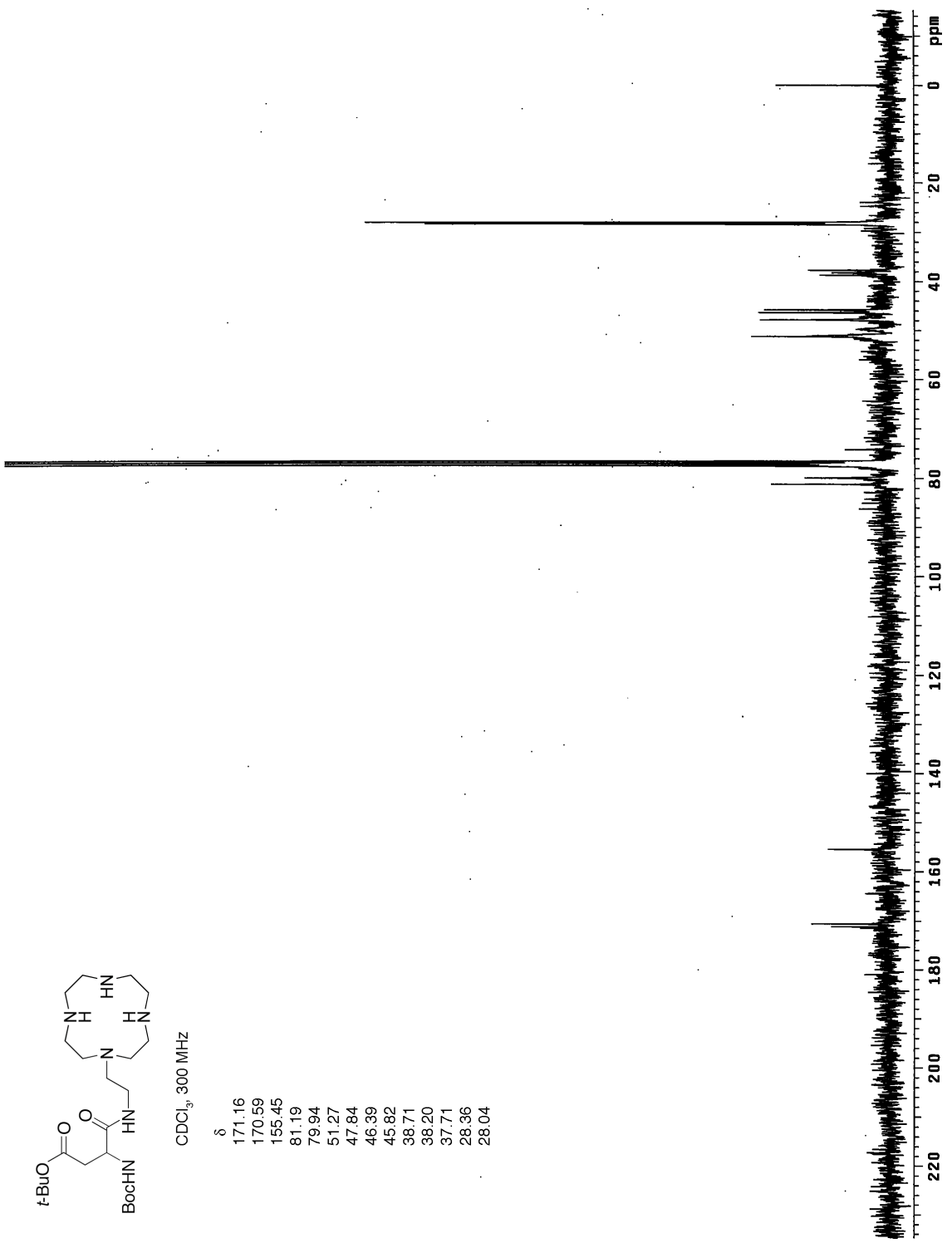
t-BuO
O
O
BocHN
HN
N
HN
NH
N
H
N
H
N
CDCl3, 300 MHz
δ
171.16
170.59
155.45
81.19
79.94
51.27
47.84
46.39
45.82
38.71
38.20
37.71
28.36
28.04
ppm
0
20
40
60
80
100
120
140
160
180
200
220

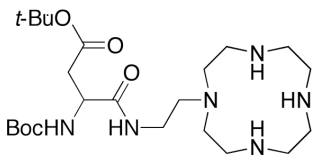

$CDCl_3$, 300 MHz

δ	m	int
5.8	br	1H
4.4	br	1H
3.5 - 4.4	m	22H
1.47	s	18H

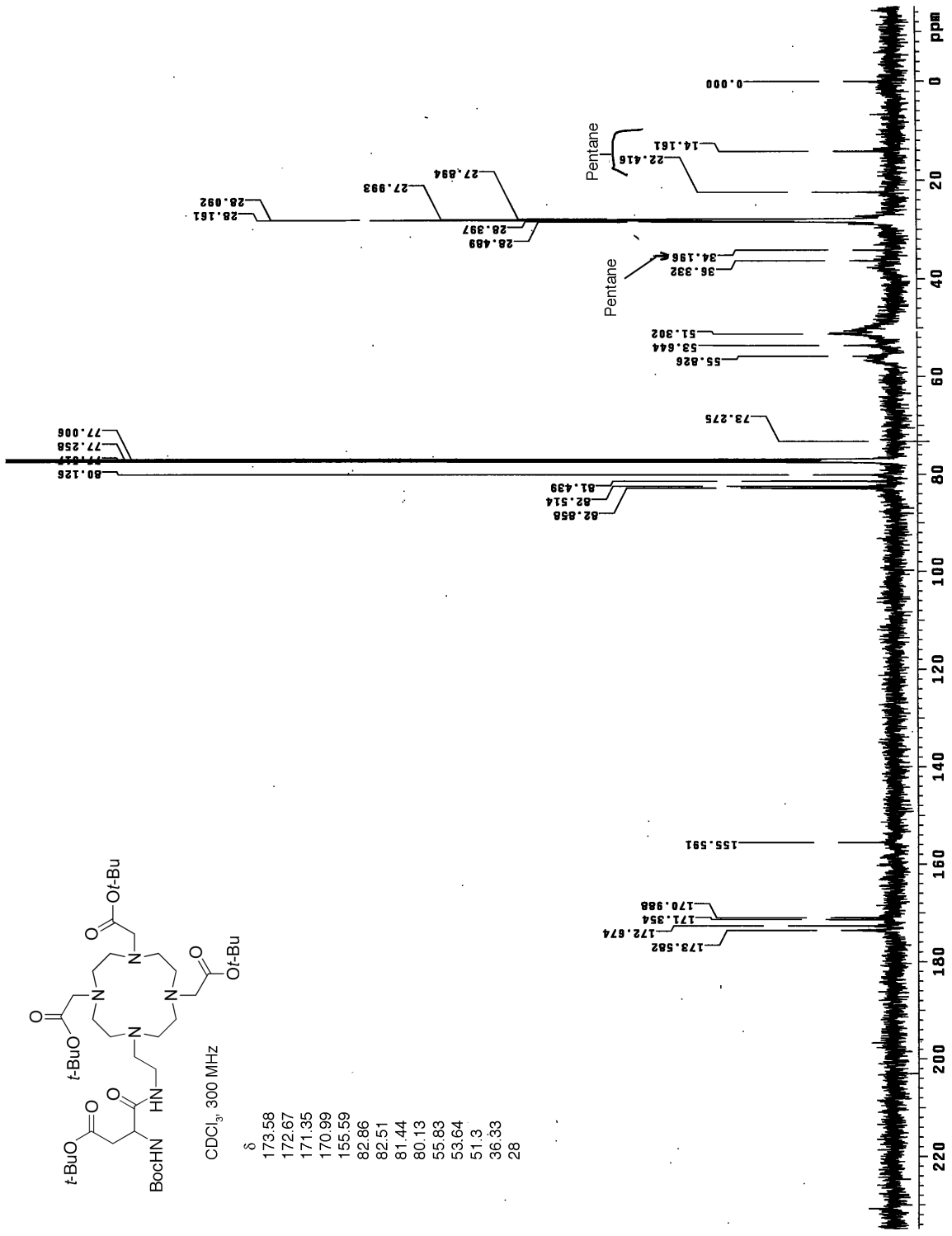

$CDCl_3$, 300 MHz

δ
173.58
172.67
171.35
170.99
155.59
82.86
82.51
81.44
80.13
55.83
53.64
51.3
36.33
28

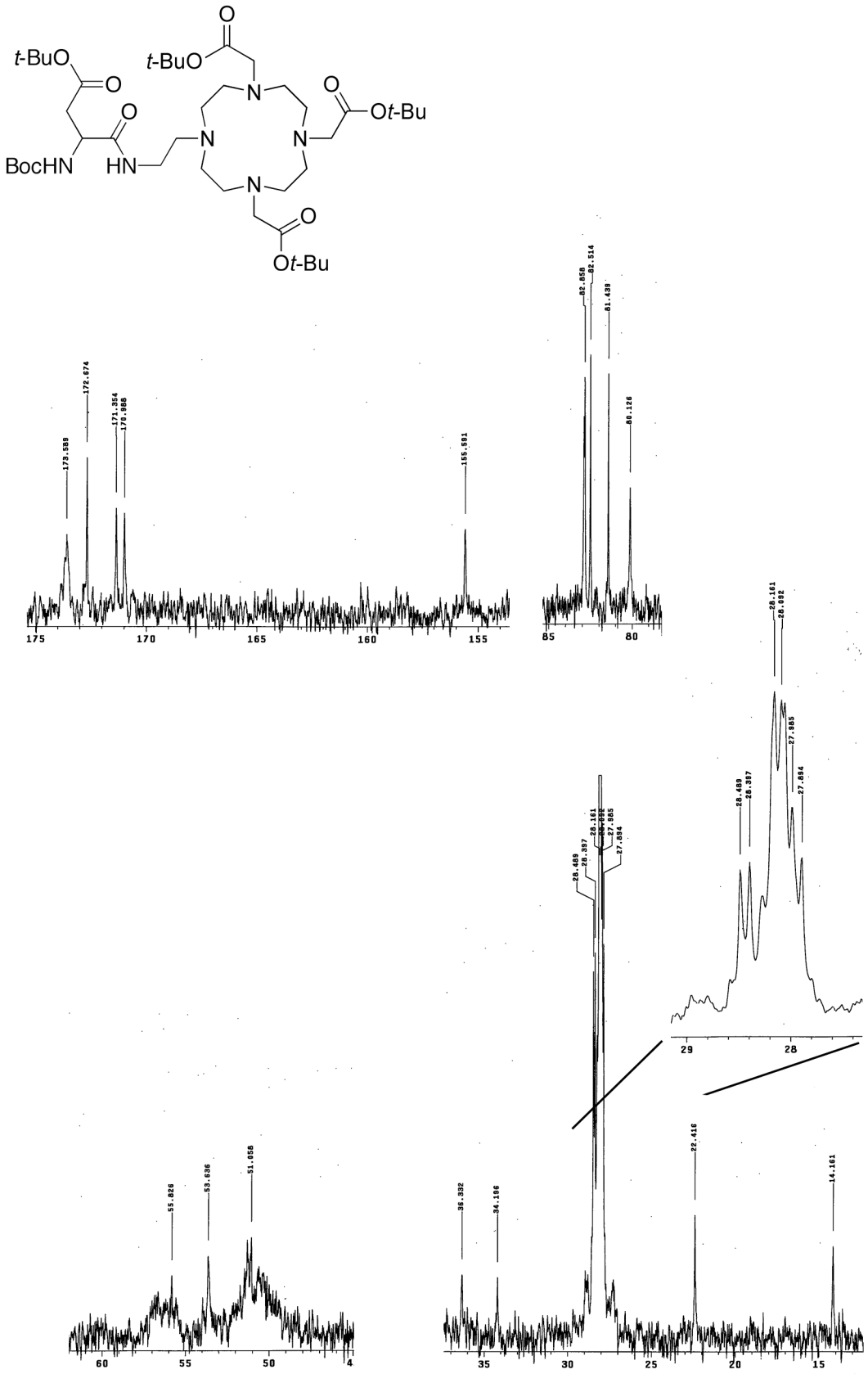
t-BuO
t-BuO
O
O
O
Ot-Bu
BocHN
HN
N
N
N
O
Ot-Bu
173.589
172.674
171.384
170.988
155.591
82.858
82.514
81.439
80.126
28.469
28.397
28.161
28.092
27.885
27.694
55.826
53.636
51.658
36.332
34.196
22.416
14.161

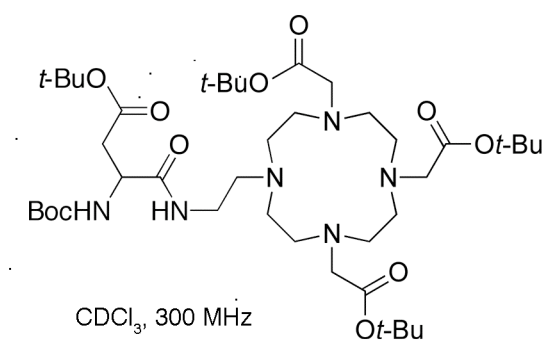

$CDCl_3$, 300 MHz

δ	m	int
7.22	s	1H
5.76	d	1H
4.41	d	1H
3.4 - 2.2	m	28H
1.49 - 1.43	m	45H

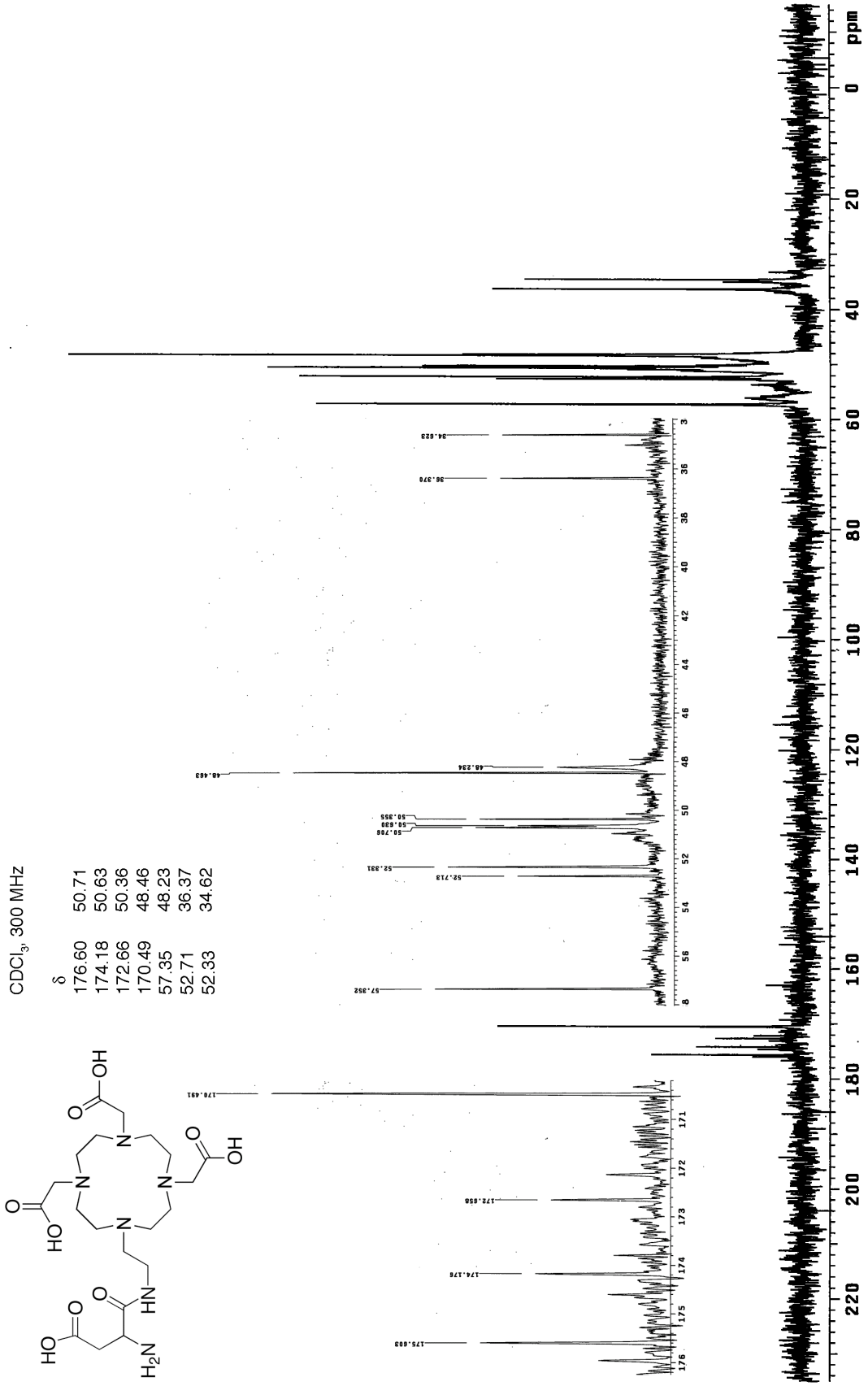
CDCl3, 300 MHz
δ
176.60
174.18
172.66
170.49
57.35
52.71
52.33
50.71
50.63
50.36
48.46
48.23
36.37
34.62
ppm

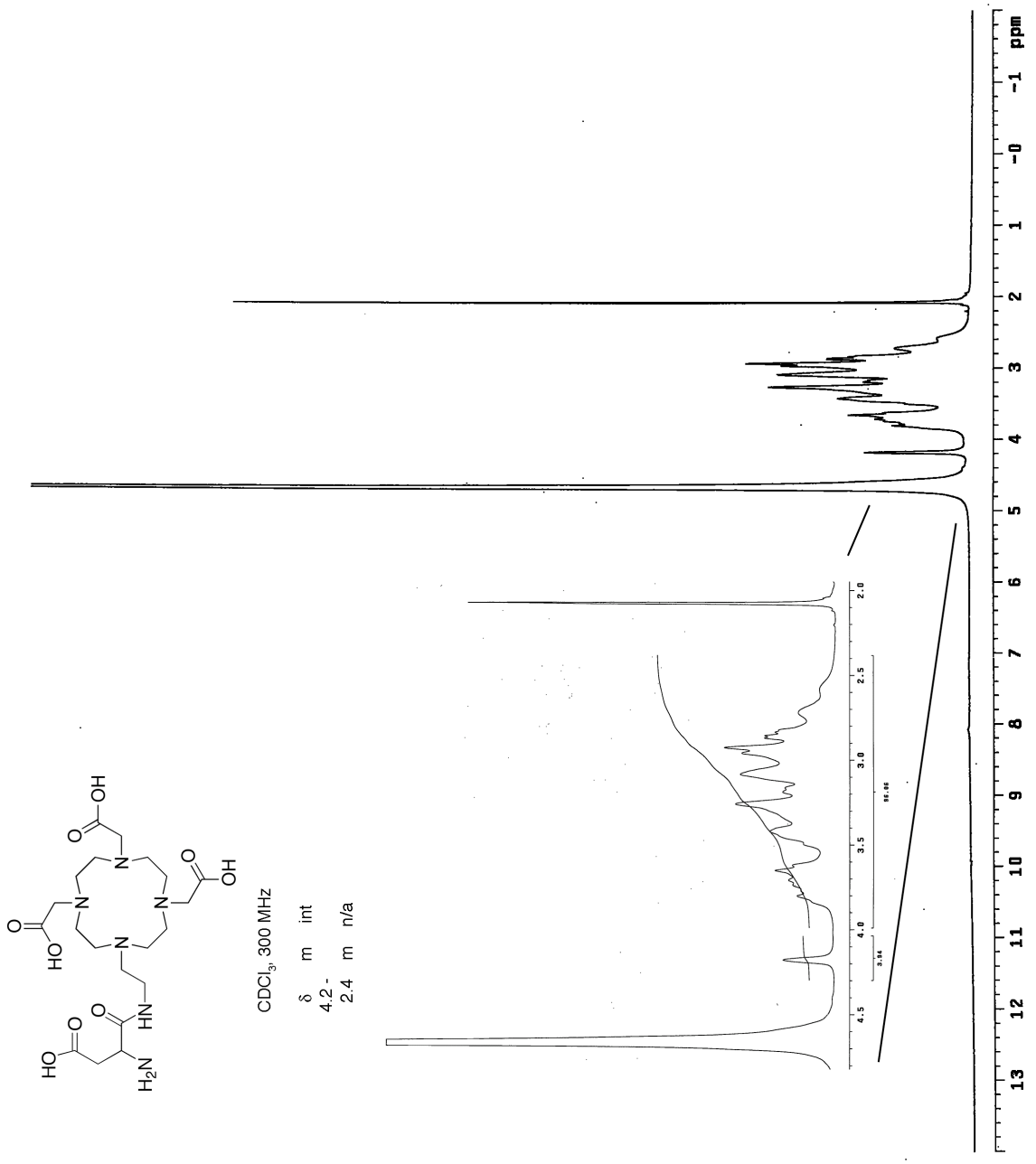
CDCl3, 300 MHz
δ m int
4.2 - 2.4 m n/a
ppm

	A	B	C	D	E	F	G	H
1		Direct fit				Instructions		
2		Relaxivity=	4.64165526510838	mM-1s-1		Enter the observed T1 data and the concentration data in the appropriate cells (in yellow). Go to the "Solver" item under the "Tools" menu. Set E16 as the "Target Cell" to be minimized by changing D3.		
3								
4								
5								
6	mM	T1 Obs	T1 calc	S				
7	30	0.0025	=1/((1/B$14)+(C$3*A7))	=(1-(B7/C7))^2				
8	15	0.005	=1/((1/B$14)+(C$3*A8))	=(1-(B8/C8))^2				
9	9	0.01	=1/((1/B$14)+(C$3*A9))	=(1-(B9/C9))^2				
10	4	0.02	=1/((1/B$14)+(C$3*A10))	=(1-(B10/C10))^2				
11	2	0.04	=1/((1/B$14)+(C$3*A11))	=(1-(B11/C11))^2				
12	1	0.08	=1/((1/B$14)+(C$3*A12))	=(1-(B12/C12))^2				
13	0	3.1	=1/((1/B$14)+(C$3*A13))	=(1-(B13/C13))^2				
14								
15			S total=	=SUM(D7:D13)				
16								
17								
18								
19		Distribution Free Calculation						
20		Relaxivity=	=MEDIAN(B25:G31)	mM-1s-1				
21								
22								
23		Distribution Free Calculation						
24	1/t1obs							
25	=1/B7	=($A25-$A$32)/($A7-A14)	=($A25-$A$31)/($A7-A13)	=($A25-$A$30)/($A7-A12)	=($A25-$A$29)/($A7-A11)	=($A25-$A$28)/($A7-A10)	=($A25-$A$27)/($A7-A9)	
26	=1/B8	=($A26-$A$32)/($A8-A14)	=($A26-$A$31)/($A8-A13)	=($A26-$A$30)/($A8-A12)	=($A26-$A$29)/($A8-A11)	=($A26-$A$28)/($A8-A10)		
27	=1/B9	=($A27-$A$32)/($A9-A14)	=($A27-$A$31)/($A9-A13)	=($A27-$A$30)/($A9-A12)	=($A27-$A$29)/($A9-A11)			
28	=1/B10	=($A28-$A$32)/($A10-A14)	=($A28-$A$31)/($A10-A13)	=($A28-$A$30)/($A10-A12)				
29	=1/B11	=($A29-$A$32)/($A11-A14)	=($A29-$A$31)/($A11-A13)					
30	=1/B12	=($A30-$A$32)/($A12-A14)						
31	=1/B13							
32								